AN ANALYSIS OF GEOMAGNETIC VARIATIONS IN WESTERN BRITISH COLUMBIA

by

HUGH GORDON MILLER

B.Sc. (Hons.) Memorial University of Newfoundland 1968

M.Sc. Memorial University of Newfoundland 1970

A THESIS SUBMITTED IN PARTIAL FULFILMENT OF

THE REQUIREMENTS FOR THE DEGREE OF

DOCTOR OF PHILOSOPHY

in the Department

of

GEOPHYSICS

We accept this thesis as conforming to the

required standard

THE UNIVERSITY OF BRITISH COLUMBIA

August, 1973

In presenting this thesis in partial fulfilment of the requirements for an advanced degree at the University of British Columbia, I agree that the Library shall make it freely available for reference and study. I further agree that permission for extensive copying of this thesis for scholarly purposes may be granted by the Head of my Department or by his representatives. It is understood that copying or publication of this thesis for financial gain shall not be allowed without my written permission.

Department of Geophysics and Astronomy

The University of British Columbia
Vancouver 8, Canada

Date September 2, 1973

ABSTRACT

Geomagnetic variation anomalies in the western structural province of the Canadian Cordillera are examined. Data were collected at five temporary geomagnetic observatories and analysed using single station transfer functions, induction ellipses, and I-ratios. These data and the single station transfer functions from Cochrane and Hyndman (1970) and Dragert (1973) were interpreted.

Geological and geophysical evidence suggest a different tectonic history for the northern and southern parts of British Columbia. The geomagnetic variations provide further evidence for this difference.

Analog and numerical model studies indicate that several major features are causing the geomagnetic variations in the region. First there is a strong coast effect caused by the ocean-land conductivity contrast. The model studies show that an explanation of the observed coast effect requires a zone of high conductivity close to the surface and lying beneath both the ocean and the land. Second there is a strong correlation between the magnitude and direction of the inland induction arrows and the general structural trend. It is concluded that these inland induction arrows are caused by induced currents flowing along the structural province boundaries, possibly at the Mohorovicic discontinuity which has considerable variation in depth from province to province. Third, the offset of the induction arrows from a simple orientation perpendicular to the general structure suggests the presence of three east-west conductors. The major one is the Souther (1970) volcanic zone through the central region analysed. The other two are the edge of the North American craton south of Cache Creek and a

proposed crustal discontinuity north of the Prince Rupert - Prince George profile.

This interpretation is consistent with the known geological and geophysical information regarding the tectonic history of British Columbia.

TABLE OF CONTENTS

APPENDICES

LIST OF TABLES

LIST OF FIGURES

ACKNOWLEDGEMENTS

The candidate wishes to acknowledge the assistance received from the following persons:

Dr. R. M. Ellis, my research supervisor, for his many suggestions and comments during the course of the research.

The late Dr. B. Caner, who originally proposed the survey using the new locations, designed the floating recording system, and supervised the field work.

Dr. R. D. Hyndman who through many stimulating discussions greatly enhanced my knowledge of the techniques used in geomagnetic depth sounding.

Dr. H. W. Dosso and his graduate students at the Department of Physics, University of Victoria for their permission to use the model tanks and for their technical assistance in obtaining the analog data.

Personnel from the Department of Geophysics and Astronomy and the Victoria Magnetic Observatory who serviced the Cache Creek, Bella Bella, and Tatla Lake stations.

National Research Council of Canada for a graduate scholarship and for support through an operating grant to Dr. R. M. Ellis.

The Department of Energy, Mines, and Resources for funds supporting the field work through the Victoria Magnetic Observatory.

Mrs. Hilary Hayles for her patient typing of the thesis.

Last, but by no means least, my wife, Christine, for her assistance with all the drafting of diagrams and for her patience and understanding during the course of the research.

CHAPTER 1

INTRODUCTION

1.1 Scope of Thesis

In this thesis the geomagnetic coast effect and associated variation anomalies in western British Columbia are interpreted using both new data and the earlier information of Cochrane and Hyndman (1970) and Dragert (1973) presented as profiles (Fig. 1.1). Geomagnetic models are developed in conjunction with the present understanding of the tectonics of this region. Modifications to these tectonically derived models are required to explain the observed geomagnetic variations; thus the geomagnetic variations provide further insight into the tectonics of the region.

1.2 Geomagnetic Variations and the Coast Effect

Current flow in the ionosphere induces secondary currents in the earth which give rise to secondary geomagnetic fields. For a uniform sheet current over a horizontally stratified medium, the induced magnetic field has the same horizontal component as the inducing field but the vertical field is in the opposite direction. The total field, therefore, has a horizontal component which is twice the size of the inducing field and no vertical component (Rikitake, 1966). The presence of a vertical component indicates either limited source dimensions or lateral inhomogeneities. For the frequency range of interest (0.16×10^{-3} to 1.15×10^{-7} Hz) and at mid-latitudes, the predominant cause of vertical fields is geological inhomogeneities (Lambert and Caner, 1965). It has been found that these variations in the vertical field and the associated

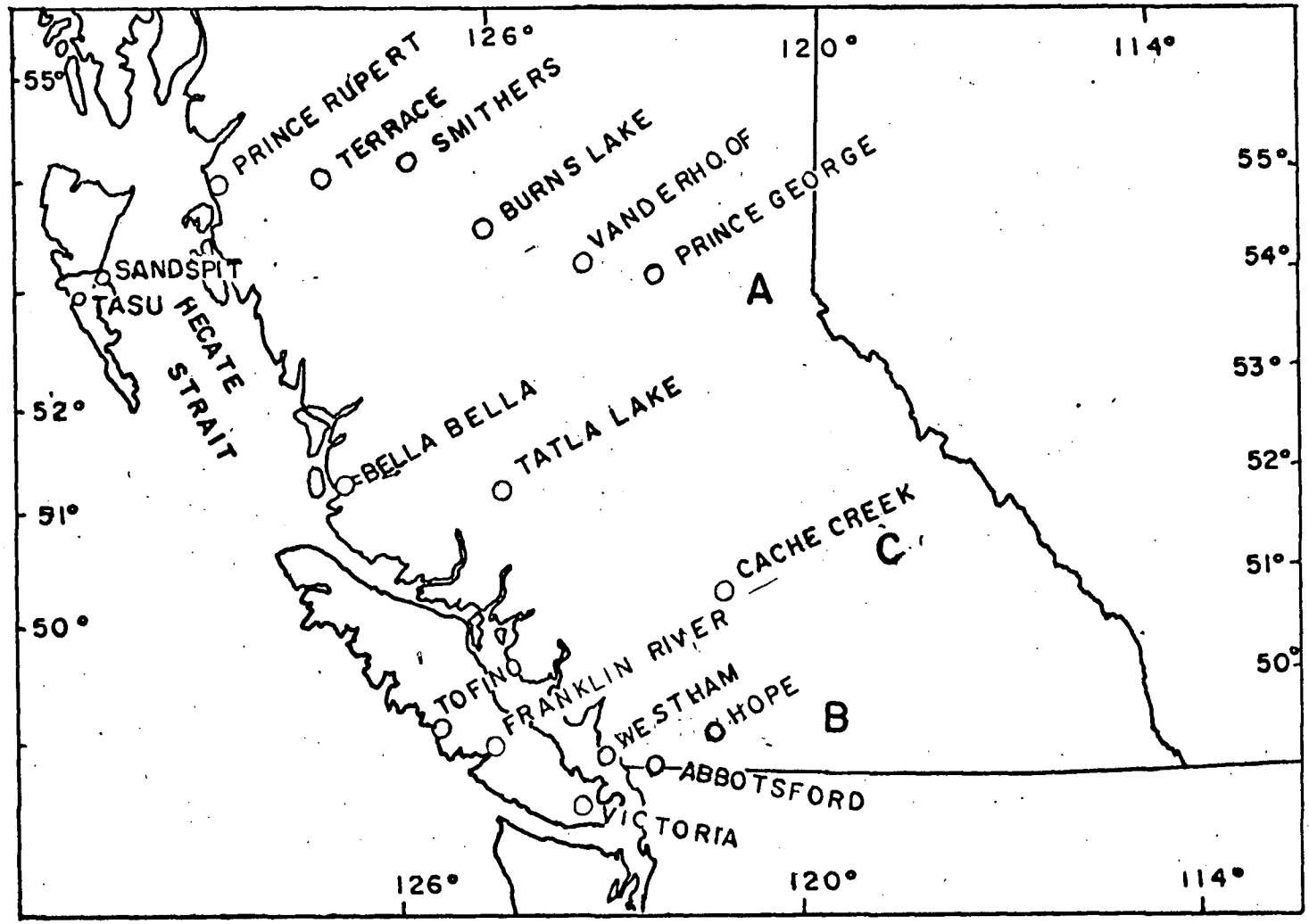

Fig. 1.1 Location map for geomagnetic observatories analysed in this study
A - Dragert (1973) profile Prince Rupert to Prince George.
B - Cochrane and Hyndman (1970), Tofino to Hope.
C - Present study, Tasu to Cache Creek.

changes in the horizontal fields may be used to interpret the subsurface structure (Rikitake, 1966). These interpretative techniques will be discussed in Chapter 2.

The geomagnetic coast effect is the earliest known form of geomagnetic variation anomaly. A major source of this anomaly is the large electrical conductivity contrast between the ocean and land which causes current concentration along the boundary giving rise to large components of the vertical magnetic field. In addition, geological and thermal differences between the oceanic and continental crust and upper mantle contribute to this effect. This will be particularily true at complex margins such as trenches. The coast effect has now been observed at many locations (Parkinson, 1959; Schmucker, 1964; Lambert and Caner, 1965; Hyndman and Cochrane, 1972 and others). As expected the size of the vertical component has been found to decrease as one progresses inland. The maximum effect is observed at periods between 30 and 60 minutes (Everett and Hyndman,1967; Schmucker, 1970; Cochrane and Hyndman, 1970). Variations in the form of coast effect are found confirming that subsurface structures associated with the coast play a major role (Lambert and Caner, 1965). (It should be noted that the exact form of the land-sea margin does not affect the results at periods longer than 10 minutes.)

A boundary of particular interest is a subduction zone where water-saturated material from an oceanic plate descends beneath the continent. Such a zone will be more conductive than the continent and will damp the geomagnetic variations caused by the induced currents at the land-water boundary. In quiescent zones, cooling and dehydration will occur thus giving rise to further variations in the form of the coast effect. The observed geomagnetic variations, therefore, yield data on

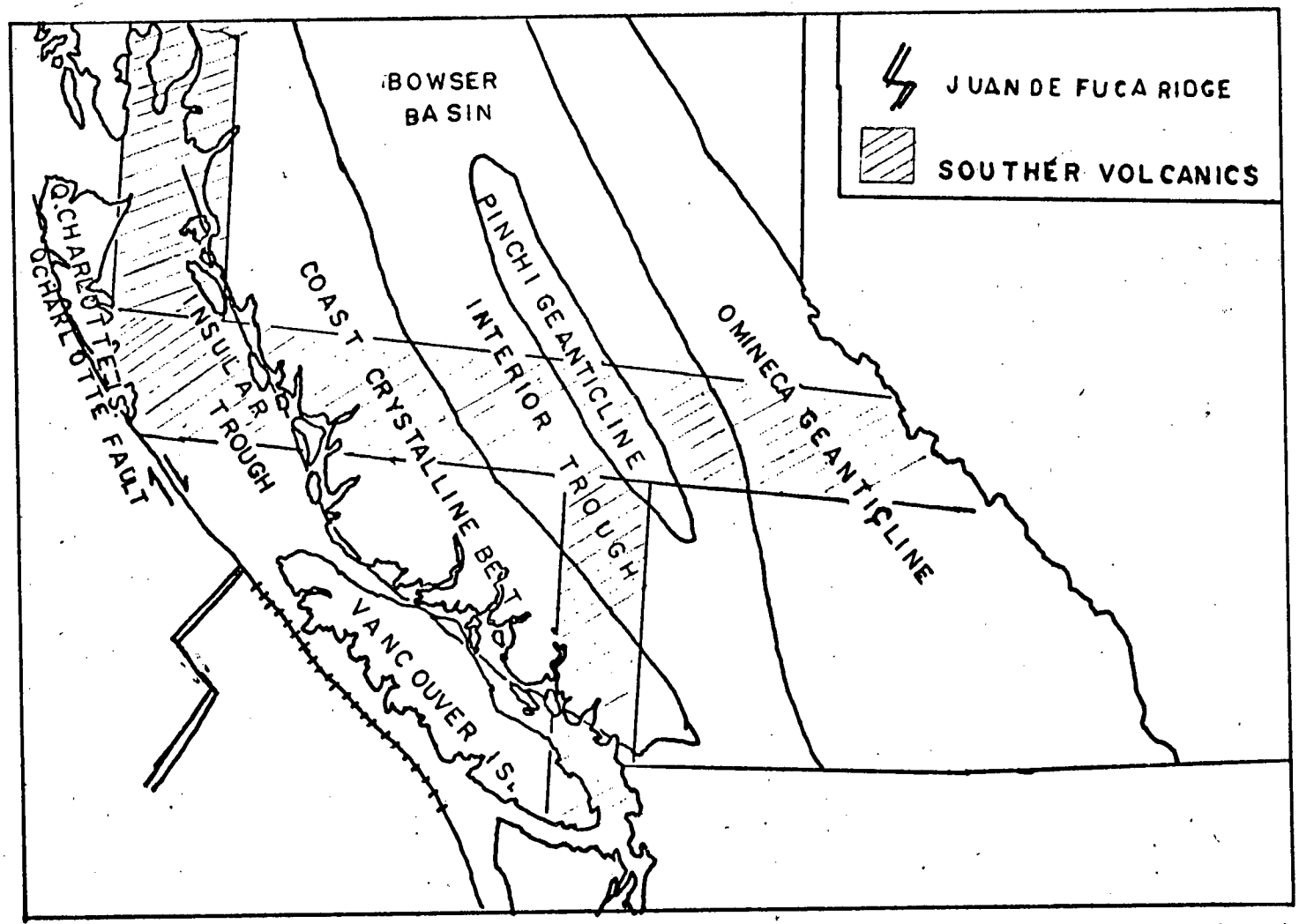

Fig. 1.2 General geology of British Columbia and adjacent Pacific after Souther (1970) and Tiffin et al., (1972).

both the present and past tectonic activity at the continental boundary.

1.3 Tectonics of Western British Columbia

The geological setting of the coastal and adjoining regions of British Columbia is complex (Roddick, et al., 1967; Monger, 1972) due to several phases of crustal evolution which have each left their characteristic imprint. There are four northwesterly trending structural provinces in the Canadian Cordillera: the Insular Trough, consisting of marine sediments and volcanics; the Coast crystalline belt which is a granodiorite suite; the Interior Trough with marine sediments and recent volcanic accumulations of considerable thickness; and the Omineca geanticline and the adjacent miogeosynclinal belt forming a structural couplet at the eastern part of the Cordillera (Fig. 1.2). All the geomagnetic observatories considered in this thesis were located in the first three provinces. For geologic discussion the region is divided into northern and southern parts by 51^{0} N latitude.

The geological history of the Canadian Cordillera for the Precambrian and Early Paleozoic is difficult to deduce since there are few outcrops of these old rocks and the rocks which do outcrop have been affected by subsequent events. Berry et al., (1971) review the geophysical evidence for the Cordillera and suggest that the North American craton extended further west in the southern region than in the northern during the Paleozoic. This would mean that the craton boundary would be the site of complex plate interactions since the Paleozoic. Evidence suggests that it controlled the east-west axis of an early Paleozoic orogeny.

Since the Paleozoic the Coast Crystalline belt has been the major positive topographic feature, providing sediment to the two adjacent troughs

while the whole eugeosynclinal region was the site of complex evolution. The present dissimilarities in character originated during the Triassic (Culbert, 1971). The Triassic in the northern area was a period of slow, quiet changes typified by the production of pillow lavas overlain by shallow-water carbonate shales. The southern area was more unstable during this time. Here, a more dynamic environment prevailed as typified by the coarse pyroclastic rocks covered by basaltic and andesitic lava flows. These are indicative of an active subduction zone flowing under an island arc system (Dickinson, 1971).

Uplift in the Coast Crystalline belt occurred throughout the Jurassic. The northern and southern areas of the Insular Trough underwent similar changes as those occurring during the Triassic. By the middle Jurassic, the whole of the Insular Trough was the site of pyroclastic volcanism which may indicate that an active subduction zone then existed along the entire coast. This evolution of island arc type subduction continued throughout the Lower Jurassic during which time broad northwest trending folds were formed. Faulting formed elongate NW trending blocks. Along with some emplacement of plutons, the faulting persisted throughout the Cretaceous. This phase which first imprinted the NW trend on the Cordillera is characteristic of the terminal stage of the evolution of a geosyncline (Dickinson, 1971).

From the Tertiary to the present, volcanism in various forms has occurred in the Cordillera. In the southern area the calc-alkaline lavas characteristic of volcanism above an active trench were produced, while in the north the lava type changed during the Miocene from the calc-alkaline type to alkali-olivine basalt. This change indicates that subduction ceased in the northern area during the Miocene. The effusion of

the alkali-olivine basalt, which is formed at great depth, may be indicative of new zones of weakness in the upper mantle. This geological evidence suggests that subduction in the northern area had ceased at least 13 million years ago, but may still be occurring in the southern area.

On the basis of the locations of the Quaternary volcanoes (Souther, 1970) proposes two north-south zones of volcanism offset by an east-west zone (Fig. 1.2).

A comprehensive analysis of the plate tectonic history of the west coast of North America during the Cenozoic has been presented by Atwater (1970). The following pertain to British Columbia.

(1) The southern region is currently an active zone where spreading is occurring from the Juan de Fuca ridge (Fig. 1.2). Slow subduction may yet be occurring as the plate formed at the ridge is consumed at the continental margin.

(2) The northern region is experiencing dextral movement along a transform fault, the Queen Charlotte Fault (Fig. 1.2). Active subduction may have occurred in this region prior to the Miocene.

Tiffin et al., (1972), in a detailed interpretation of the geology in a relatively small area from the triple point to the northern part of Vancouver Island, support these conclusions.

1.4 Geophysical Information

There is a limited collection of geophysical data directly

applicable to the region. In the north a crustal section from the continental margin to the Interior Trough may be constructed (Fig. 1.3) using the seismic results (Johnson et al., 1972; Forsyth, 1973). This section shows that the top of the intermediate layer (velocity 6.3-6.8 km/sec) dips from 7 km. depth beneath the ocean to 10 km. beneath the Queen Charlotte Islands and 24 km. beneath the Coast crystalline belt. Jacoby (1971) reports that on a similar profile across the southern region the depth to the Mohorovicic discontinuity changes from greater than 50 km. beneath Vancouver Island to about 40 km. beneath the Strait of Georgia and 35 km. beneath the Interior Trough.

The thickness of the crust is examined by Stacey (1973) on the basis of gravity data accumulated and interpreted along a profile from the continental margin off Vancouver Island to the plains in Alberta. Stacey concludes that the region beneath Vancouver Island has an abnormal structure with a high density lower crust or a lower than usual density upper mantle. He considers this to be compatible with a zone of subduction beneath Vancouver Island which is either currently active or has been recently active.

Previous geomagnetic investigations (Lambert and Caner, 1965; Caner et al., 1967; Caner et al., 1969) have been interpreted in terms of a horizontal layer of high conductivity extending from a depth of 15 km. to a depth of 40 km. This layer has been detected beneath all of British Columbia west of the Rocky Mountain Trench. The magnetotelluric results also suggest this zone is found beneath Vancouver Island, there extending from 10 km. to 65 km. depth (Caner and Auld, 1968; Neinaber et al., 1973). From its depth this would appear to correlate well with the seismic intermediate zone. Its existence in north-central British

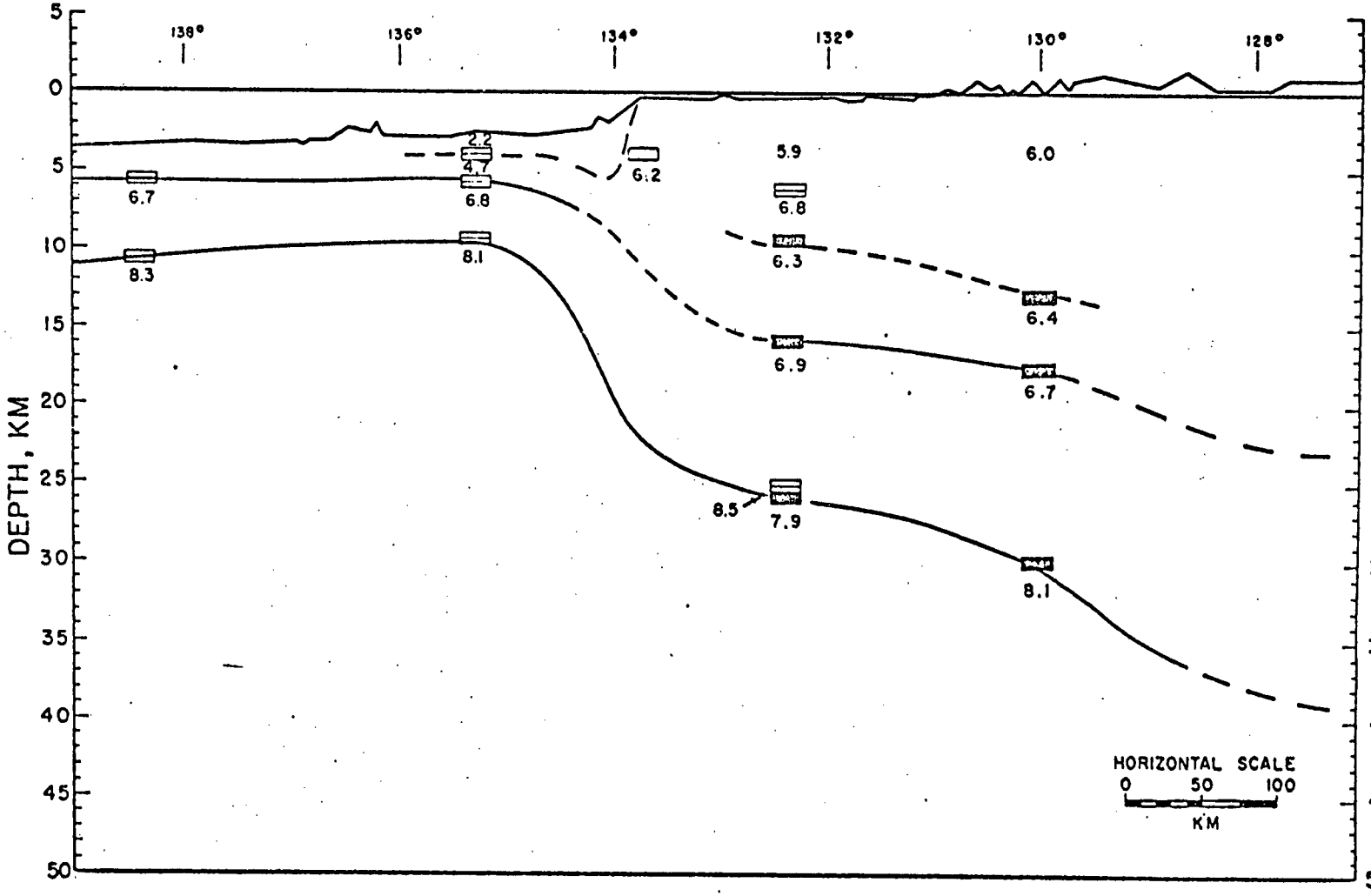

Fig. 1.3a Crustal cross-section through Dixon Entrance from Johnson et al., (1972). at latitude $54^{0}30'$ N. All velocities in units of KM/sec.

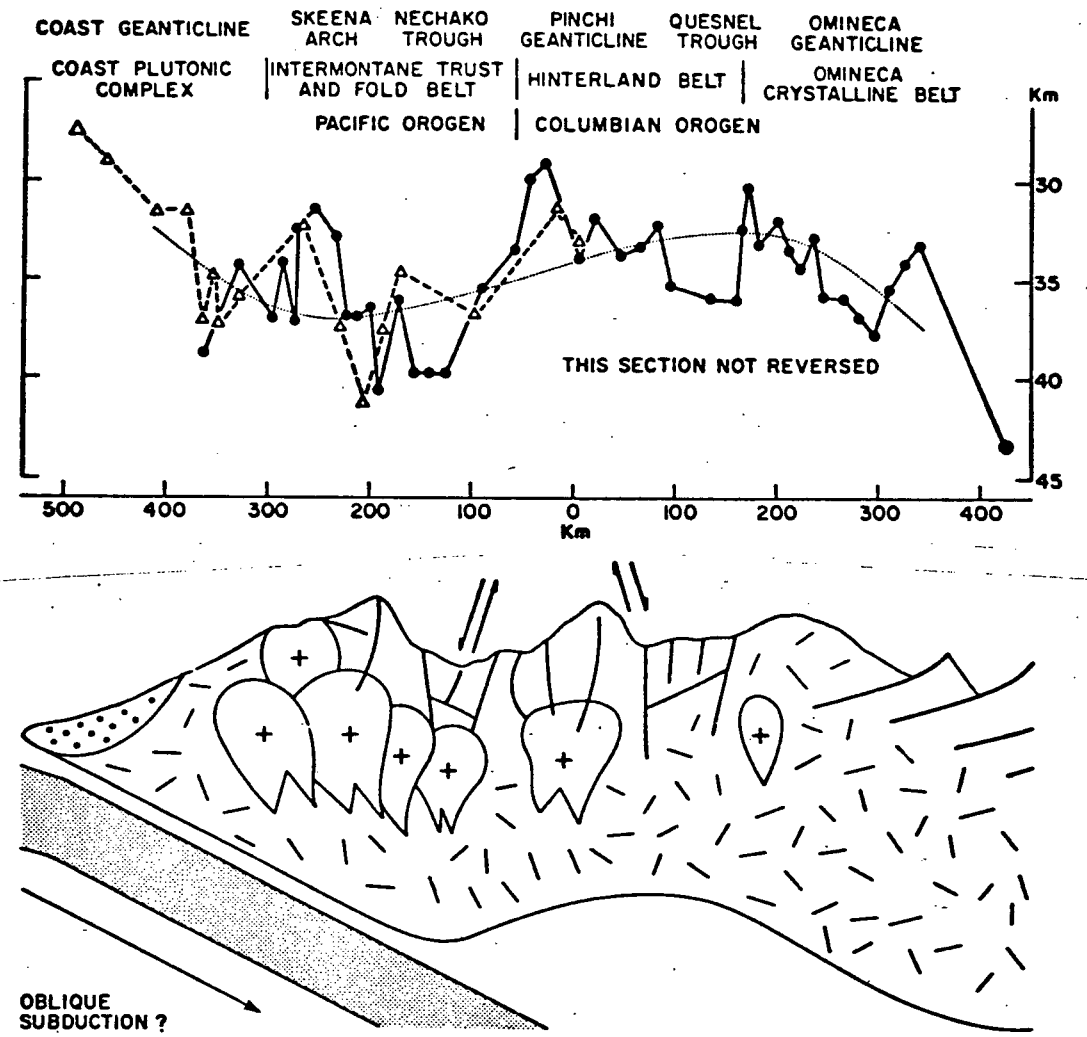

Fig. 1.3b Deep crustal structure Prince Rupert to Prince George(from Forsyth (1973)).

Columbia is mentioned in the only available work on the area (Dragert, 1970) but not modelled.

The cause of this high conductivity in the lower crust has been alternately proposed as temperature variations or hydration coupled with partial melting. Caner originally favoured temperature variations as the cause (Caner, et al., 1967) but in his last paper on the region (Caner, 1969) suggested that hydration and partial melting hypothesis was more probable physically. He points out that the conductivity required would necessitate a temperature in excess of 900^0 C. at a depth of 15 km. and an inversion in temperature while hydration would require only a few percent water content which would lower the melting temperature of the layer sufficiently to allow melting without elevated temperatures. With the accent now on plate tectonics and the effects of downgoing slabs Oxburgh and Turcotte (1970) have calculated the thermal regime around a subducting slab. These results appear to show that the temperatures required by Caner for the high conductivity could be attained near the top of the subduction region but would not be sustained at sufficiently large distances from the subduction region to explain the persistence of the high conductivity from the coast to the Rocky Mountain Trench. It would appear that the cause of the high conductivity in the lower crust is not simple. The existence of such a layer in the regions far from active subduction zones and in regions where subduction ceased 13 million years ago indicates that hydration is a more probable explanation for these regions. Near the present subduction zone a combination of hydration and thermal effects is probable since in such a region there is a downgoing slab pulling water saturated sediments with it.

The presence of the water will lead to depressed melting points for

the materials at the surface of the slab. The heat from the hotter adjacent mantle will tend to melt the material in the slab. Both these effects together may lead to a higher electrical conductivity of the slab with respect to the surrounding material.

Further evidence for the change in the subduction pattern is obtained from an analysis of the aeromagnetic fields recorded at flight altitudes of 5.5 km. over the land and adjacent Pacific Ocean (Haines et al., 1971). The characteristic oceanic lineations are observed over the Pacific with the pattern indicative of a change in spreading rate and direction 13 million years ago. Over the land the fields are varied, the major changes in character occurring at or near the structural boundaries. In the Interior Trough region the fields are flat supporting the proposal of high temperatures in excess of 750^{0}C. at 35 km. depth.

In summary the geological and geophysical evidence indicates that the Canadian Cordillera is a complicated region which has been the site of many plate interactions. At present the northern region is experiencing dextral movement along the Queen Charlotte Fault while the southern is a region of current or recent subduction.

1.5 Geomagnetic Implications

The physical parameter which determines the response of a material to electromagnetic disturbances in the frequency range under consideration is the electrical conductivity. The electrical conductivity of a rock may be determined as a function of temperature, pressure, water content, and composition by laboratory measurements (Watanabe, 1970). Such measurements have shown that similar rock types have a wide range of conductivity values (Keller and Frischknect, 1970) (Table 1.1) which reflect variations in the local conditions under which the rocks were formed and were reworked by subsequent events. While these results show considerable

variation in resistivity within a given rock type, they do show consistent differences between varying rock types which make these values applicable to large rock units required in geomagnetic studies.

Knowledge of these general patterns of rock conductivity enable the geological information to be used to predict zones of induced current concentration. Since the Insular Trough is composed mainly of marine sediments and volcanics it can be expected to have a higher conductivity than the adjoining Coast crystalline belt. Similarily the Interior Trough with its volcanics should have a higher conductivity than the Coast crystalline belt. The east-west volcanic zone proposed by Souther (1970) should also have a higher conductivity than the rocks adjoining it. These conductivities suggest a complicated current pattern with the northwest-southeast currents induced along the Coast crystalline-Insular Trough and Coast crystalline-Interior Trough deflected by the east-west volcanic zone. The crustal structure suggests that subsurface electrical current concentrations should occur beneath the Queen Charlotte Islands where the warped high conductivity layer meets the less conductive continental material. Further concentrations may be expected along the boundary between the volcanic zone at depth and the adjoining material. If any unknown structures are present with significant conductivity contrast with the surrounding material, induced currents may be expected to concentrate at these boundaries.

The geological and geophysical evidence points to a differing conductivity structure between the northern and southern region for several reasons. First, the southern region is active or recently became dormant, thus the effect of temperature upon conductivity should still be evident. The role of the hydration of the downgoing slab should also be

evident. From the seismic evidence it appears that the mantle is deeper beneath the southern region while the magnetotelluric evidence suggests that the higher conductivity layer starts at approximately the same depth as in the north. This would give a greater thickness for this layer in the south which should provide more rapid damping of the vertical field as one progresses inland.

1.6 Objectives

The objective of this thesis is to interpret the coast effect and related geomagnetic variations in western British Columbia. The data from the two previous studies which reveal the coast effect (Cochrane and Hyndman, 1970; Dragert, 1970, 1973) have been incorporated into this work. These profiles were located in north-central British Columbia from Prince Rupert to Prince George and in southern British Columbia from Tofino to Hope (Fig. 1.1). The closest location to the continental margin is Tofino which lies 55 km. from the 200 m. bathymetric contour.

Both these surveys ignored an opportunity to examine the coast effect in a region in which the effect would be most evident and vary most rapidly. The Queen Charlotte Islands (Fig. 1.1) lie adjacent to the continental shelf, hence the coast effect due to the presence of the land-sea interface should be quite pronounced on the west coast of the islands. Since the area is one of subduction which ceased 13 million years ago, the underlying structure should be conductive, which should cause secondary effects along with the coast effect. Using stations such as those on the Queen Charlotte's it may be possible to resolve the contributions to the geomagnetic variations from the water and the structure. To minimize the effects of distance from the source fields all stations should be on

the same line of geomagnetic latitude. When such a line is plotted through Tasu it is found that stations can be located within 0.5^0 by placing them at the locations chosen (Table 3.1). All these locations are readily accessible by road or regular airline flights and have the a-c power required for the equipment. The two locations in the Queen Charlotte Islands, Tasu and Sandspit, represent the first time in British Columbia that data has been collected from sites this close to the continental margin.

An interpretation of the coast effect in terms of tectonic structure requires that the data be processed in a form which may be compared with model studies. To do this the transfer function technique (Chapter 2) was used and compared with numerical model studies (Chapter 4) to provide a structural cross-section similar to a seismic crustal section. The effects of three dimensional structures were examined using the electromagnetic analog modelling tanks at the Department of Physics, University of Victoria.

Interpretation in this manner represents the first time that a detailed study of the coast effect in British Columbia has been compared with models derived from tectonic information. It also represents the first time that major tectonic features of British Columbia have been modelled using the electromagnetic analog modelling technique.

TABLE 1.1

General Resistivity Ωm.

Age	Marine Sed.	Terrestial Sed.	Extrusive Basalt, Rhyolite	Intrusive Granite, Gabbro	Chemical Precipitates
Quaternary Tertiary	1-10	15-50	10-200	500-2000	50-5000
Mesozoic	5-20	25-100	20-500	500-2000	$100-10^4$
Carboniferous Paleozoic	10-40	50-300	50-1000	1000-5000	$200-10^5$
Early Paleozoic	40-200	100-500	100-2000	1000-5000	10^4-10^5
Precambrian	100-2000	300-5000	200-5000	5000-20000	10^4-10^5

CHAPTER 2

GEOMAGNETIC DEPTH SOUNDING

Geomagnetic depth sounding is a technique employed to deduce sub-surface electrical conductivity variations using simultaneous, three component, geomagnetic data from an array of magnetic observatories. The electrical conductivity distribution in the crust and upper mantle may be estimated by an analysis of geomagnetic variations in the frequency band 0.16×10^{-3} Hz to 1.15×10^{-7} Hz (periods of 10 minutes to 24 hours). These periods correspond to disturbances which induce currents in the crust and upper mantle of the earth.

2.1 Maxwell's Equations as Related to Geomagnetic Depth Sounding

Maxwell's equations express the relationship between the electrical and magnetic fields and the physical properties of a medium. For a uniform, homogeneous medium these equations are

$$\nabla \cdot \underline{D} = 0 \qquad \nabla \cdot \underline{B} = 0$$

$$\nabla \times \underline{E} = -\frac{\partial \underline{B}}{\partial t} \qquad \nabla \times \underline{H} = \underline{J} + \frac{\partial \underline{D}}{\partial t} \tag{2.1}$$

Using the empirical relations $\underline{D} = \varepsilon \underline{E}$, $\underline{B} = \mu \underline{H}$ and $\underline{J} = \sigma \underline{E}$ and sinusoidal time variation it can be shown that

$$\nabla \times \nabla \times \underline{H} = i\mu\sigma\omega\underline{H} + \mu\varepsilon\omega^2\underline{H}$$

$$\nabla \times \nabla \times \underline{E} = i\mu\sigma\omega\underline{E} + \mu\varepsilon\omega^2\underline{E} \tag{2.2}$$

The magnitude of the ratio of the first term on the right hand side to the second term on the right hand side is $\sigma/\omega\varepsilon$. Considering typical values for the earth where $\sigma = 10^{-3}$ (ohm m)$^{-1}$, $\varepsilon = \varepsilon_0 = 8.85 \times 10^{-11}$ farad/m and for the highest frequency under consideration $\omega = 2/60$ sec^{-1} shows that $\sigma/\omega\varepsilon = 10^8$. Thus the second term on the right hand side of equation (2.2) can be ignored for the problem under consideration.

A further simplification to (2.2) can be made which renders the problem tractable in cartesian coordinates. Two effects must be considered in making this simplification. First the effect of the curvature of the earth must be considered. Since the profile length under consideration is approximately 500 km. which is small compared to the circumference of the earth, the problem may be considered in terms of a disturbance incident upon a flat earth. Secondly, the spatial wavenumber of the source fields must be considered. Caner et al. (1967) deduce that the source field is uniform over at least 600-800 km. for short periods (10 minutes) and that the spatial wavenumber is effectively infinite at longer periods. Thus the source fields may be regarded as uniform for the periods being investigated and the problem reduces to one of a plane disturbance incident upon a flat earth. Cartesian coordinates may be used in all regions for which (2.2) must be solved. Equation (2.2) then becomes

$$\nabla^2 \underline{H} = i\mu\omega\sigma\underline{H}$$

$$\nabla^2 \underline{E} = i\mu\omega\sigma\underline{E} \qquad (2.3)$$

These equations show the dependence of the magnetic field upon the frequency of the disturbance and upon the electrical conductivity of the medium. By solving (2.3) for $\underline{H}$, the corresponding $\underline{E}$ may be determined

from the appropriate equation in (2.1) . These equations also show that the quantity $\omega\sigma\mu$ has dimensions of L^2. L, the skin depth, indicates the depth of penetration of a disturbance in a medium before being attenuated to 1/e of its initial value. Since the skin depth is a function of both the frequency and conductivity a change in either parameter will affect penetration depth of a disturbance. This variation of the skin depth with frequency requires that a different calculation of the magnetic fields be carried out for each frequency.

2.2 Analysis Techniques

Several techniques exist for analysing the geomagnetic variations recorded at an array of stations irregularly spaced along a profile. The first technique is the Parkinson Arrow (Parkinson, 1959) where the magnitude of the arrow is the ratio of the incremental change in the vertical direction to the incremental change in the total horizontal field for the same increment in time. The azimuthal direction of the arrow is determined from the incremental changes in the horizontal components.

$$|PA| = \frac{Z(t) - Z(t+\tau)}{\sqrt{\{H(t) - H(t+\tau)\}^2 + \{D(t) - D(t+\tau)\}^2}} \qquad (2.4)$$

$$\text{THETA}\ (\tau) = \arctan \frac{D(t) - D(t+\tau)}{H(t) - H(t+\tau)}$$

where H is the magnetic north component

D is the magnetic east component

Z is the vertical magnetic component

τ is the time increment

PA is the magnitude of the Parkinson arrow

THETA (τ) is the azimuthal dependence measured clockwise from magnetic north.

A second angle, the tilt angle may be defined

$$TA(\tau) = \text{arc tan } PA$$

Analysis of long record lengths ($T >> \tau$) for a particular locality has shown that the magnitudes and amplitudes of the Parkinson arrows tend to fall on a plane.

The observations also tend to fall around two preferred azimuthal directions 180° apart. This phenomenon is interpreted by Parkinson as indicative of two things. Forst the magnitude of the vertical field is a linear function of the magnitude of the horizontal field. Secondly, the two preferred directions, one for instantaneous positive vertical changes and the second for negative vertical changes indicates that a preferred direction of the horizontal field changes exists. Since all the changes lie on a plane of confinement as defined by Parkinson (1959), it is possible to use the direction of the total horizontal component of the field changes as an indicator of the location of the induced current concentration. An analogy may be drawn between these field changes and the magnetic field around a wire carrying a sinusoidally varying current. If the reference frame is chosen correctly, when the ratio of the vertical to horizontal field is positive, the horizontal field component points toward the wire. By using the direction associated with positive Z/H ratios. Parkinson thus devised the Parkinson arrow which points towards the induced current.

The Parkinson arrow provides then a technique for determining the location and strike of the major conductor from the instantaneous changes in the magnetic field. Its most serious flaw is that it cannot be readily interpreted in regions of complex structure since it provides no phase information.

A similar problem in interpretation is faced by the I ratio (Lambert and Caner, 1965) presented in Appendix 4. Essentially the I ratio is the magnitude of the Parkinson arrow calculated for selected events of a particular period. Like the Parkinson arrow, the I ratio removes source effects by averaging over a number of events. However, for the I ratio the averaging is a numerical averaging of the magnitudes only and not a vector averaging incorporating directions as well. Also, like the Parkinson arrow, the I ratio reveals no phase information. As used in this thesis the I ratio is based upon the power spectra for the three components. This approach means that the I ratios as calculated may be strongly contaminated by source effects since no technique of removing the part of the vertical field which is not coherent with the horizontal field is used. The I ratios are used only to delimit regions of induced current concentration and are not used in any quantitative comparisons with the numerical models.

The third technique used in the analysis of geomagnetic data is the transfer function and the single station transfer function. Parkinson's observation that the vertical field was linearly dependent upon the induced horizontal field has led to the formulation of the following relation, termed Parkinson's relation:

$$\Delta Z = z_D \, \Delta D + z_H \, \Delta H \qquad (2.6)$$

where ΔZ is the induced vertical field change

ΔD is the change in the eastward horizontal field

ΔH is the change in the northward horizontal field

z_D and z_H are the transfer functions showing the relationship between Z, D, H.

Everett and Hyndman (1967) and Schmucker (1964, 1970) have extended this relationship to the concept of a linear relationship between the anomalous induced fields and the normal inducing fields.

$$\underline{F_a} = T\,\underline{F_N} \tag{2.7}$$

where $\underline{F_a}$ is the anomalous field

$\underline{F_N}$ is the normal field

T is the transfer matrix

In general $\underline{F_0} = \underline{F_a} + \underline{F_N}$ where $\underline{F_0}$ is the observed field at a given location. Given $\underline{F_N}$ and $\underline{F_0}$, $\underline{F_a}$ may be determined and the matrix T may be found at a specified location. The major problem is the determination of $\underline{F_N}$. The usual criterion for the determination of $\underline{F_N}$ is that the vertical field at the reference, "normal", station be zero or close to zero at all frequencies. The selection of a normal station has usually been based upon a visual inspection of records (Caner, et al., 1967) a procedure which is not accurate since it is easy to detect the absence of high frequency vertical fields but the presence of lower frequency vertical fields may be overlooked by this procedure. If a station is chosen as a reference location, its fields are subtracted from the observed fields

at the remaining locations and (2.7) may then be solved for T at all except the reference station.

That this assumption is suspect is obvious from the above discussion of the selection criterion for a normal station. This criterion also ignores variations in the horizontal fields which may be indicative of different horizontal layering beneath stations. The use of the reference station technique in regions of complex geology such as British Columbia is discussed by Cochrane and Hyndman (1970) who conclude that for analysis of geomagnetic data in this region, no suitable reference station exists. They suggest that the best approach is to use data from a single station to calculate z_D and z_H from (2.6). The z_D and z_H so derived may be directly compared with model results as could the z_D and and z_H calculated from the reference station approach.

The use of data from a single station in essence assumes that $H_N = H_0$, $D_N = D_0$ and $Z = Z_a$, which reduces (2.7) to

$$Z_a = z_D D + z_H H \tag{2.8}$$

This form also implicitly assumes that there is no long term correlation between Z_N and either of the horizontal components H_N and D_N. Everett and Hyndman (1967) and Schmucker (1964) derive the following solution of (2.8) for z_D and z_H from the auto and cross spectral relationships S(DD), S(HH), S(HD) etc.

$$z_D = \frac{S(HH)\ S(DZ) - S(HD)^*\ S(HZ)}{S(DD)\ S(HH) - |S(HD)|^2} \tag{2.9}$$

$$z_H = \frac{S(DD)\ S(HZ) - S(HD)^{*}S(DZ)}{S(DD)\ S(HH) - |S(HD)|^2} \qquad (2.9)$$

The computed parameters, z_H and z_D, are known as the single station transfer functions. These may be interpreted directly, combined to give the single station induction arrow (Appendices 2, 1) or combined to provide an induction ellipse (Appendix 3).

Up to this point the analysis technique has followed the procedures outlined by Schmucker (1964) and Everett and Hyndman (1967). The computation of the induction ellipse is given, but a passing reference by these authors indicates that in regions of complicated structure the ellipse may be a better indicator than the induction arrow of the complexity of the induced fields. This suggestion merits further consideration.

For a simple two dimensional conductor the in phase part of the transfer function will be perpendicular to the induced current flow. For this simple case the Parkinson arrow and the transfer function provide the same information since the out of phase part is zero. For more complicated situations the out of phase part is non-zero indicating secondary coupling and the in phase part is the resultant of several in phase vectors each due to a different conductor. The direction of the in phase part is no longer perpendicular to the induced current flow (Appendix 2, 3). This indeterminancy can be partially resolved by using the induction ellipse. (Everett and Hyndman, 1967).

The induction ellipse is a technique for resolving the induction arrows, both real and imaginary, on to a set of mutually perpendicular axes. The orientation of the major axis represents the direction of the total horizontal field associated with the equivalent conductor. The

induction ellipse may be derived from (2.9) as shown in Appendix 3. Use of the induction ellipse enables the interpreter to deduce the complexity of the situation by comparing the ratio of the major to minor axis. Computation of the ellipse incorporates all information from the induction arrows into a simple form which resolves the in phase and out of phase resultants into two mutually perpendicular ellipse axes each having in phase and out of phase information.

The induction ellipse technique is especially powerful in the case of two mutually perpendicular or nearly perpendicular conductors for which the response of one is marginally greater than the response of the second i.e. the major to minor axis ratio is about 2 or 3. In such a case the direction of the major axis of the ellipse will be perpendicular to the the major conductor. The magnitude of the minor axis will provide essential information about the second conductor which would have been masked if the induction arrow alone had been used (a specific example is presented in Appendix 3). It is obvious that if many conductors of varying orientation and approximately equal strength are present even the induction ellipse technique will not help in determining the contributions to the resultant induction arrow from each conductor.

Geological information suggests that two major conducting directions should be present. The coast and its associated tectonics appear to be intersected by the volcanics (Souther, 1970). Thus ellipse analysis was used to try and resolve the relative contributions from the two conducting directions. It is the author's opinion that in a complex geological situation such as the one being analysed in this study, the ellipse analysis is an invaluable tool in resolving the major and secondary effects.

The second feature of the analysis which the author feels tends

to be overlooked is the importance of the out of phase part of the transfer functions and the ellipses. The out of phase part is related to coupling between conductors. Consideration of this part may be useful in regions of complicated structure for interpreting deep conductors.

The phase responses of the transfer functions and induction ellipses are poorly understood parameters. It has usually been considered sufficient to match the in phase component observed to the in phase component calculated for models and essentially ignore the matching of out of phase components. In analysis of transfer functions the out of phase part has not been used to be diagnostic of any structure. The reasoning behind such an approach is difficult to understand. For a simple conductor embedded in a uniform medium having a large conductivity contrast with the conductor, the calculated out of phase part is small but for any deviation from this situation the out of phase part may be significant. It appears from model studies that significant changes in the out of phase component may be more diagnostic of transitions in conductive structure than the in phase for conductors buried beneath a conductive overburden.

In physical terms the in phase component represents the sum of the magnetic coupling effects due to the induced currents in the anomalous structures. The out of phase component then represents the effect of secondary magnetic fields produced by the induced current in the first structure coupling with the second structure to induce a secondary current in the second conductor which is out of phase with the primary induced current. The reverse situation is also true since the primary induced current in the second structure will couple with the first structure to produce a secondary induced current in it which is out of phase with the primary induced current. Thus magnetic fields

which have in phase and out of phase parts may be experienced by an observer sitting above these locations. This argument may be illustrated by recourse to simple electrical circuit theory. The in phase part represents the current through the resistive part of the impedance while the out of phase represents the inductive impedance which may include inductive coupling with adjacent circuits. In the analogy here the voltage across the resistor plus the self-inductance of the inductor would be the in phase part even though this contains a phase angle and the voltage across the mutual inductance part would be the out of phase part. But it is impossible to measure the out of phase mutual inductance part directly. Circuit theory predicts that the mutual inductance

$$M = k\sqrt{L_1 L_2}$$

where L_1 and L_2 are the self inductances in the respective circuits, and $k \leq 1$ (Winch, 1963). Thus the coupling ratio of the out of phase part to the in phase part at a given location is given by

$$CR = \frac{kL_1\kappa(r_1) + kL_1\kappa(r_2)}{\kappa(r_1)L_1 + \kappa(r_2)L_1} = \frac{kL_1[\kappa(r_1) + \kappa(r_2)]}{L_1[\kappa(r_1) + \kappa(r_2)]} = k$$

where $\kappa(r)$ is function of distance from conductor and geometry of conductor and k is a complicated function of the geometry of the conductors. Since $k \leq 1$, the phase angle is constrained to be less than 45^0 for simple cases of two conductor coupling. The magnitude of the phase angle then is indicative of the degree of coupling between conductors which is a measure of the complexity of the situation. In regions where the coupling is occurring k may be larger in magnitude indicating more complicated

structure in this region.

In a situation where the magnitude of the response is controlled mainly by one or two major near surface high conductivity structures, overlying a complex subsurface structure, the in phase part may show a monotonically decreasing response while the phase angle will show abrupt changes in coupling in this region. In essence then the in phase part shows the resistive response while the out of phase part shows the inductive response between the layers and structures.

CHAPTER 3

DATA PRESENTATION AND VISUAL INTERPRETATION

3.1 Data

The present data employed for analysis of geomagnetic variations near the west coast of Canada emanates from three sources. The primary data were gathered from temporary geomagnetic observatories erected during May and operative until July 1971 at Tasu, Sandspit, Bella Bella, Tatla Lake, and Cache Creek in British Columbia (Fig. 1.1, Table 3.1). The secondary data were the single station transfer functions of Cochrane and Hyndman (1970) for southern British Columbia and Dragert (1973) for north central British Columbia.

All data were analysed in the single station transfer function format; the Cochrane and Hyndman (1970) data and the data from the new locations were also analysed using the induction ellipse technique.

3.2 Instrumentation

The systems for recording the primary data will now be discussed. The system at the major stations of Tasu, Sandspit, Bella Bella, and Cache Creek was the Askania Variograph. This instrument records three component temperature compensated magnetic traces plus a base line and temperature record on photographic paper. The chart advance speed of 20 mm/hr. permitted unattended operation for a period of three weeks. The major problem in previous surveys using Askania systems were frequency fluctuations in the local power supply and loss of record due to power failures. To eliminate these problems the systems were designed

TABLE 3.1

STATION LOCATIONS

Station	Latitude	Longitude	Geomagnetic Latitude
Tasu	$52^0 46'$ N	$132^0 3'$ W	$59^0 16'$
Sandspit	$53^0 15'$ N	$131^0 50'$ W	$59^0 8'$
Bella Bella	$52^0 9'$ N	$128^0 13'$ W	$58^0 39'$
Tatla Lake	$51^0 53'$ N	$124^0 19'$ W	$58^0 56'$
Cache Creek	$50^0 48'$ N	$121^0 40'$ W	$58^0 15'$

TABLE 3.2

CALIBRATION CONSTANTS FOR ASKANIA SYSTEMS

Location	Instrument	constant γ/mm D	Z	H	std. error γ/mm D	Z	H
Tasu	75	2.47	2.88	3.51	.007	.004	.004
Sandspit	77	2.48	3.13	2.67	.005	.003	.001
Bella Bella	76	2.66	3.02	3.31	.006	.004	.008
Cache Creek	78	2.58	3.12	2.90	.006	.003	.008
Tatla	Fluxgate	1.97	3.94	3.94	?	?	?

by Dr. Caner to be floating with respect to the local power supply (Fig. 3.1). In the event of a power failure the system could operate by battery power for 36 hours.

Since fluctuations in the local power supply frequency cause variations in the chart advance speed, the chart drive system was driven by a precision 60 Hz output from Sprengnether chronometers. Time fiducial marks for the records were obtained from the Sprengnether chronometers coupled to the timing circuit in the Askania control systems. Using this arrangement hourly time marks were recorded, these time marks being accurate to ±15 seconds since the chronometers were periodically checked against WWVB standard time broadcasts.

At Tatla Lake the magnetic variations were detected using a three component fluxgate magnetometer and recorded on chart paper using a Texas Instrument chart recorder. The timing and drive systems were similar to the systems used for the Askania instruments.

The Askania systems have calibration circuits for each component built into the control system. By means of this circuit a precisely controlled current produced a deflection on the record. Using the manufacturer's specifications for the calibration coil, a sensitivity for each trace was determined. By repeating the calibration procedure at least twice on each film, a large number of calibrations were obtained for a particular trace. The mean and standard error of estimate of the sensitivity were calculated for each component and each instrument (Table 3.2).

The Tatla Lake fluxgate system did not have a calibration circuit built in the control system. The attenuator settings on the chart recorder were noted only as the equipment was being dismantled. By

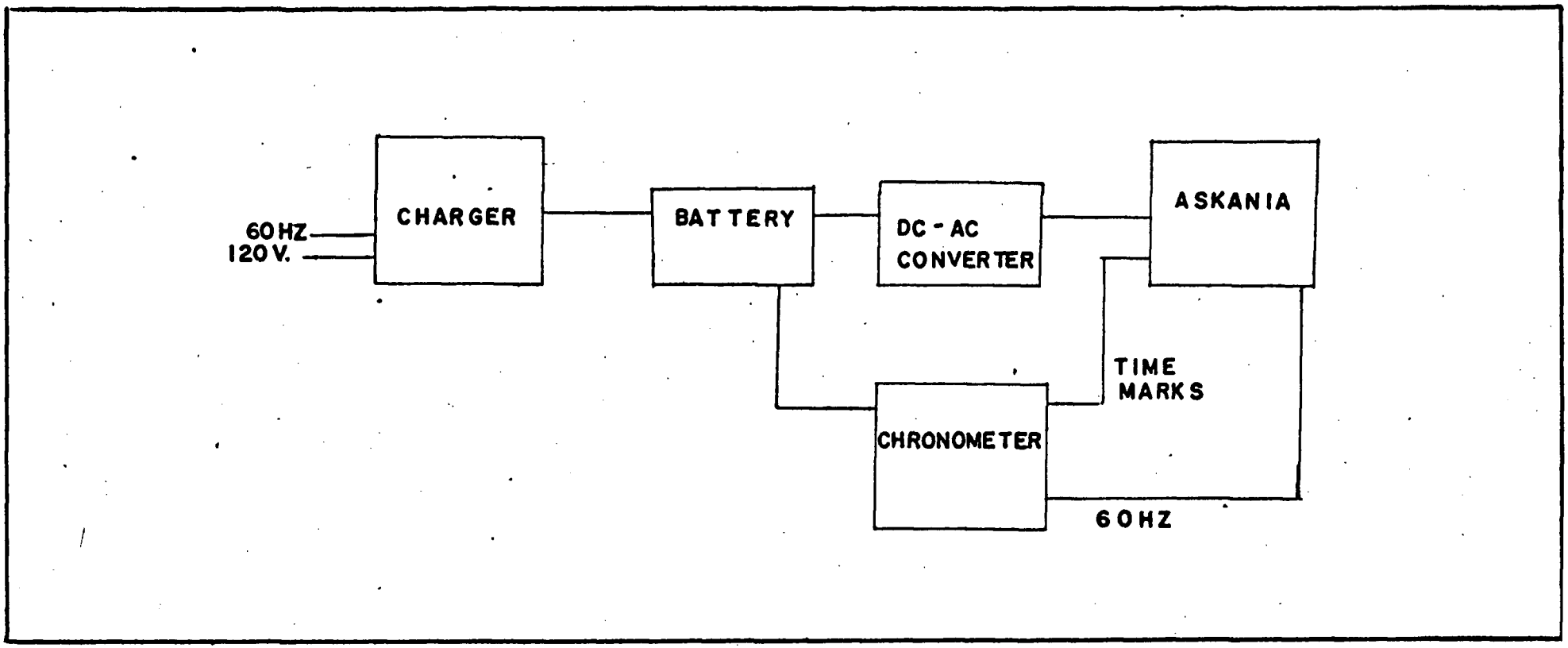

Fig. 3.1 Recording system block diagram illustrating the use of the floating system to provide independent operation in the event of a local power failure.

comparing the H and D components recorded at Tatla Lake and those recorded at Victoria Magnetic Observatory for the same events, it was possible to obtain an estimate of the sensitivities for the various components. These estimates were confirmed through discussion with Mr. D. Auld about the usual sensitivity settings of this equipment. It should be noted that any variation in the sensitivity would be by a factor of two which would readily be apparent on comparison of the Tatla Lake and Victoria records. Thus the sensitivities given (Table 3.2) for the fluxgate are considered accurate to a few percent.

3.3 Data Selection

The field systems recorded several geomagnetically disturbed periods of varying intensity. Of these periods the following four, recorded simultaneously at all stations, were selected for detailed analysis:

(1) 2100 UT May 29 to 1900 UT May 30

(2) 1200 UT June 1 to 1000 UT June 2

(3) 1200 UT June 2 to 1000 UT June 3

(4) 0200 UT June 6 to 0000 UT June 7

The records of the disturbed period May 29 to June 3 contained sections of record where there were severe problems in following the trace of a given component due to repeated crossing of other traces and therefore these record sections could not be digitized. Several other periods of activity were not recorded at all stations due to equipment problems. To ensure that all stations were affected by uniform source fields having the same orientations only simultaneous records were analysed. By

means of model studies it was found that the orientation of the source can seriously affect the geomagnetic variations, hence by using the same sections of records for all stations, the scatter in the transfer functions can at least be ascribed to the same events.

The data analysed for the other locations came from Cochrane and Hyndman (1970) and Dragert (1973).

3.4 Interpretation

A) Amplitude Ratios These ratios show the enhancement of the vertical component and the total horizontal field relative to the respective components at Cache Creek (Fig. 3.2). No attempt is made to calculate the error bars for these amplitude ratios as they are used solely as indicators of possible induced current concentration.

The weighted average spectral energies for each magnetic component were determined at each location using the techniques of Appendix 1. These spectral energies may be used to define the vertical amplitude ratio and the horizontal amplitude ratio as follows.

Let VA(J) be the vertical amplitude at a station at period J.

$$\text{Then } VA(J) = \sqrt{\frac{\overline{S(ZZ(J))}_{\text{station}}}{\overline{S(ZZ(J))}_{\text{cache}}}}$$

where $\overline{S(ZZ(J))}_{\text{station}}$ is the total weighted spectral energy in the vertical component at the station

$\overline{S(ZZ(J))}_{\text{cache}}$ is the total weighted spectral energy in the vertical component at Cache Creek.

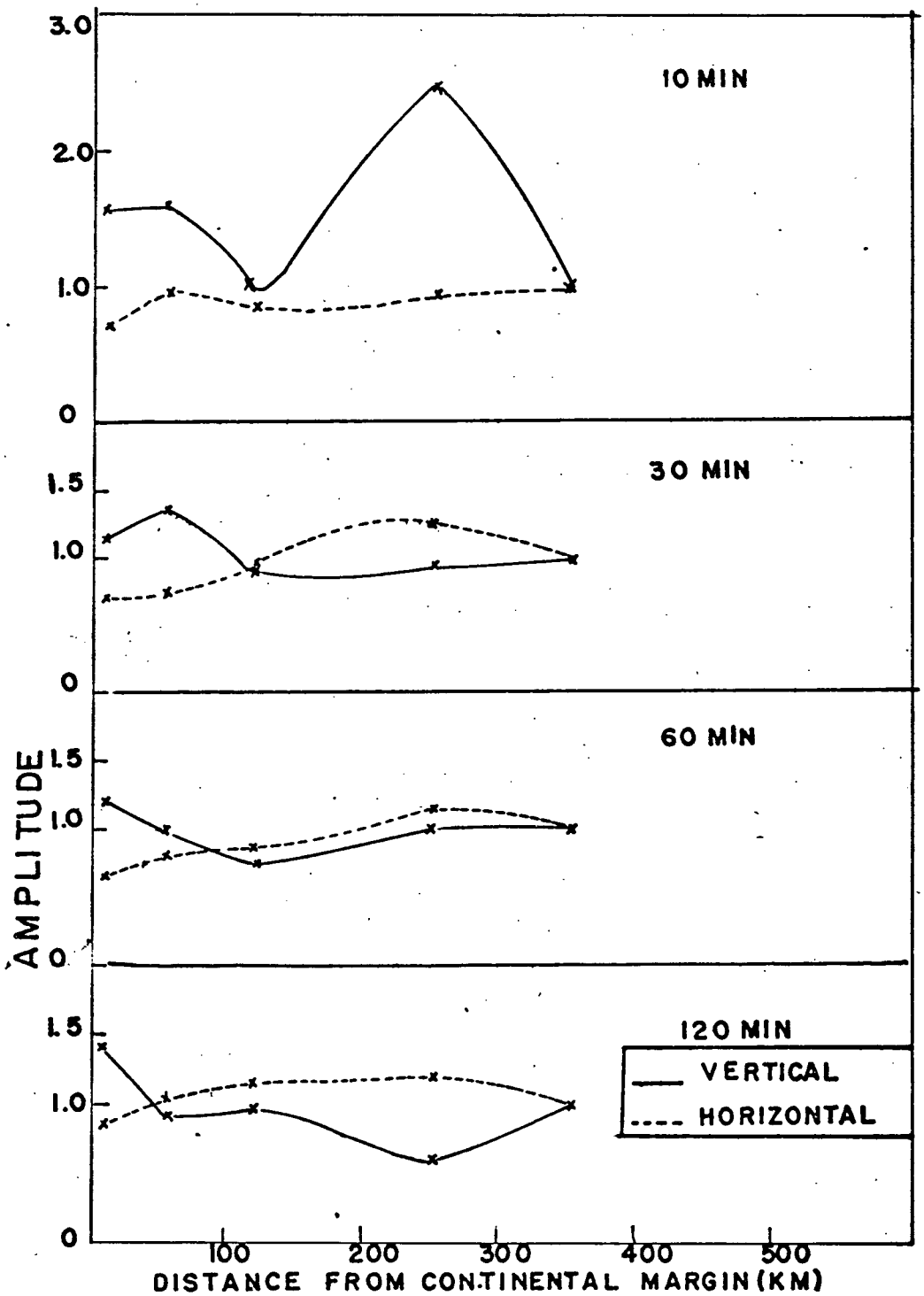

Fig. 3.2 Vertical amplitude ratios and horizontal amplitude ratios for all stations on new profile. Amplitude ratios are measured relative to Cache Creek.

Similarly one can define the horizontal amplitude ratio at a station for period J as HA(J)

where $$HA(J) = \sqrt{\frac{\overline{S(DD(J))} + \overline{S(HH(J)}_{station}}{\overline{S(DD(J))} + \overline{S(HH(J))}_{cache}}}$$

$S(DD(J)) + S(HH(J))_{station}$ is the total weighted spectral energy in the total horizontal field at frequency J for the station

$S(DD(J)) + S(HH(J))_{cache}$ is the total weighted spectral energy in the total horizontal field at frequency J for Cache Creek.

The curves of Figure 3.2 show that there is considerable variation in the vertical amplitude ratio at 10 minutes period. The large peak at Tatla Lake and the smaller peaks at Tasu and Sandspit indicate a larger local near surface current distribution near Tatla Lake. A smaller induced current is found beneath Tasu and Sandspit.

At longer periods the Tatla Lake vertical component maximum disappears but the one related to Tasu and Sandspit appears at all periods indicating that a major discontinuity in conductivity is found near Tasu. This conductivity contrast has considerable depth extent since even the longest period of 120 minutes is affected (Table 3.3).

The horizontal amplitude ratios exhibit less variation both with location and period than the vertical ratios. The spatial variations in the horizontal field are less than 25% which may appear large, however model studies have shown this variation is not unexpected in regions of complex structure.

The amplitude ratios indicate then that the coast and possibly

TABLE 3.3

Variation of skin depth with conductivity and period

conductivity σ (ohm m^{-1})	period T (min.)	skin depth L (km.)
1.0	120	30.1
	60	21.3
	30	15.1
	10	8.7
.1	120	95.5
	60	67.5
	30	47.7
	10	27.5
.01	120	302
	60	213
	30	151
	10	87.2
.001	120	955
	60	675
	30	477
	10	276
ocean .28	120	57.0
	60	40.3
	30	28.5
	10	16.5
land .027	120	180
	60	127
	30	90
	10	52

its associated structures influence the observed vertical and horizontal magnetic fields. Local discontinuities in conductivity near Tatla Lake may also be the sites of induced currents.

B) I Ratios The I ratios are presented here to show how the induced current locations may be quickly deduced from the power spectra of the data and to tie this study together with the work of Lambert and Caner (1965) on the coast effect. No error bars are presented for these ratios since no comparison is made between these and model results.

Lambert and Caner (1965) and Caner and Cannon (1965) have presented the I ratio as a quantity which may be measured directly from records and used to locate recording sites for close analysis of an anomalous region. The values of the I ratio calculated by these authors have been based upon events having periods from 5 to 20 minutes. Only average values of the I ratio for a number of events have been calculated by them so no frequency dependence has been examined. The I ratios are calculated in this study from the total weighted spectral energies (Appendix 1 and 4).

The previous workers divided British Columbia into two parts: a high I region east of the Rocky Mountains and a low I region to the west. The low I region was typified by I values less than 0.3 for periods between 5 and 20 minutes. The I ratio for the present study (Fig. 3.3) only approach this value of 0.3 for 10 minutes period at Tatla Lake and Cache Creek. Toward the coast the I ratios increase for 10 minutes period. This is expected since the zone of induced currents is being approached as shown by the increase in the Z component in the amplitude ratios. Lambert and Caner (1965) had classified Tofino (Fig. 1.1) as an anomalous

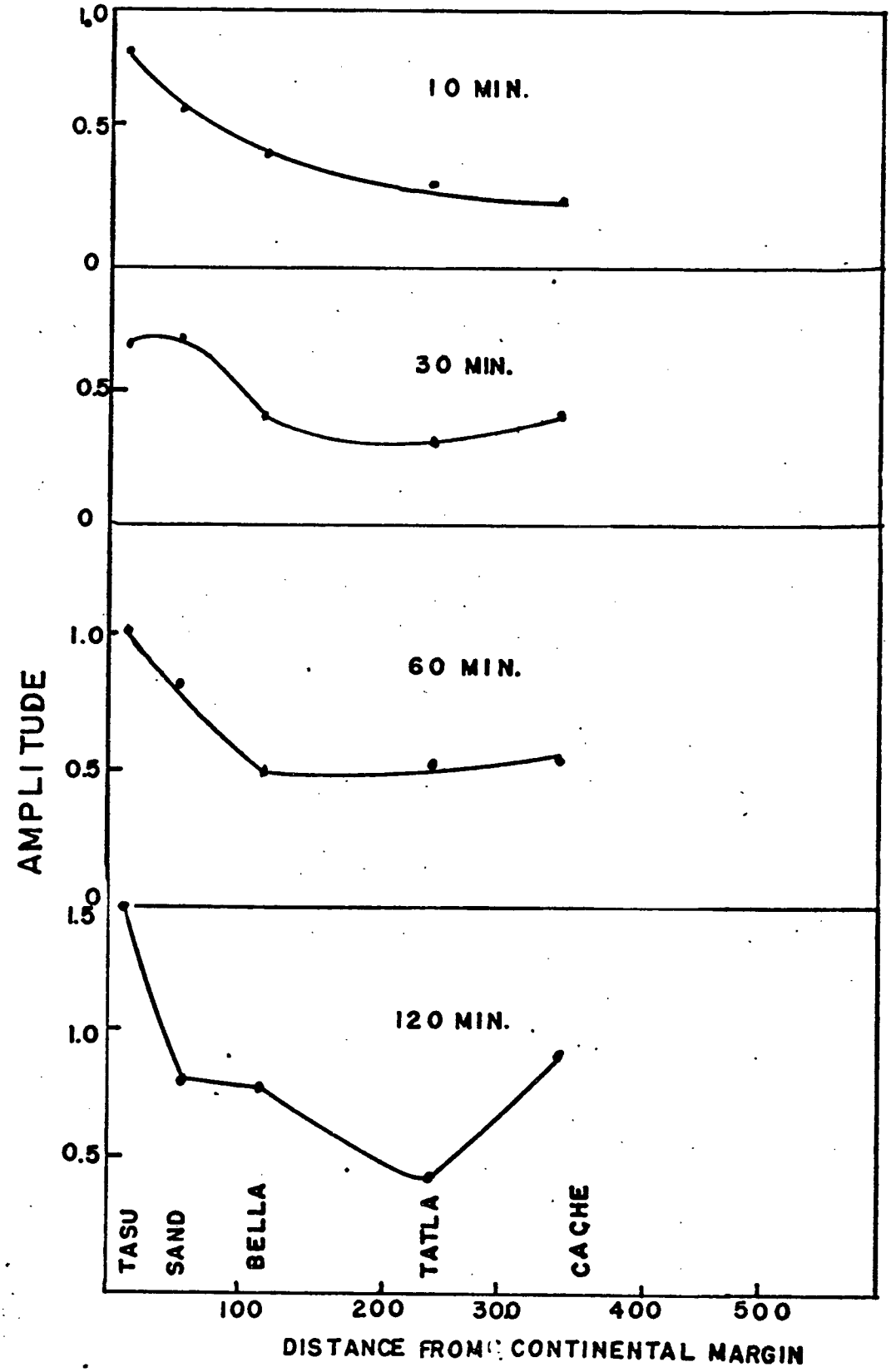

Fig. 3.3 I-ratios as functions of distance from continental margin for periods of 10, 30, 60, and 120 min.

station since its I ratio was higher than those for the rest of western British Columbia but classify the other stations on the southern profile as low I locations.

At longer periods the I ratios still indicate that the major induced current concentration occurs at the coast since the largest I ratios are calculated for locations near the coast. The I ratio increases at Cache Creek indicating that Cache Creek is not a normal low I location. This normal classification was based upon the I ratios calculated by Cannon (1967) for events in the 5 - 20 minute period range. The higher I ratios for Cache Creek at longer periods indicate that the feature controlling the induced currents in the region of Cache Creek is deeply buried.

The I ratios have added another induced current to the induced current flow at the continental margin deduced from the amplitude ratios. This second induced current influences the geomagnetic variations in the region of Cache Creek. No azimuth or phase information may be deduced from the data presented as I ratios and amplitude ratios, hence the strikes of the conductors may not be deduced.

C) Transfer Functions The phase and azimuth information which cannot be obtained from the I ratios and amplitude ratios, is an essential part of the single station transfer function information. The single station transfer functions were calculated as functions of period at each location on the new profile. The magnitude vs. period responses are illustrated in Fig. 3.4 to 3.8 and the azimuth vs. period responses are shown in Fig. 3.9. Error bars have been calculated for the magnitudes, as outlined in Appendix 2.

The size of the error bars increases, in general, as the con-

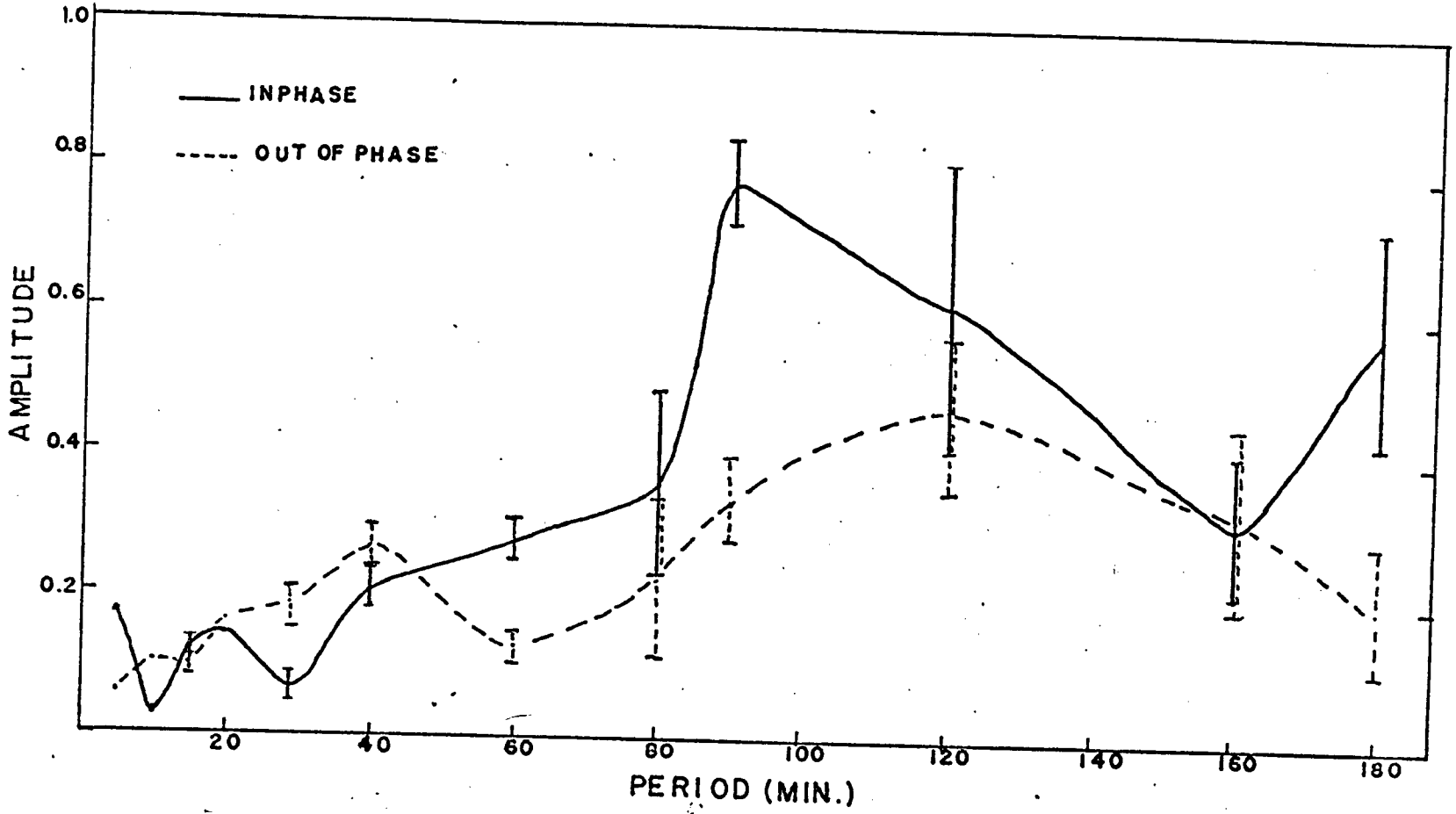

Fig. 3.4 Induction arrow magnitude vs. frequency response for Cache Creek. Error bars are standard errors of estimate.

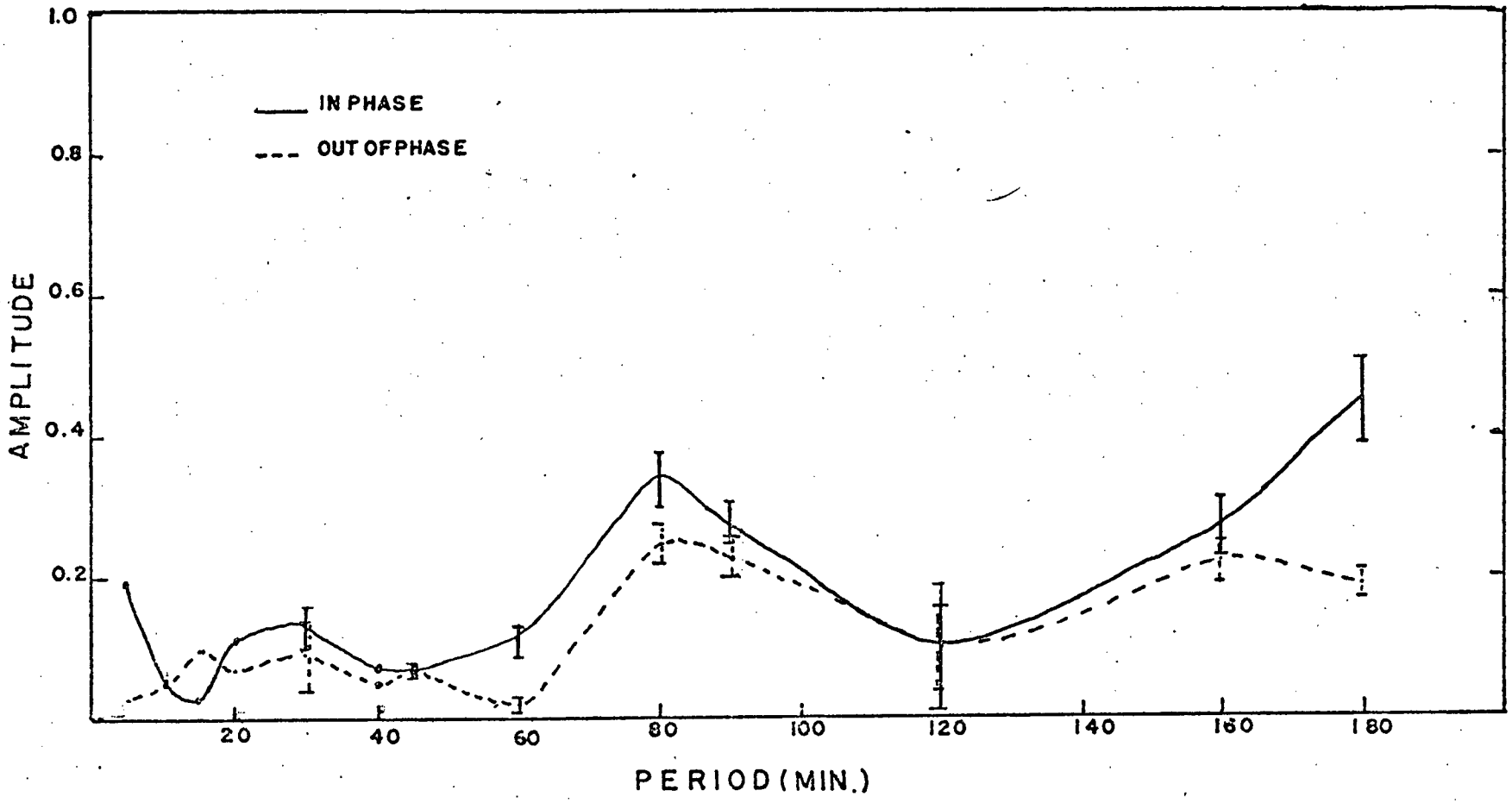

Fig. 3.5 Induction arrow magnitude vs. frequency response for Tatla Lake. Error bars are standard errors of estimate.

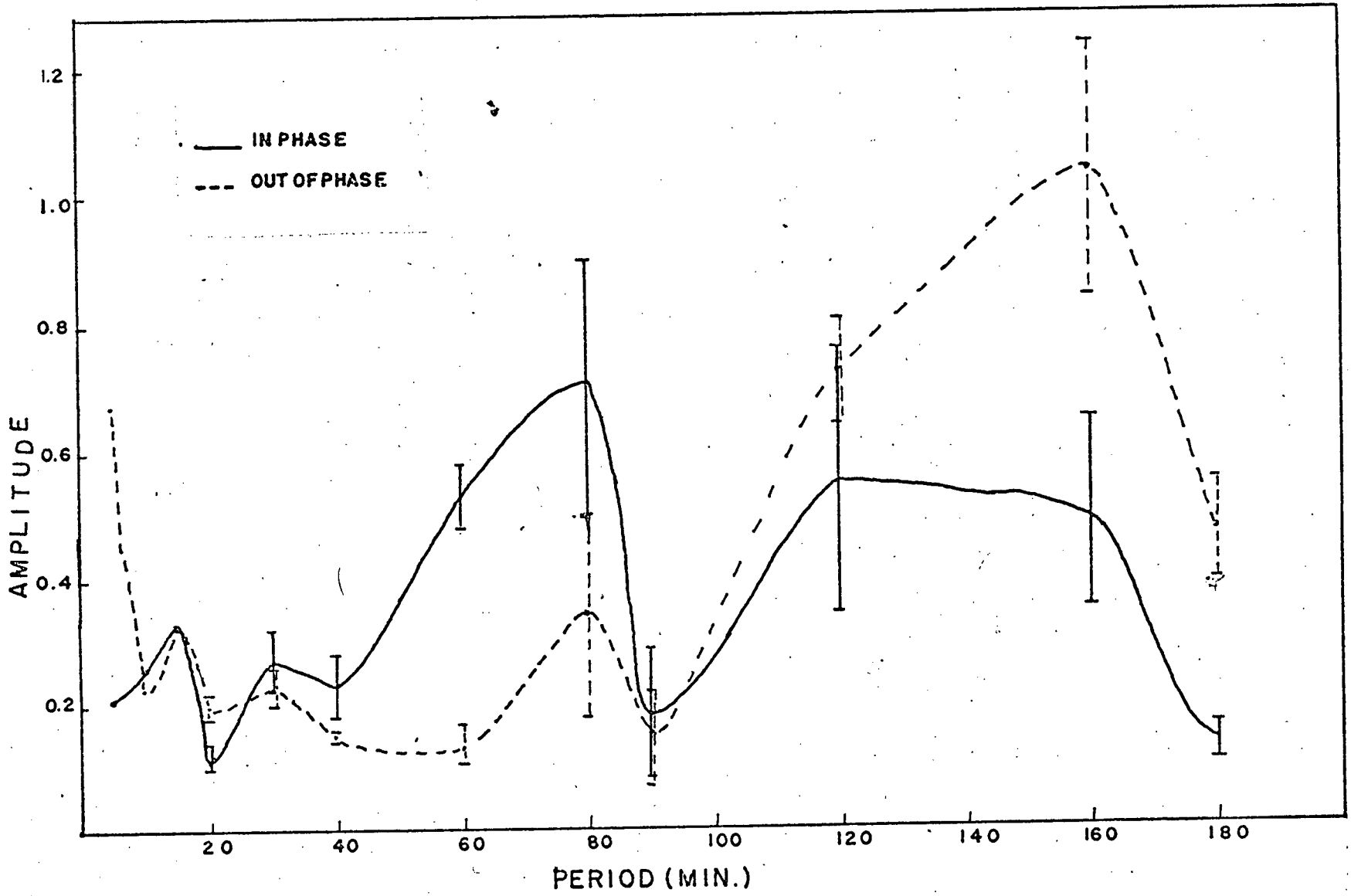

Fig 3.6 Induction arrow magnitude vs. frequency response at Bella Bella. Error bars are standard errors of estimate.

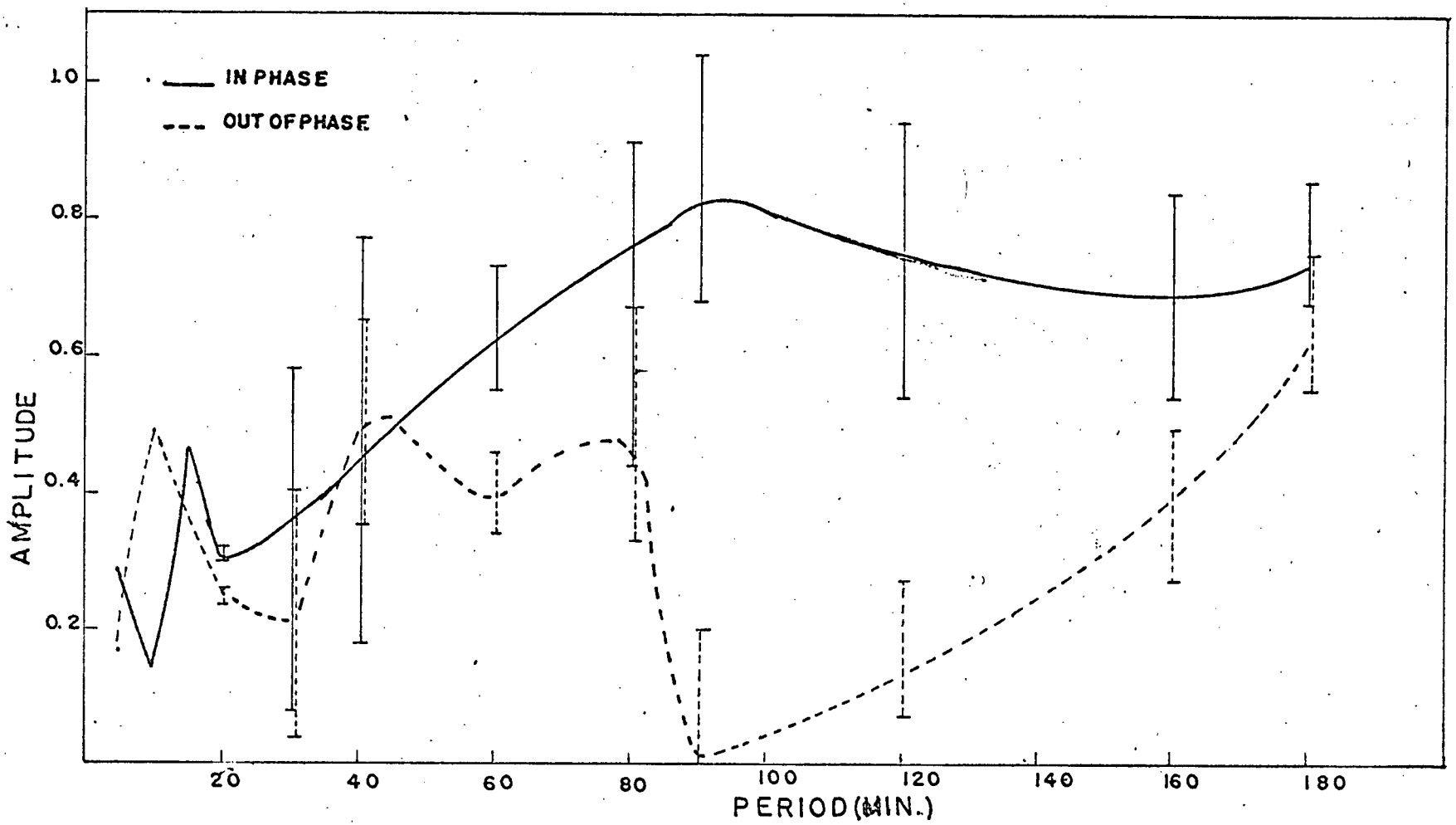

Fig. 3.7 Induction arrow magnitude vs. frequency response at Sandspit. Error bars are standard errors of estimate.

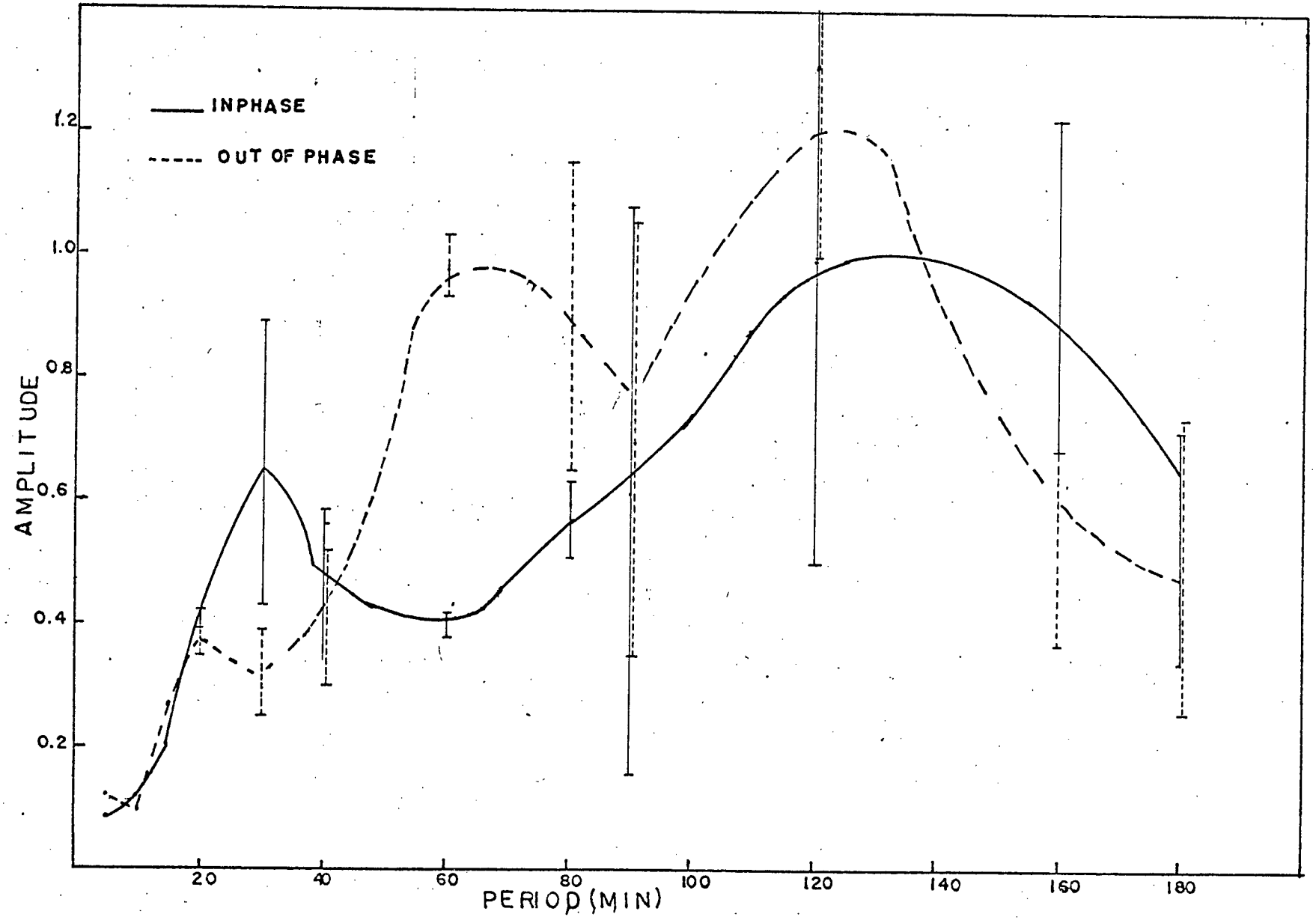

Fig. 3.8 Induction arrow magnitude vs. frequency at Tasu. Error bars are standard errors of estimate.

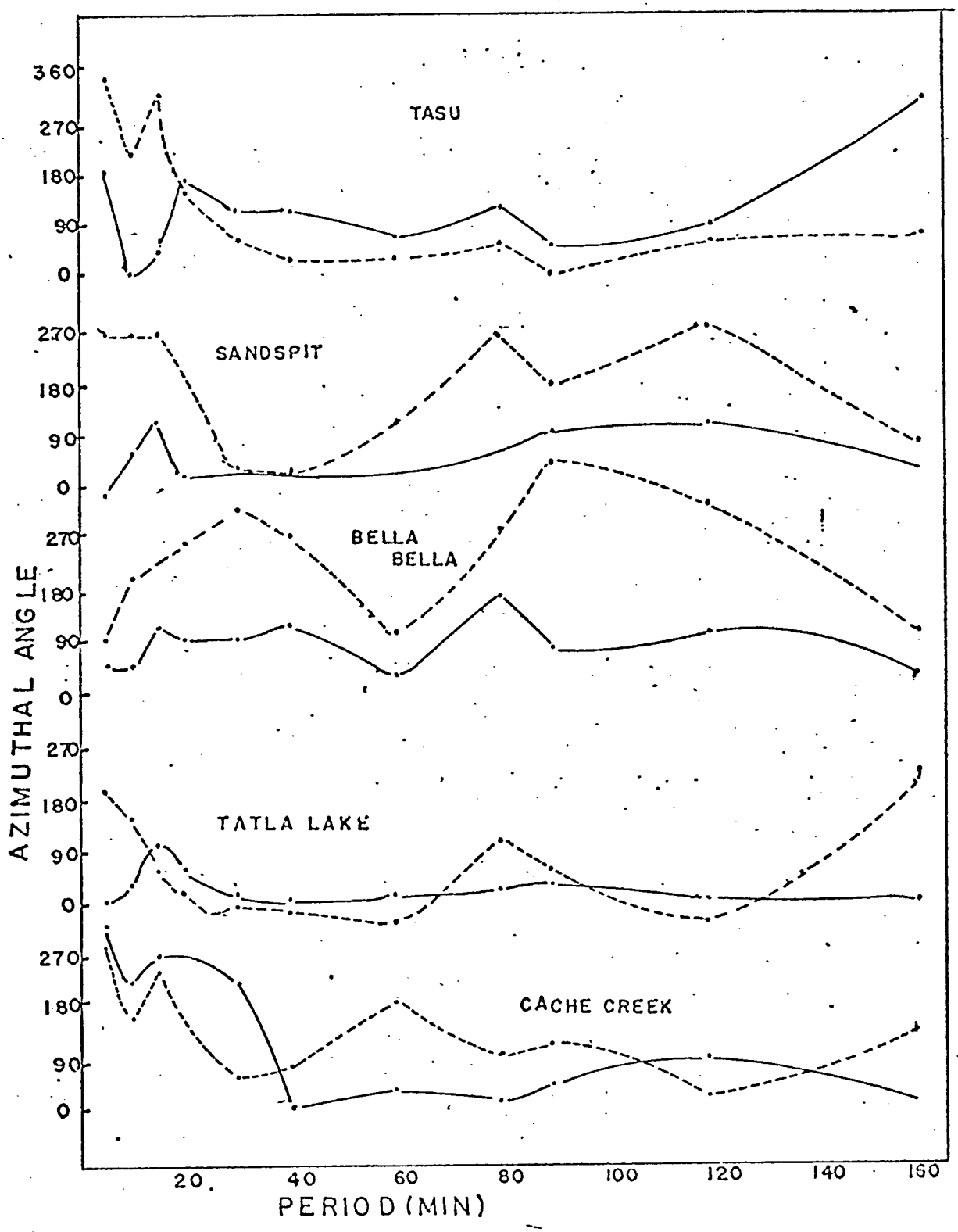

Fig. 3.9 Azimuthal angle direction of in phase and out of phase induction arrows. Directions measured in degrees east of magnetic north.

tinental margin is approached (Fig. 3.4 to 3.8). The reason for this increase, as deduced by the candidate from analog model studies, is the differing induction effects by sources of dissimilar orientation in a set of conductors which intersect one another. The experimental evidence for this is presented in the next chapter in the section dealing with the analog model results. In essence the presence of two almost orthognal conductors means that at the intersection, the two induced currents can flow either north-south or east-west. The stronger conductor is the coast and its parallel subsurface structure, hence for source fields parallel to this a larger magnitude transfer function is found than for source fields perpendicular to the coast.

The curves (Fig. 3.4 to 3.8) even with the large error bars do show significant trends which are caused by the presence of conductors in which the induced currents flow. The trend is well established at all stations and in general increases as the period increases. Thus the models which may be used to achieve a match of these curves should reproduce the general pattern of observations but not necessarily the particular values.

The magnitude response curves (Fig. 3.4 to 3.8) for the transfer functions show that all locations are influenced by several conductors since all the magnitude response curves have several maxima. The magnitude responses at short periods, less than 30 minutes period, are due to conductivity anomalies in the crust while the longer period responses originate in the upper mantle. The effect of the coast and its associated structures appears to be a maximum in the 40-90 minute range. This interpretation is supported by the azimuthal dependence of the induction arrow (Fig. 3.9). At periods

below 30 minutes there is considerable variation in the direction showing that no preferred induction direction controls all the induction arrows. At the intermediate period, however, the arrows all swing around to point toward the coast. For the long periods, the arrows show considerable azimuthal fluctuation again indicating the presence of deep conductors. An examination of the amplitude and azimuthal response at each station shows the orientation and depth of the conductors influencing that station.

i) Cache Creek (CACH) The magnitude vs. period response (Fig. 3.4) has two distinct maxima in the in phase component, with a trend toward a third. The small maximum at 20 minute period points to a conductor to the east of the station (Fig. 3.8). The large maximum at 80 minutes period points to the southwest indicating it may be associated with the coast effect or the general tectonic trend, however the magnitude, approximately 0.82 is large for a location far from the coast. Thus this maximum may be more readily envisaged in terms of a change from one structural province to another, the two structural provinces causing a discontinuity in some conductor at depth. The discontinuity is required to explain the de-coupling of the out of phase and in phase components.

ii) Tatla Lake (TATL) The magnitude response at Tatla Lake (Fig. 3.5) is much smaller at 80 - 120 minutes than at Cache Creek. This indicates that Tatla Lake is little influenced by this conductor which lies to the southwest of the station. Since the magnitude, approximately 0.4, is about one-half the magnitude at Cache Creek for the same period and the azimuthal direction (Fig. 3.9) is approximately the same for both

stations, it is unlikely that the same conductor controls the magnitude response at both locations. The simplest explanation for the combined Cache Creek and Tatla Lake data is that two parallel conductors control the magnitude response at these locations. Tatla Lake is located between the two conductors while Cache Creek is located to the east of both of them. These conductors have the general strike of the coast and of the structural provinces, so the proposal made for explaining the Cache Creek magnitude, namely a current flow associated with a structural boundary is given more support.

At short periods, there is a small maximum at 30 minute period and another at 5 minutes. The 30 minutes maximum has a similar azimuth to the 90 minute maximum indicating that it is caused by a conductor parallel to the coast. The out of phase component does not deviate from its general trend of paralleling the in phase component. Thus except at 5 minutes there is little evidence for a change in the coupling between structures, hence it appears no discontinuities exist in the vicinity of Tatla Lake.

iii) Bella Bella (BELL) The magnitude of the transfer function at Bella Bella (Fig. 3.6) exhibits a completely different character than that at either of the previous two stations. There are four maxima in the in phase component, three of these are distinct maxima with only the one at 30 minutes being questionable. The out of phase component does not simply parallel the in phase component, thus significant changes in coupling between structures muct occur in the proximity of the station. The azimuthal dependence (Fig. 3.9) shows the coupling changes even more emphatically. For periods less than 10 minutes the in phase vector points to the southwest then swings to the west for periods between 15 and 40

minutes and basically to the north west for periods greater than 60 minutes except for a drastic change at 80 minutes to point almost due north. It is difficult to interpret these variations in the orientation of the in phase component in terms of any one structure or direction. The most plausible explanation is that Bella Bella is influenced by two conductors: the coast and its associated structural trend striking northwest-southeast and the Souther (1970) volcanic zone striking east-west to the north of the station. Such a configuration could explain the observed variations in magnitude and direction. The direction has swung around to the south indicating the major conductor lies to the north of the station. At longer periods the in-phase vector points to a conductor to the northwest again. The out-of-phase azimuthal component does not move in harmony with the in-phase azimuthal component indicating that the inductive coupling is occurring between non-parallel structures. At periods greater than 80 minutes the out-of-phase component dominates indicating that there is large coupling between structures. The in-phase and out-of-phase induction arrows for Bella Bella are perpendicular to neither the coast nor the Souther (1970) east-west volcanic zone which means that at this location the observed transfer functions are complicated functions resulting from several structures.

iv) Sandspit Sandspit has fairly simple magnitude (Fig. 3.7) and azimuthal (Fig. 3.9) response. The magnitude is generally higher for the in phase component than for the preceding locations indicating proximity to the major conduction zone. The significant decrease in the out of phase component at 90 minutes period indicates that for long periods Sandspit essentially "sees" a single conductor. Since the

out of phase part increases again at periods greater than 160 minutes some very deep structure may be involved. The error bars are larger here than for the inland stations, showing the strong dependence upon source direction which occurs at locations near the major conducting bodies. In general, the azimuthal dependence at Sandspit is slowly varying. At short periods it indicates currents in the surrounding water and structure; at periods between 30 and 80 minutes it is perpendicular to the continental margin, and swings around to a more easterly direction at longer periods. It is at these longer periods that the out of phase part decreases in magnitude and from the azimuthal response of the out of phase part it can be seen that its direction significantly changes. The azimuthal responses indicate that the deep conductor is not perfectly parallel to the continental margin.

y) Tasu The magnitude response at Tasu is the most complicated and most highly varying of all locations. The larger error bars indicate that no one structure is controlling the induction process at this location. Model studies have shown that a pattern of variation in the magnitude response exhibited here may be caused by differing source orientations inducing currents in two orthogonal conductors (Chapter 4). A peak in the in-phase response occurs at 30 or 40 minutes period, this appears to be associated with the coast effect or the Queen Charlotte Fault. At shorter periods the response decreases indicating the presence of a highly conducting near surface body which damps the effect of induction at the land-sea boundary. The most significant feature at Tasu is the large out of phase component indicating that considerable coupling between structures occurs in the vicinity of this station. Since

such coupling is not found at Sandspit on the other side of the Queen Charlotte Islands it must be concluded that the structure or structures involved are close to Tasu or that the distance between the high conductivity layers changes significantly across the Queen Charlotte Islands. The azimuthal response at Tasu also shows considerable variation. At periods less than 20 minutes it varies considerably, then at periods between 20 and 40 minutes it points southeast for the in-phase part. This would indicate the in-phase part at these periods is controlled by an east-west conductor. At longer periods it swings to the northeast indicating that the coast and associated structures are the dominant features. The out-of-phase part shows a similar response for the periods greater than 60 minutes indicating that the coupling exhibited by the magnitude of the out-of-phase component is due to structures associated with the general structural trend, since it is perpendicular to the trend.

D) Induction Arrows The features noted in the above discussion may be quite easily seen on the geographic plots (Fig. 3.10 to 3.13) for the induction arrows and on similar plots (Fig. 3.14 to 3.17) for the induction ellipses. On these diagrams the direction of the in phase component is 180^0 different than the direction shown in Fig. 3.9. This manner of presentation of the in phase component is also used with the major axis of the induction ellipses. By using this convention the induction arrows and ellipse major axes point toward the zone of high conductivity in agreement with the Parkinson arrows. Included on these diagrams for the induction arrows (Fig 3.10 to 3.13) are the Dragert (1973) and Cochrane and Hyndman (1970) data; on the induction ellipse diagrams the calculated induction ellipses

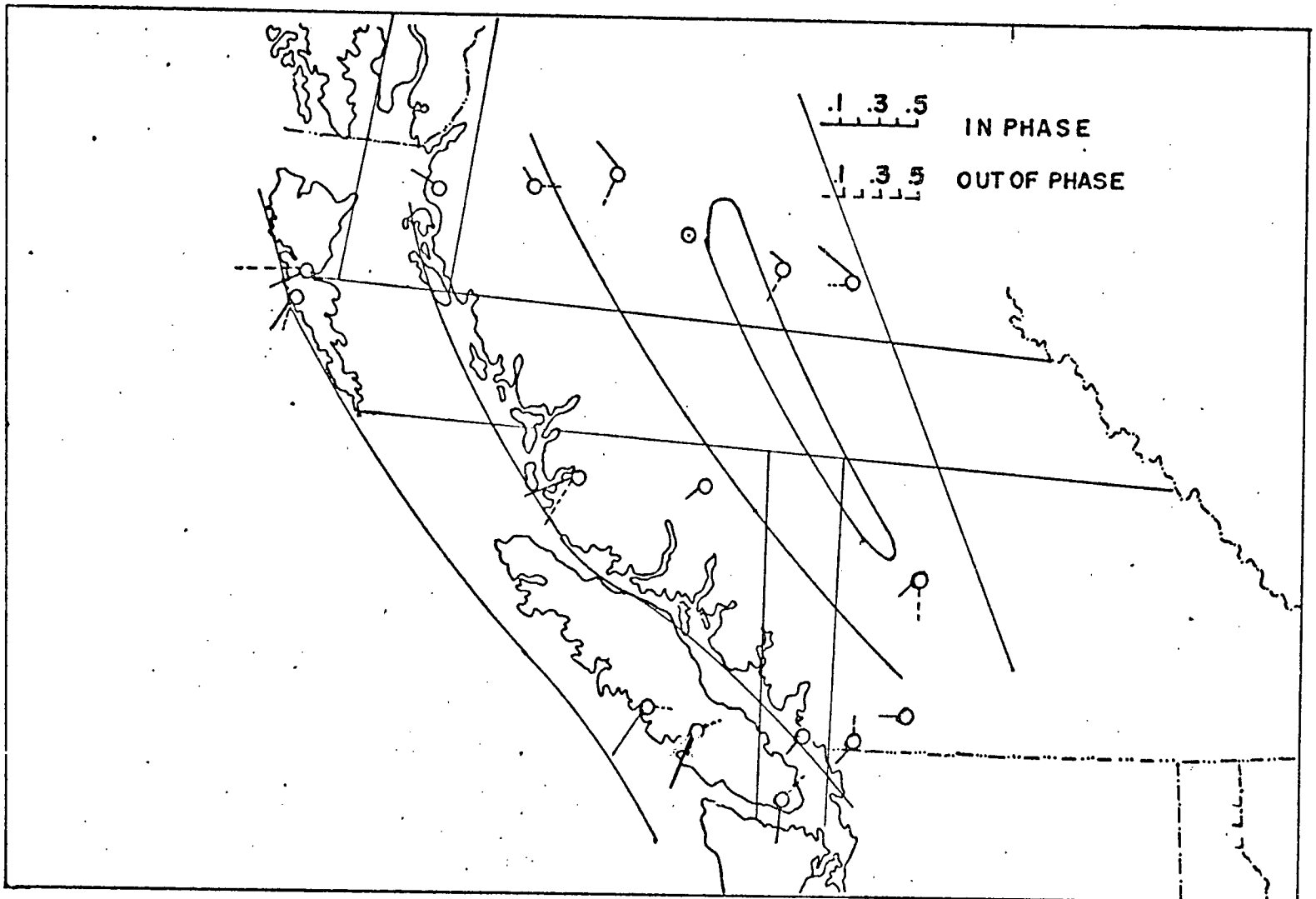

Fig. 3.10 Geographic plot of induction arrows at 10 minutes period showing relation to geologic boundaries (Fig. 1.2). In phase arrows plotted in accordance with Parkinson convention.

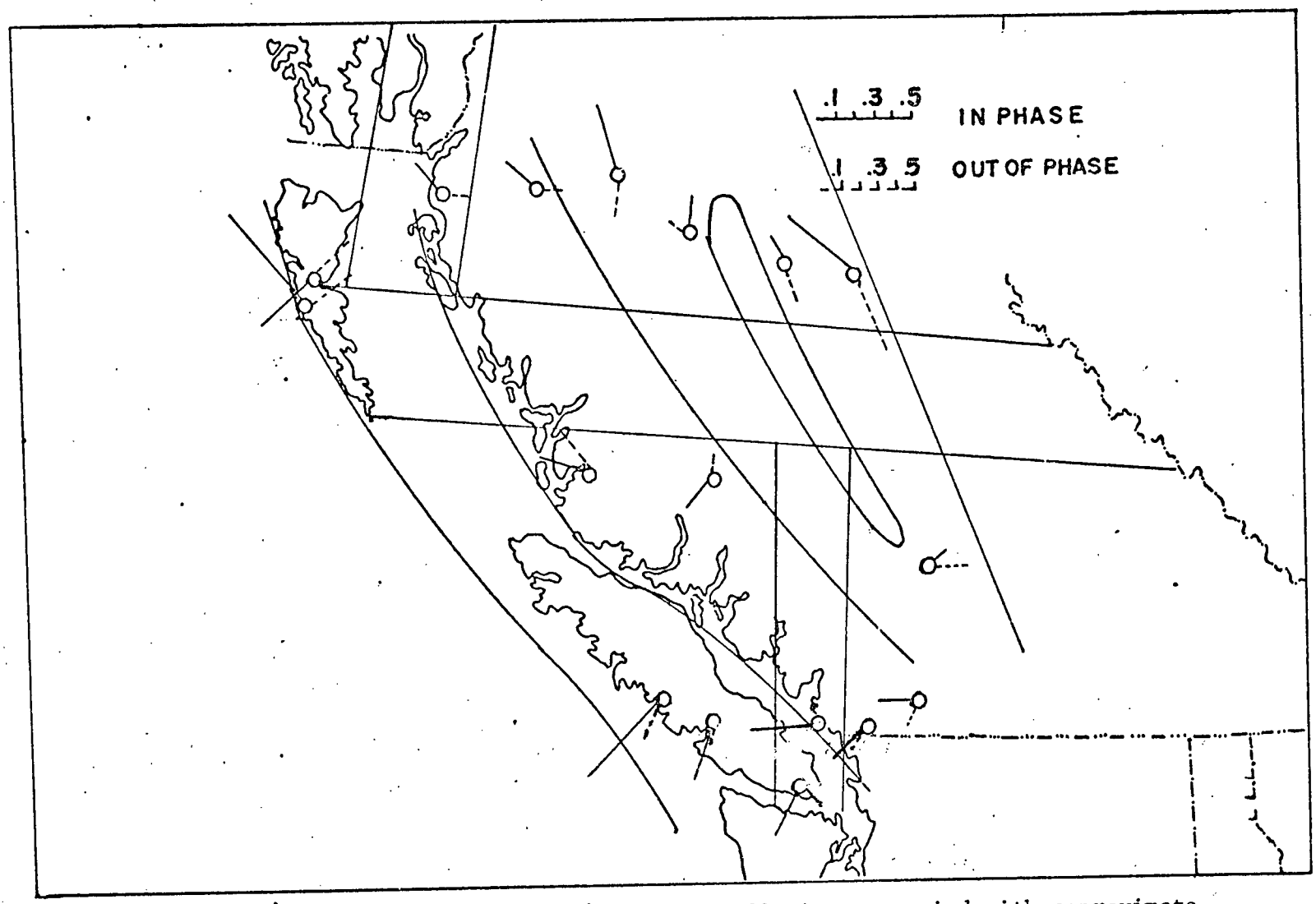

Fig. 3.11 Geographic plot of induction arrows at 30 minutes period with approximate geological boundaries.

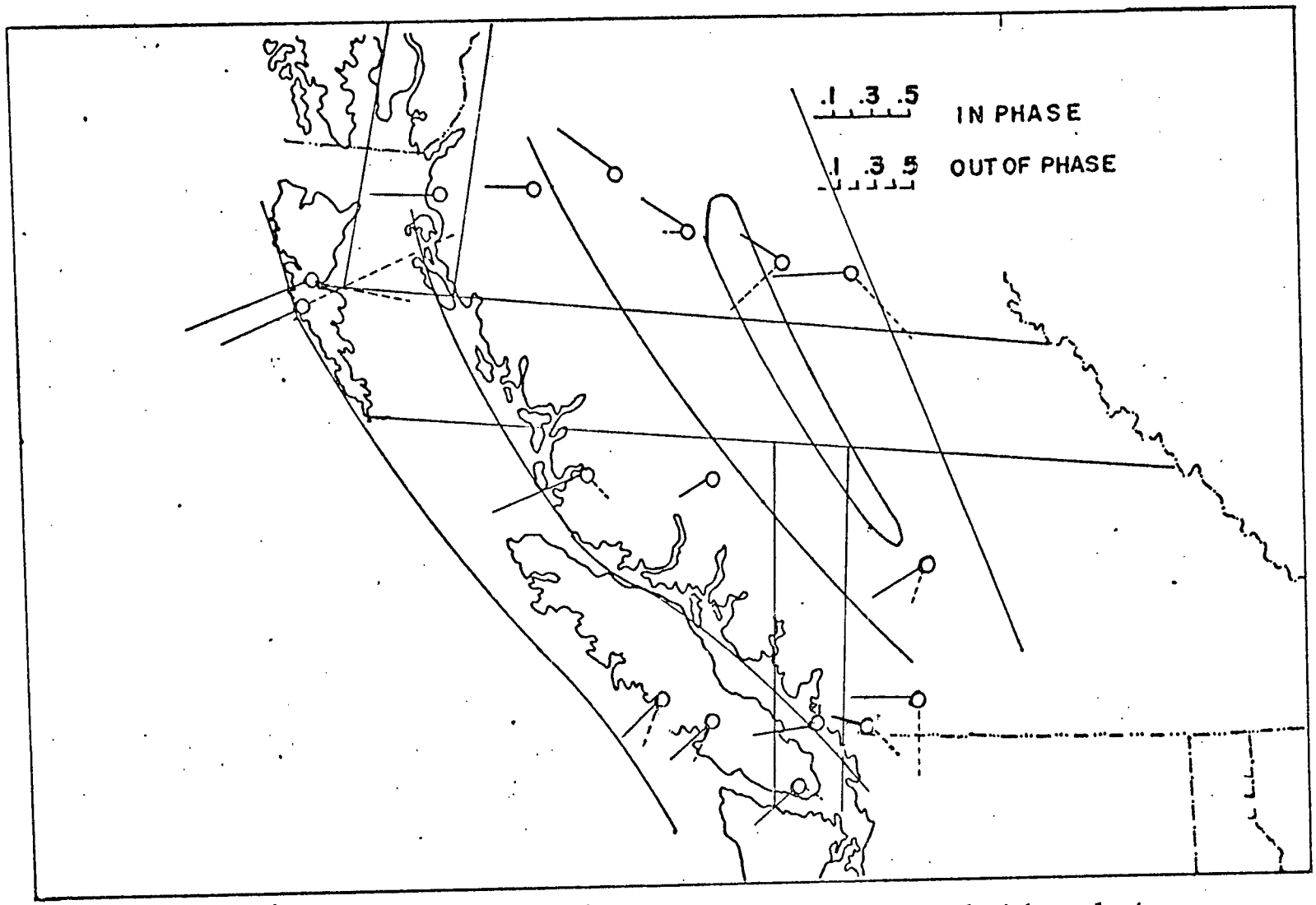

Fig. 3.12 Geographic plot of induction arrows at 60 minutes period with geologic boundaries.

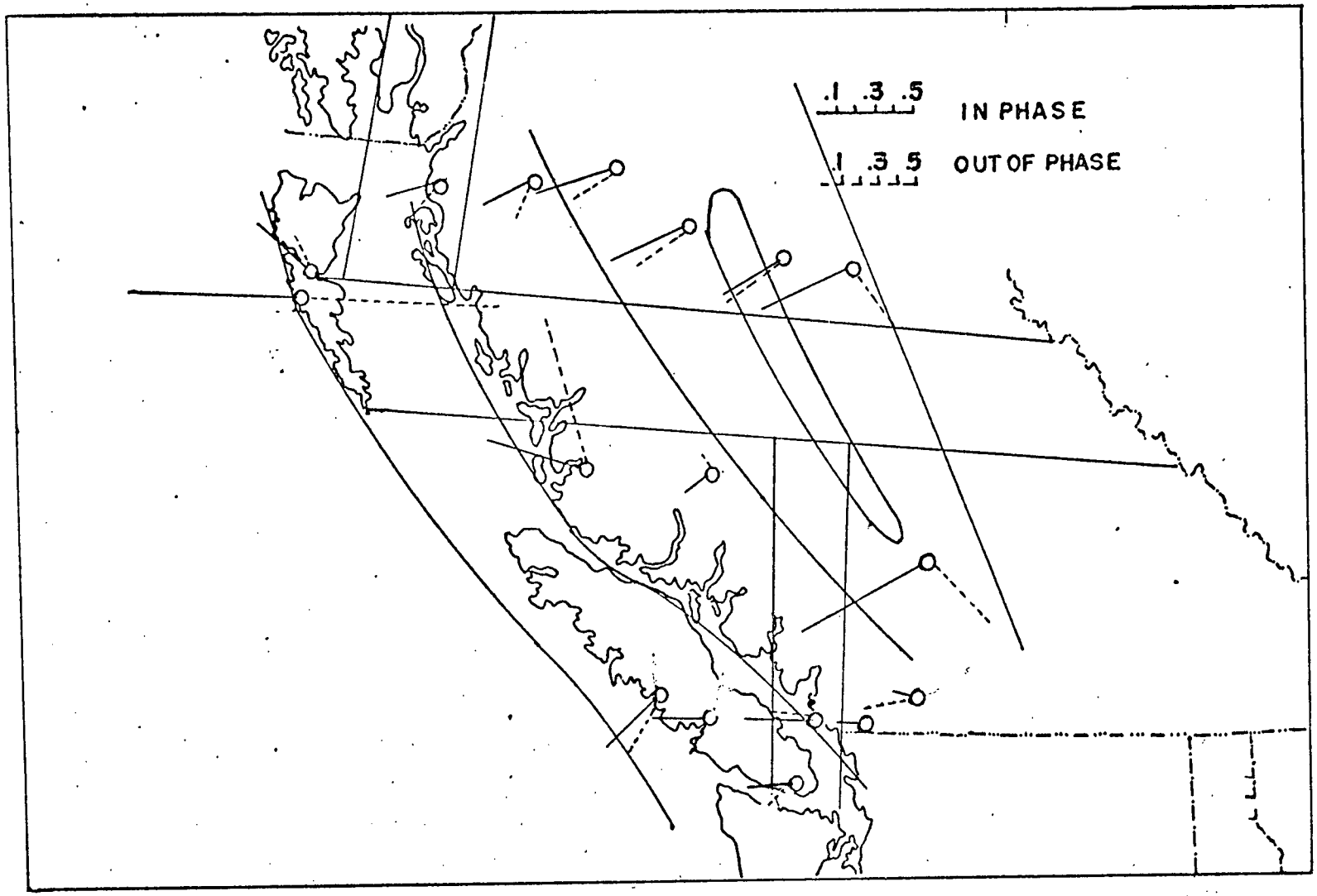

Fig. 3.13 Geographic plot of induction arrows at 120 minutes period with geological boundaries included.

from the present survey and from the Cochrane and Hyndman data are presented (Fig. 3.14 to 3.17).

The induction arrows show considerable variation in magnitude and direction. A visual analysis based upon the surface geology and its probable depth continuation is possible. At 10 minutes period (Fig. 3.10) the induction arrows are controlled by local zones of conductivity contrast. The coastal stations all point to the nearest salt water e.g. Tasu, Sandspit, Bella Bella from the present survey, Tofino, Franklin River (FRA), Victoria, Westham from the Cochrane and Hyndman (1970) results and Prince Rupert from the Dragert (1973) profile. Inland the responses vary. The northern vectors (Dragert, 1973) point to the north or northwest indicating that a conductive zone exists to the north of these stations. Dragert has interpreted these vectors as evidence for induced currents in the sediments in the Bowser Basin (Fig. 1.2). The northwest turning of these vectors at Prince Rupert and Terrace may be explained, in the candidates opinion, by adding an effect due to the general structural trend to the effect of the basin to the north or northeast. A similar structural effect may be added to the inland vectors on this profile since induced currents may be expected to flow along the boundary between the conducting sediments and sea water of the Insular Trough and the resistive crystalline rocks of the Coast Mountains. Similarly on the inside of the Coast Mountains a conductivity contrast occurs between the sediments and the volcanics of the Interior Trough and Coast crystalline belt. On the central profile the inland locations of Tatla Lake and Cache Creek see local conductors. The observed direction and magnitude at Tatla Lake are compatible with the attenuation of the coast effect. Cache Creek shows an entirely anomalous behavior. (Fig. 3.10). A consideration of the

structural boundaries shows that it may be explained by a current flow along the boundary between the Interior Trough and the Omineca geanticline. A near surface conductivity contrast is expected across this boundary since it marks the transition from the eugeosynclinal belt with its marine sediments and volcanics to the miogeosynclinal belt with its sediments derived from the craton.

At 30 minutes (Fig. 3.11) the coast effect and the effect of the general tectonic trend are becoming more evident. On the northern profile the Bowser Basin still exerts considerable control, however, the out of phase components indicate that considerable coupling is occurring between conductors. The vectors in the southern profile are obviously influenced by a strong coast effect possibly enhanced by a structural effect. The central profile is again not typical. Cache Creek continues the anomalous behavior shown at 10 minutes indicating that the structural boundary must continue deeper. The relatively large out of phase component at Cache Creek indicates that the boundary may mark a structural discontinuity at depth causing a large out of phase component due to coupling between structures. Bella Bella has a vector which may be explained by invoking the Souther (1970) east west volcanic zone. It is tempting to invoke the same zone to explain the Tasu vector, however this would involve placing the boundary of the east-west zone between Tasu and Sandspit. This location of the boundary is not on solid geological ground, however it must be noted that this is approximately the location for the boundary proposed by Souther. The large out of phase component at Tasu indicates that considerable coupling between two structures is occurring so the presence of the volcanic zone in this region cannot be ignored.

The vectors at 60 minutes period show a classic coast effect (Fig. 3.12) for the outer stations of the central and southern profiles. The northern stations appear to be influenced by the coast at Prince Rupert, but as Dragert points out the magnitudes inland are too large to be due to the effect of the coast alone. Dragert has explained the orientation of the vectors on the basis of the Souther volcanic zones claiming that the rotation of the vectors is caused by these zones. The candidate suggests that such an explanation is untenable. If as Dragert claims, the arrows are rotated by the east-west and north-south volcanic zone and influenced at short periods by the Bowser Basin sediments, then it is impossible to construct a simple set of vectors using these zones which will have resultants such as those observed at 30 and 60 minutes. A more logical explanation is that the observed vectors are caused by induction arrows perpendicular to the structural trend, these arrows being perturbed by the arrows due to the induction in the Bowser Basin and the east-west volcanic zone. The effect of this volcanic zone is to rotate southward the vectors due to the induced currents at the structural province boundaries. But the opposite is observed i.e. the vectors due to the structural trend are rotated northward suggesting that an appreciable east-west zone of induced current exists to the north of the profile. It is difficult to explain this zone on the basis of the sediments in the Bowser Basin since these are essentially surface cover. It is necessary to suggest that the causative feature for such vectors penetrates through the crust. No geological evidence for such a zone has as yet been reported.

The vectors for the southern and central profiles do not deviate from a classic coastal effect orientation. It is difficult, however, to explain the magnitude of the Cache Creek vector at such a distance from

the coast. As before it is possible to explain the Cache Creek vector in terms of induced currents flowing at structural boundaries, however the direction has now reversed. The orientation of the vector at Hope and the large out of phase component there at 60 minutes period seems to indicate the presence of a conductor not associated with the structural trend.

At 120 minutes (Fig. 3.13) all the northern vectors have rotated to an orientation perpendicular to the structural trend. The magnitudes and orientations of the out of phase components suggest structural boundaries near Smithers and Prince George. The Souther volcanic zone helps rotate the vectors to this orientation but is not the cause of the large magnitudes. The Cache Creek vector is swinging more to the south indicating that there may be a zone striking east-west at considerable depth. Such a boundary would lie at some distance north of Hope but nearer to and south of Cache Creek. This would roughly agree with the location of the buried Paleozoic craton edge proposed by Berry et al., (1971) on the basis of geophysical evidence.

The Souther volcanic zone may easily explain the rotation of the vectors away from coast effect at Bella Bella at all periods. Similarly the presence of such a zone on the Queen Charlotte Islands would explain the complexities in the Tasu and Sandspit vectors. Insufficient evidence from the geomagnetic data precludes an accurate delineation of the zone by geomagnetic means alone.

The interpretation presented here has attempted to resolve the observed vectors into two or more parts which agree with known geology. In an attempt to obtain mathematical justification for this the Cochrane and Hyndman (1970) and present data were re-analysed using the induction ellipse technique described in Appendix 3. These ellipses are presented

in Fig. 3.14 to 3.17 which show the major and minor axis at each location.

E) Induction Ellipses The basic interpretation presented above is not changed. They show large major/minor ratios for most of the inland stations except Cache Creek and Hope. The orientation of the major axes at these two locations for periods of 30 minutes and 120 minutes supports the hypothesis that the induction effects in this region are caused by an east-west conductor at depth and by a northwest-southeast conductor. The complexity of the induced fields at the coastal locations of the present survey indicates that more than one conducting direction is involved at Tasu, Sandspit and Bella Bella. This is in agreement with the location of the volcanic zone of Souther (1970) and suggests that it has considerable depth extent. This would imply that the east-west zone of volcanics may represent a major fissure in the earth's crust and upper mantle which allowed volcanic material to rise from considerable depth (Souther, 1970). The major/minor axis ratio of nearly unity at Tasu indicates there is no one preferred direction of induction but considerable induction does occur as evident in the large magnitudes. Hence, the structure here must be complicated. The swing of the induction arrows to almost east west for the new locations may indicate that at considerable depth the structural trend changes slightly but evidence for this is not conclusive.

3.5 Summary

The induction process in the coastal region of British Columbia is complicated. There is a strong coast effect which is perturbed by the presence of conductors associated with the tectonic structural trend

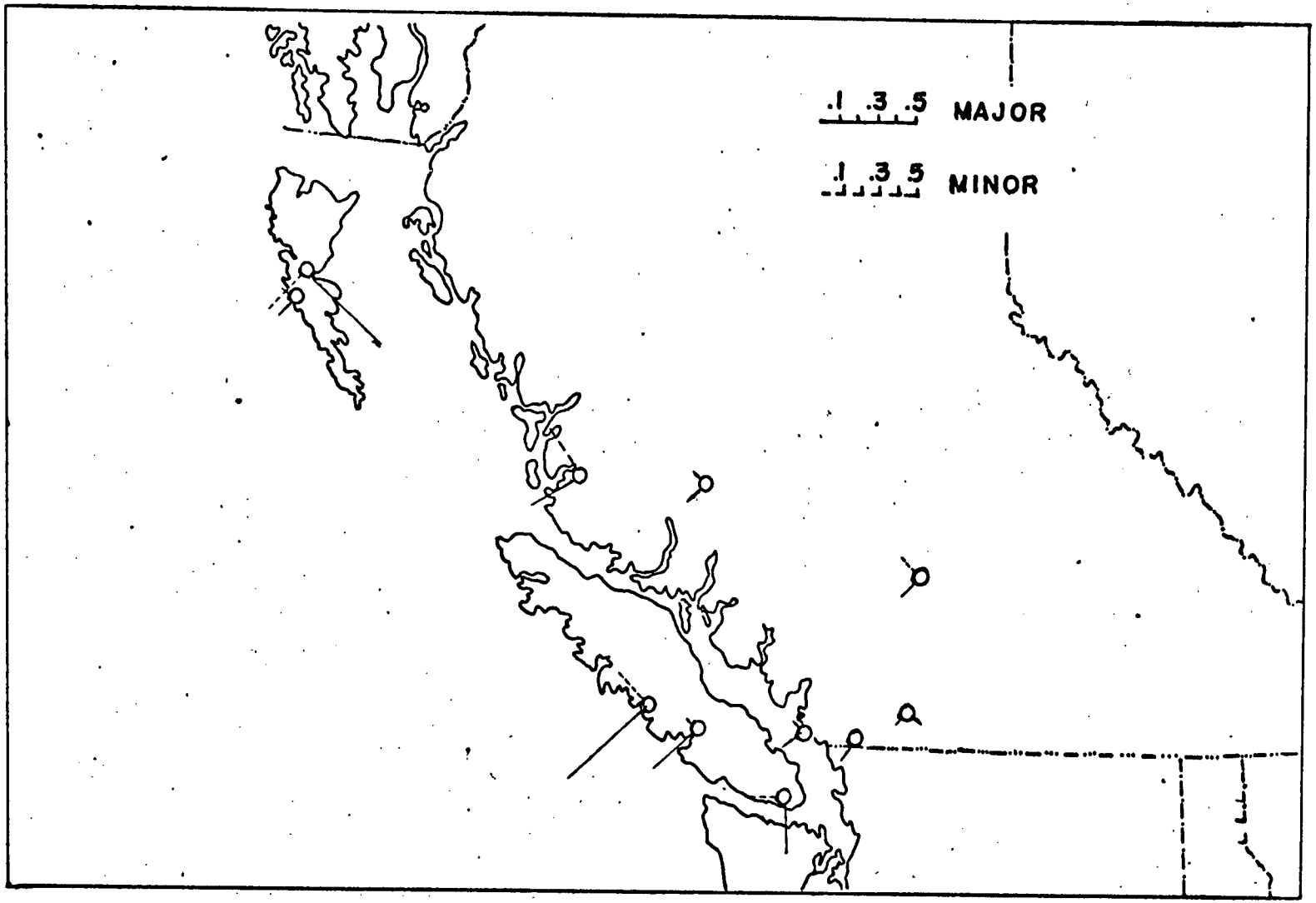

Fig. 3.14 Geographic plot of induction ellipses at 10 minutes period. Major axis plotted negative to agree with Parkinson convention.

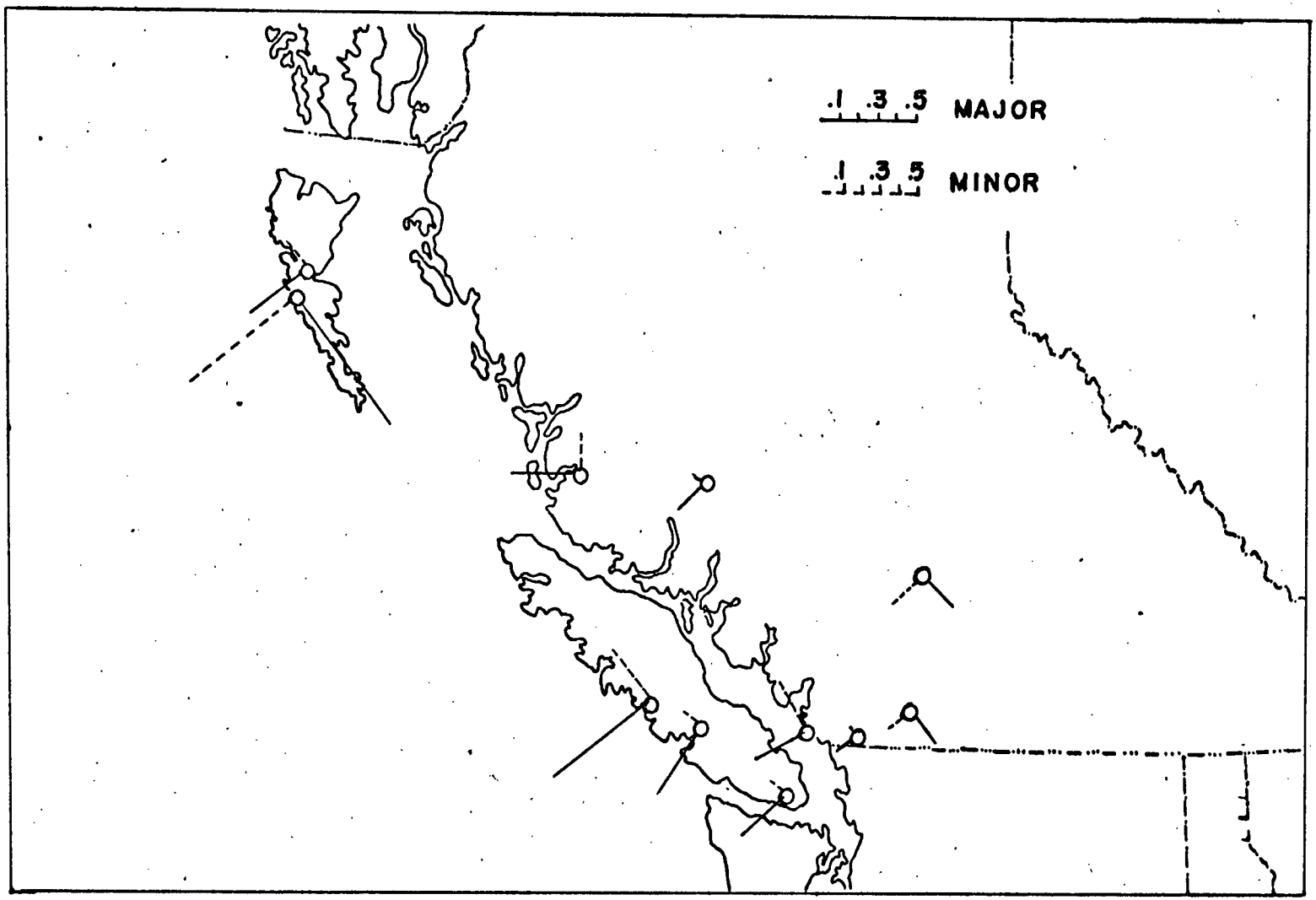

Fig. 3.15 Geographic plot of induction ellipses at 30 minutes period.

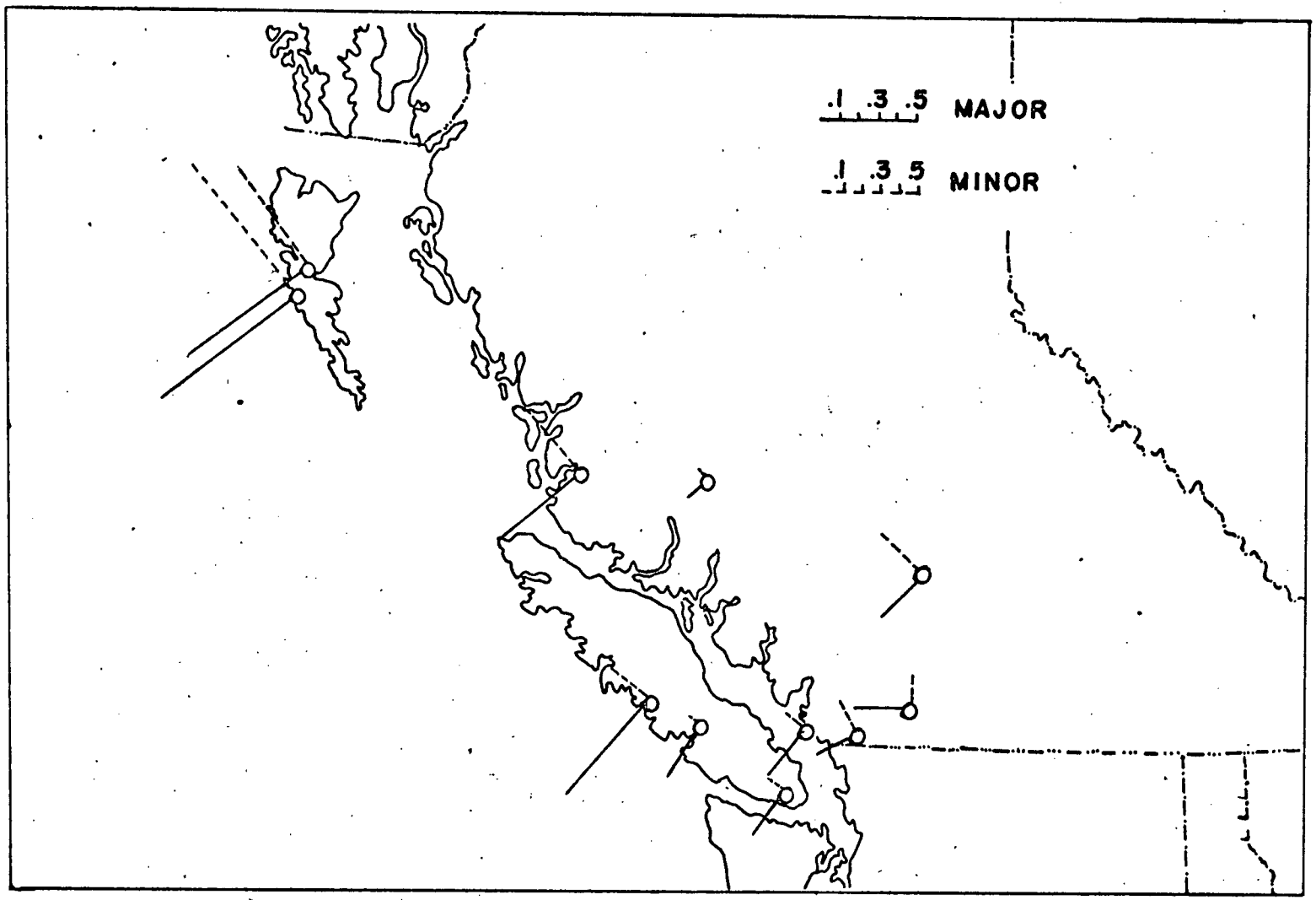

Fig. 3.16 Geographic plot of induction ellipses at 60 minutes period.

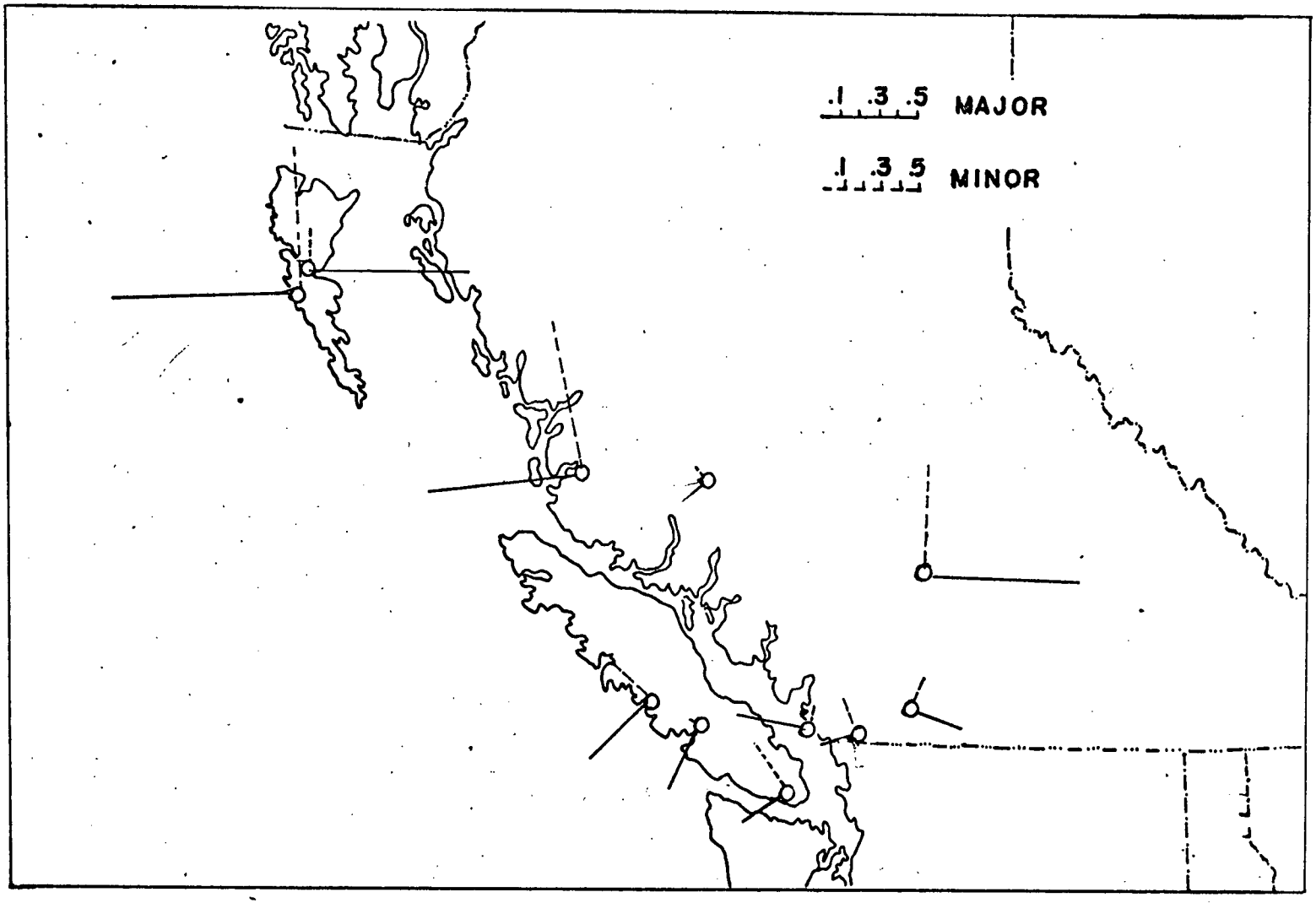

Fig. 3.17 Geographic plot of induction ellipses at 120 minutes.

of the area and apparently also with the ancient craton edge. It is possible by detailed inspection of each induction vector and ellipse and a reinterpretation of the northern profile to draw the above conclusions about the orientation and location of the conductors.

The location of the induced currents may be estimated from Table 3.3. The land and sea conductivity and skin depth estimates are derived from models discussed in the succeeding chapter, and represent the integrated conductivity of the upper 50 km. of the earth and overlying ocean. As can be seen from this table the currents can be expected to flow in the crust and upper mantle. The variations in Moho topography may provide the conductivity contrasts needed to provide current concentrations since the conductivity contrast between deeper crustal wedges and the adjacent mantle material may be two orders of magnitude.(Watanabe, 1970).

A detailed interpretation in terms of structures and their dimensions must be undertaken to examine the causes of the observed geomagnetic variations. Since the evidence presented here indicates that the observed data can be explained by three dimensional structures, both these and the simpler two dimensional models must be employed. These models were constructed and the results of these model studies are presented in the next chapter.

CHAPTER 4

MODEL STUDIES

4.1 Introduction

The interpretation of geomagnetic data in terms of the physical properties and dimensions of the anomalous structures can be facilitated by electromagnetic model studies. The structure, so determined, must incorporate and be compatible with the known geological and geophysical constraints.

Three techniques for determining the electromagnetic response of a structure are available. The first is an analytic solution of Maxwell's equations for the geometry of a particular structure. Only recently (Weaver and Thompson, 1972) has the problem for the coast effect been formulated and solved. The Weaver and Thompson approach assumes that the ocean and land can be represented by two quarter spaces with the appropriate conductivity contrast. This assumption, and hence their solution, is valid as long as the skin depth of the disturbance in the water is much less than the average depth of oceans. This means that their solution is valid only for periods of less than 10 minutes. Integrated conductivities may be used for longer periods. The use of quarter spaces limits the applicability of this technique to simple geological problems.

Two techniques which may be used to provide geologically useful models for the geomagnetic variation anomalies are the two dimensional numerical model studies and the electromagnetic scale model analog technique. Some three dimensional numerical model studies have been attempted by extending the two dimensional technique to calculate the effect of two islands off a two dimensional continent (Lines, 1972). The full three

dimensional problem has not as yet been formulated, and even the quasi three dimensional approach used by Lines requires considerable computing time. The two dimensional numerical technique and the three dimensional analog scale models were used for model studies in this investigation.

4.2 Numerical Modelling

The numerical modelling of two dimensional electromagnetic induction problems is a recent technique (Madden and Swift, 1969; Wright, 1969; Jones and Price, 1970). The basic problem is formulated from Maxwell's equations which may be separated into two distinct problems depending upon the orientation of the electric and magnetic fields. The case most closely analagous to the geological problem is the E polarization where all currents flow along the strike of the conductors. These currents give rise to magnetic fields which have horizontal components perpendicular to strike and have vertical components. The second case is the H polarization where the magnetic field is parallel to strike causing horizontal electric fields perpendicular to strike and vertical electric fields. These in turn cause vertical magnetic fields. The E polarization case is most applicable here in view of the general orientation of the source fields relative to the strike of the structure being considered.

The observed data with which to compare the model results are the single station transfer functions resolved on a line perpendicular to the mean strike of the continental margin. The formulation of the E polarization for use in computing is presented in Appendix 5.

The use of the E polarization case introduces several problems associated with the boundary conditions and computing techniques. These problems are inter-related since the formulation of the boundary conditions

poses the problem of matching the theoretical infinite boundary conditions to a finite grid of points.

The boundary conditions require that the fields at the grid edge be unaffected by the presence of the anomalous structures. Thus the grid must be large enough to satisfy this condition yet the spacing in the region of the anomalous structure must be small enough to provide detailed information. This is achieved by using a logarithmically increasing grid spacing (Cochrane and Hyndman, personal communication). The computer programme to calculate the fields is one formulated by Cochrane and Hyndman (personal communication) based upon Swift's (1971) technique. By using the logarithmically increasing spacing vertically and horizontally the Cagniard conditions of no vertical field and a horizontal field twice the magnitude of the inducing field at the lateral ends of the grid are met. The use of the upwards vertically increasing spacing means that the source region at the top of the grid is relatively unaffected by the anomalous fields. The use of a different vertically increasing spacing downwards assures that the fields at the bottom of the grid are zero.

The problem can be accurately solved on a 21 x 21 point grid. The small vertical grid spacing near the air and "land" interface fulfills the condition that the vertical grid spacing be less than a skin depth for a disturbance of the period being modelled in order to obtain accurate results. The surface conductivity is poorly known so that an integrated conductivity for the upper few kilometers is used, this conductivity being estimated from the known geological structure at the surface. By using these techniques an accurate representation of the resolved single station transfer function response for a given source field may be calculated.

The problem of the correct source field is an unsolved one. Estimates of the spatial wavenumber of the field (Caner et al, 1967; Cannon, 1967) indicate that for periods of the order of 10 minutes the field is uniform over 600-800 km. Since the spatial wavenumber increases with increasing period, the source field is uniform at all periods considered in this survey. The second problem is the orientation of the field. The use of the E polarization formulation with a uniform source implicitly assumes that the source is parallel to the strike of the conductors. The orientation of the equivalent ionospheric current source varies critically with the time of day. Thus the average current system orientation depends critically upon the record section chosen for analysis. The strongest concentration of current is on the night side of the earth between midnight and 0600 local time; this section has a predominant geomagnetic east-west orientation and contains most of the energy of the storm. Thus a record which truncates in the middle of this period has a different average current orientation than one which includes this strong night section.

A geomagnetic east-west current system has a strong component parallel to the coast line. This component is responsible for inducing magnetic fields on a line perpendicular to the coast with an E polarization. The component of the electric field perpendicular to the coast line may induce changes in the horizontal magnetic field parallel to the coast. Thus the total horizontal field is neither parallel nor perpendicular to the coast. Analog model studies which will be discussed later in this chapter show that the magnitude of the magnetic component parallel to the coast is much smaller than the magnitude of the magnetic component perpendicular to the coast. Thus the major part of the magnitude of the transfer function resolved on a line perpendicular to the coast is due to

the induction effects of the component of the source current which runs parallel to the coast. The structure deduced by modelling using the E polarization scheme is therefore as accurate a representation as possible of the features which cause perturbations in the geomagnetic field. Since there is considerable evidence presented in the previous chapter to indicate that the structures controlling the induction are three dimensional, the numerical model results should be regarded as first order attempts to explain the configuration of conductors parallel to the coast.

4.3 Analog Models

The second method for modelling the geomagnetic response of the earth is the electromagnetic scale model technique. This technique has been discussed by various authors (Dosso 1966, 1968, 1972; Hermance, 1968). Basically it utilizes the invariance of the electric and magnetic fields under the scaling condition that $\omega\sigma L^2$ = constant. Thus geophysical problems may be scaled to laboratory problems by reducing L by a factor of about 10^5 and increasing σ and ω by corresponding factors. Then frequencies in the kHz range may be used and materials such as graphite and brine may be used to represent the sea and land respectively. The major problem is to obtain materials having the correct conductivity to model the various layers in the earth.

In this thesis the modelling tank at the Department of Physics, University of Victoria was used (Dosso, 1966). The modelling system consists of three components: the source, the model, and the detector.

The first component to be considered is the source. The assumptions made in calculating the transfer functions is that the source field

is a uniform horizontal field having large dimensions compared to the size of the structure. The source field employed was a uniform sheet current which had the same physical dimensions as the model tank in which the structure was placed. This sheet current also required a return current path. By using a return path around the laboratory, the magnetic effect of this current on the inducing field at the surface of the tank was minimized. The uniform sheet current of finite dimensions introduces a second problem. The vertical field is not zero except below the centre of the source where it undergoes a 180^0 phase shift. This means that induction by the vertical component of the source field may occur as one proceeds away from the centre of the source. The horizontal field of the source is essentially uniform varying by less than 25% from the centre to the end of the profile. The frequency of the source may be changed by tuning the source system to a particular frequency. The size of the capacitor bank available limits the lowest effective frequencies which may be used with the uniform sheet source to about 500 Hz. The source is fixed in position at a height above the model tank corresponding to 110 km. above the earth, thus representing a uniform current sheet directly overhead in the ionosphere.

The second problem to be considered is the construction of the model using the available materials of graphite, brine, and aluminum foil. The purpose of the model study was to investigate the effect of the east-west zone of volcanics (Souther, 1970) on the geomagnetic field. This was to be examined using the transfer functions. Using the invariance relation $\omega\sigma L^2$ = constant with the scaling relations

$$\frac{L}{L_0} = \frac{10^{-5}}{5} \qquad \frac{f}{f_0} = 25 \times 10^5 \qquad \frac{\sigma}{\sigma_0} = 10^5$$

implies 1 cm. on the model represents 5 km. in the geophysical problem. The periods of 10, 30, and 60 minutes are represented by frequencies of 4160 Hz, 1390 Hz, and 694 Hz. It was originally planned to model the 120 minute period data using a frequency of 347 Hz. but suitable power at this frequency could not be attained using the available tuning circuits.

The modelling of the Souther volcanic zone with the surrounding continent and land was achieved as follows: The sea and its underlying structure were simulated by a sheet of graphite 120 cm. x 30 cm. x 1.00 cm. formed by cementing four 30 cm. x 30 cm. x 1 cm. blocks together with conductive cement. The volcanic zone was simulated by aluminum foil whose dimensions were 100cm x 45 cm x .0025 cm. This was placed with a 0.5 cm. overlap on the graphite in the tank of saturated brine (Fig. 4.1). The thickness of the various materials was chosen to correspond to the integrated conductivity of the upper 50 km. of the earth and overlying ocean in the oceanic section. Dosso (1966, 1972) shows that the correct magnetic response for scale models will be achieved if the ratios of the conductivities used in modelling are the same as the ratios in the geophysical situation. To achieve this, depth of the brine solution was taken to be fixed and the integrated conductivity of the tank solution was calculated. Using this and the integrated conductivities calculated from the models used in numerical studies for the sea, land, and volcanic zones, the thickness of the graphite and aluminum was determined such that the ratio of the conductivity of the aluminum to the brine equalled the ratio of the volcanics to the land, and the ratio of the graphite to the brine equalled the ratio of the sea to the land.

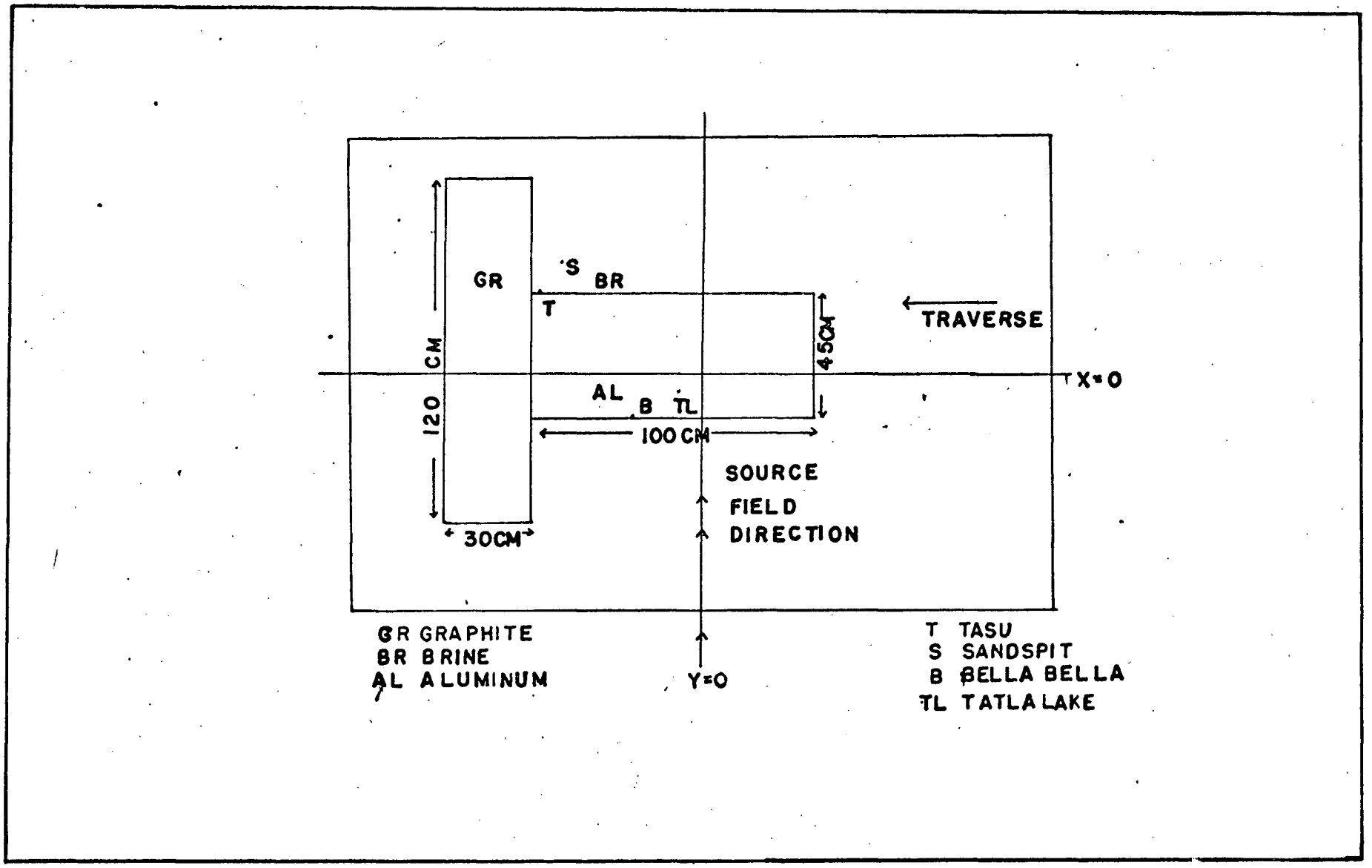

Fig. 4.1 Model configuration - analog model tanks.
a) Model orientation - E parallel

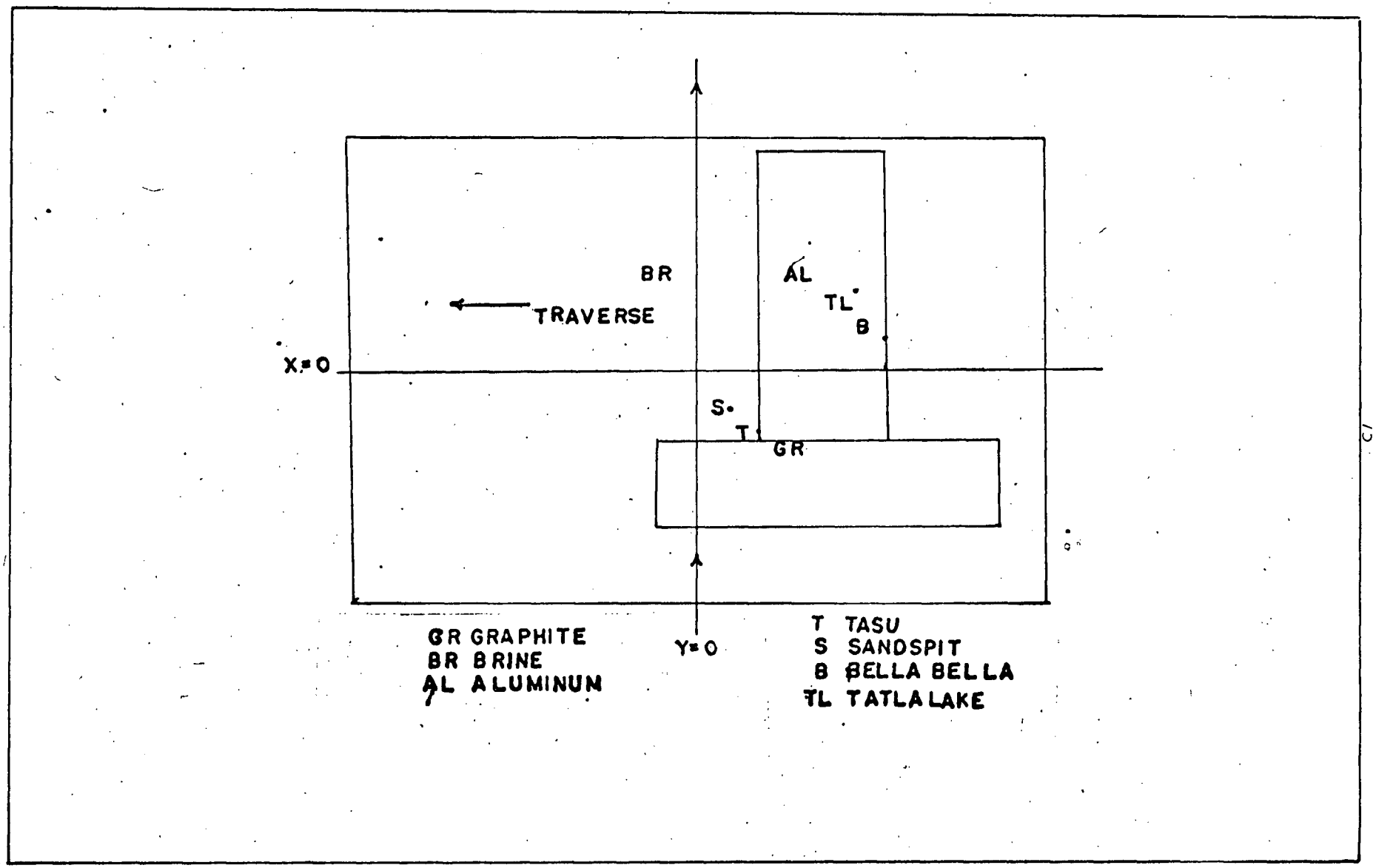

Fig. 4.1 Model configuration - analog model tanks.
b) Model orientation - E perpendicular
Graphite and aluminum dimensions same as Figure 4.1a.

The required thickness of the aluminum was calculated to be only a few microns, whereas the only size available was the .0025 cm household foil. This was used for the modelling with the realization that the integrated conductivity of both the aluminum and the graphite was approximately equal. This implies that the magnetic response of the graphite and the aluminum should be approximately equal, and hence the induced currents should concentrate more in the aluminum than would be expected in the volcanic zone, since the volcanics have a lower conductivity than the sea. This would cause greater rotation of the induction arrows towards the aluminum and possibly a diminuation in amplitude of the transfer functions. The calculation of induction arrows from these models is derived in Appendix 6.

The results of the three dimensional model study will show the effect of several aspects of the induction process which could not be modelled using the two dimensional numerical approach. First the effect of source-structure orientation (Fig. 4.1a,b) can be examined and general conclusions about the source orientation which produce the observed results may be drawn. As a consequence of these source orientation studies insight into the scatter of the transfer functions magnitude at a single location is obtained. Even though the frequency scaling relations no longer hold since the approximations made in using the integrated conductivities and the aluminum changed the relations, the model results will show the general effect of changing frequency and serve to illustrate how the frequency variations of the transfer functions arise. The interaction between two orthogonal conductors as a function of frequency may be examined, a study for which the two dimensional models could not be used.

Thus the three dimensional models are a powerful tool in investigating the general features of the induction response of a model while the two dimensional numerical models provide detailed calculations for certain aspects of the situation under the simplifying assumption of approximate two dimensionality.

The first configuration (Fig. 4.1a) corresponds to the E polarization with one important modification. In the numerical modelling of E polarization all currents are constrained to flow parallel to the land-sea boundary. In the analog model, however, current can flow transverse to this land-sea boundary along the aluminum foil thus inducing magnetic fields parallel to the land-sea boundary. Similarly for the second source orientation (Fig. 4.1b) which is analagous to the H polarization, current can flow parallel to the land-sea boundary. These models represent cases which could not be properly modelled using two dimensional studies.

Third part of the modelling system which determines the finest length scaling which may be employed is the detector system. The assumed scaling in the present studies is $L/L_0 = 10^{-5}/5$ which means 1 cm. on the model corresponds to 5 km. in the geophysical problem. This scaling is in error since the conductivities do not properly correspond to a scaling of $\sigma/\sigma_0 = 10^5$ but the models do show the effect of changing ones observation location relative to the conductive zones. The detection coils are 0.57 cm. in diameter. Thus under the assumed scaling the signal detected is a weighted average of the magnetic fields over 0.57 cm. or about 3 km. in the real situation. If the scaling is changed so that this averaging distance is doubled, the response near the land-sea interface would be appreciably flattened (Dosso, 1972). Thus the scaling of

$10^{-5}/5$ was used. This meant that Cache Creek could not be included on the models. The presence of the inland anomalous conductor at Cache Creek and its anomalous azimuth response show that it is not affected significantly by the zones being modelled, hence it was omitted on the analog models. The locations T, S, B, TL shown on the models (Fig. 4.1a,b) correspond to Tasu, Sandspit, Bella Bella, and Tatla Lake.

The data from the analog models were recorded by making traverses along the X direction (Fig. 4.1). With the model emplaced, three traverses were made at each frequency and at each X coordinate corresponding to a station location, each traverse recorded a magnetic field component and its associated phase angle. The same procedure was repeated with the model removed. These data were analysed using the technique developed in Appendix 6.

4.4 Model Results

The analog and numerical models were used together to interpret the induction processes which occur in the area. The relative insensitivity of the numerical models to subsurface structure and the scarcity of observation locations means that considerable additional geophysical and geological information had to be used in deciding upon the final models.

A) Numerical Models

The curves to be matched by the numerical models are the in phase and out of phase transfer functions resolved on a line perpendicular to the coast line (Fig. 4.2, 4.3, 4.4). Only the data from the present study and the Cochrane and Hyndman (1970) data are presented here since it is

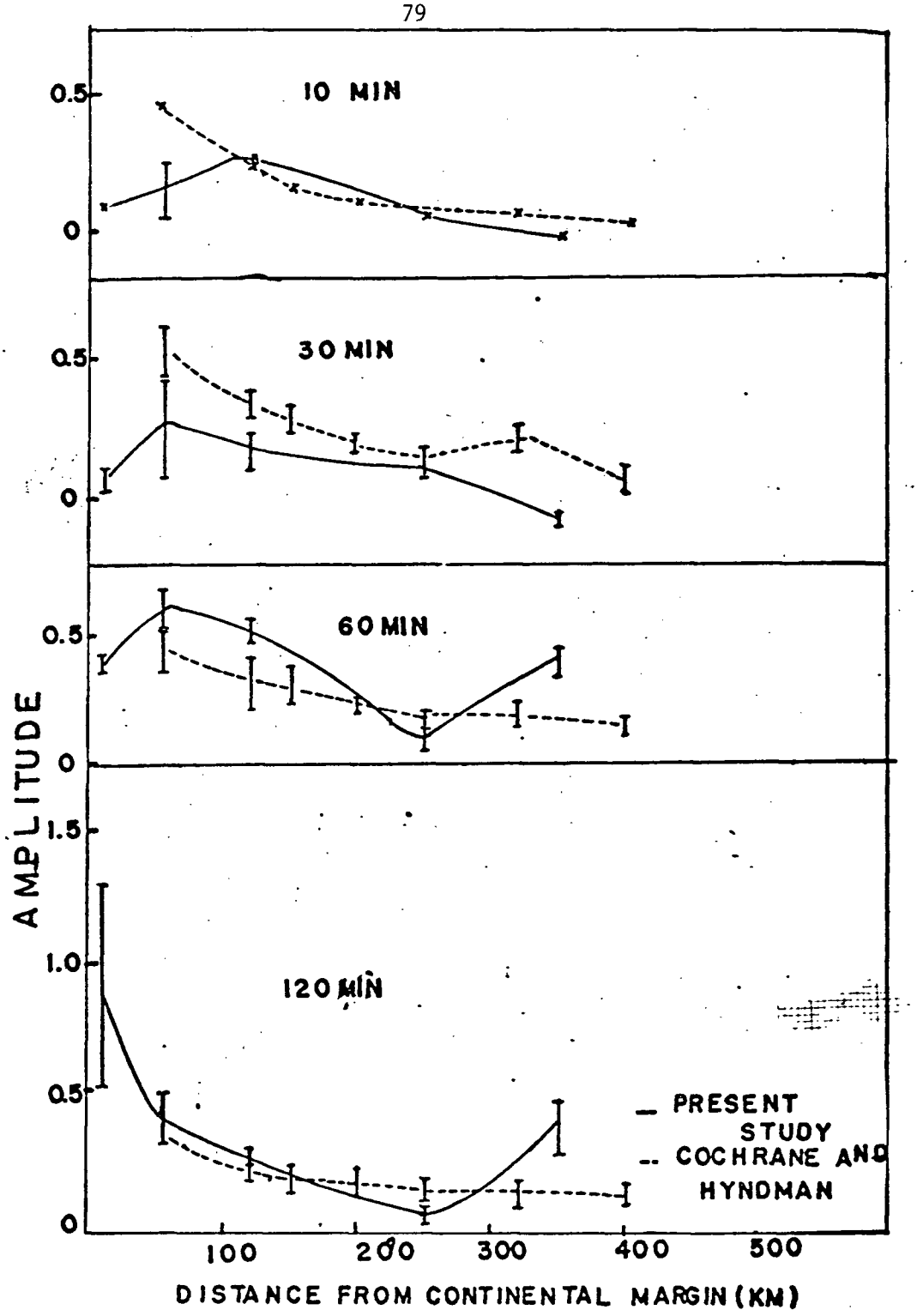

Fig. 4.2 In phase induction arrow magnitude resolved on a line perpendicular to the mean strike of the continental margin.

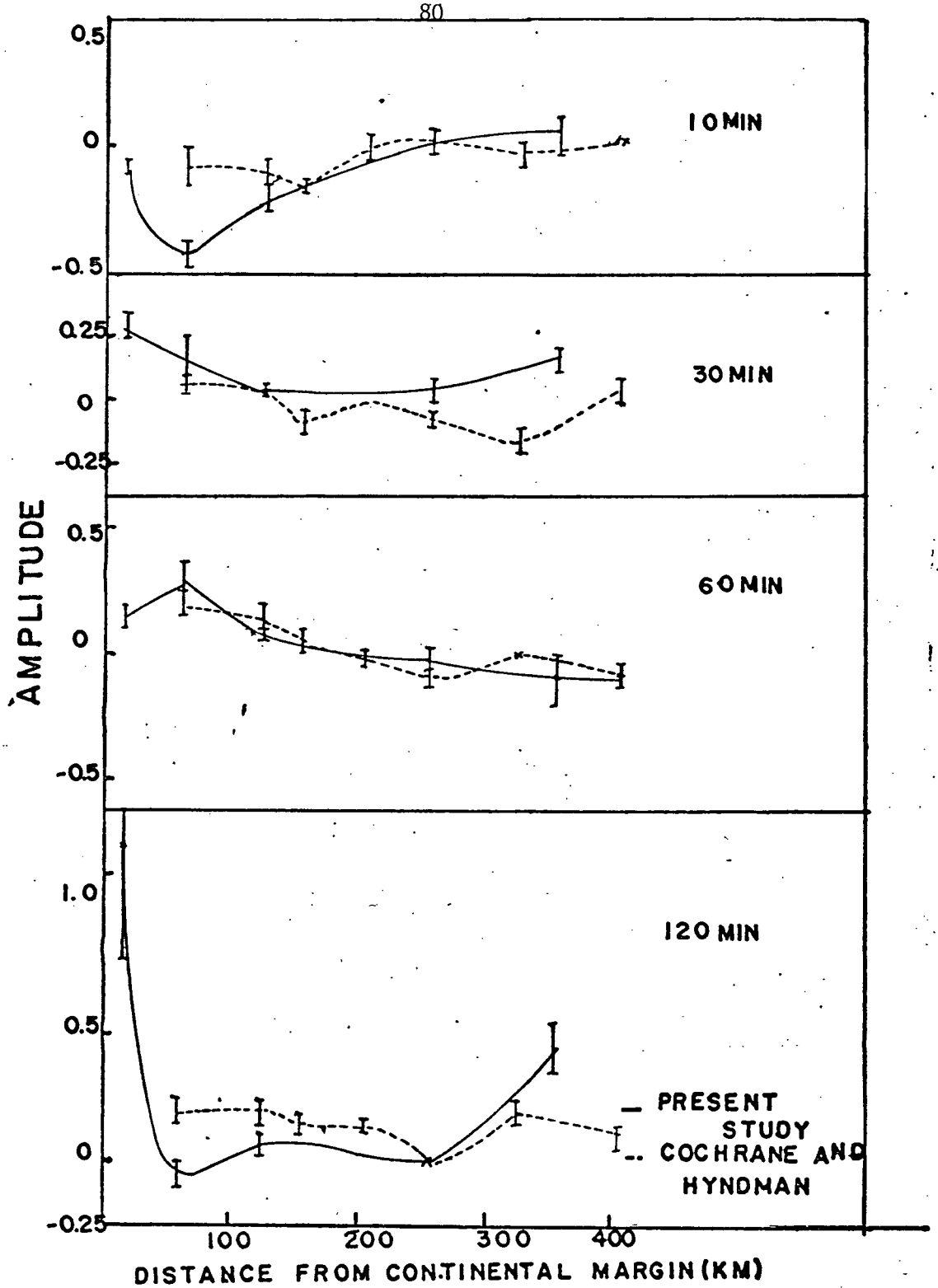

Fig. 4.3 Out of phase induction arrow resolved on a line perpendicular to the mean strike of the continental margin.

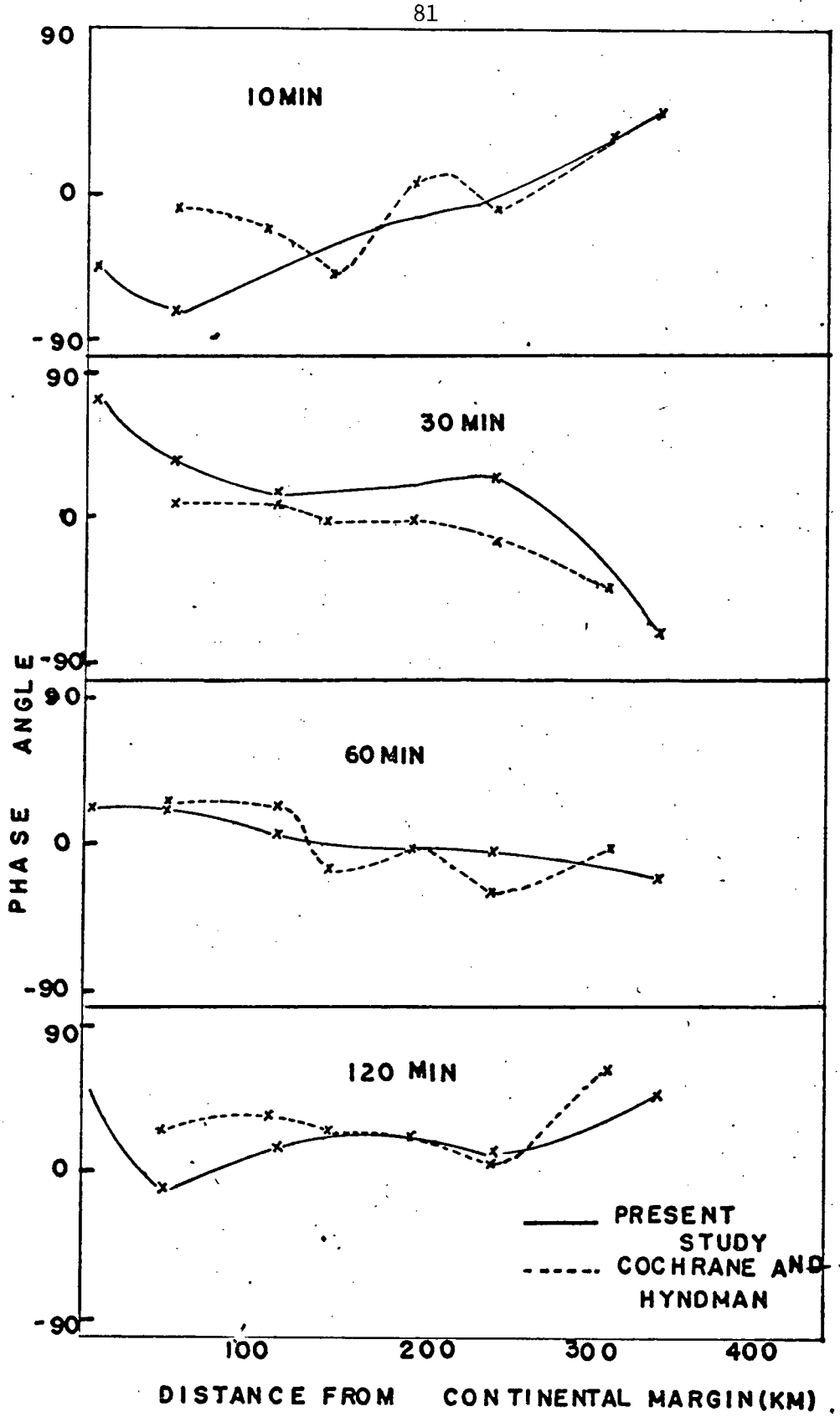

Fig. 4.4 Phase angle for resolved transfer functions at stations on present profile and Cochrane and Hyndman (1970) profile.

concluded that the Dragert (1973) data can be explained by effects connected with the structural boundaries and are not related to the coast effect except at Prince Rupert and Terrace (Fig. 1.1).

The in phase transfer functions differ significantly for the southern area, Cochrane and Hyndman, and the northern area, present survey. The differences are only apparent in the in phase component at 10 minutes and 30 minutes period, at longer periods the two sets become indistinguishable. This suggests that the crustal structure is different in the two regions while the deep structure is similar which is in agreement with the geologic and geophysical evidence for the two regions (Chapter 1). The out of phase components and phase angles exhibit different responses at all periods indicating that the distance from the continental margin to the structures which cause these changes differs. In the north such changes in the phase angle (Fig. 4.4) occur primarily beneath the Queen Charlotte Islands and Hecate Strait i.e. at distances from 10 to 120 km. from the margin. These changes would correlate with the change from oceanic to continental structure beneath the Queen Charlotte's and from the Insular Trough to the Coast Mountains at 120 km. from the margin. On the southern, Cochrane and Hyndman (1970), profile the changes in phase occur at distances from the continental margin which again correlate with changes from the Insular Trough to the Coast Mountains i.e. across Georgia Strait. Jacoby's (1971) profile suggests that these changes in phase angle may be caused by the presence of induced currents at the Mohorovicic discontinuity. The changes in the depth of the Mohorovicic discontinuity would cause changes in the coupling between the sets of induced currents, thus causing the observed out-of-phase component changes. The discontinuity in the depth may be

indicative of the edge of a crustal block at the transition zone marked by the Georgia Strait. There is some paleomagnetic evidence (Berry et al., 1971) that Vancouver Island was not formed in its present location but moved there from the south. If this were so then the Moho discontinuity observed across the Georgia Strait could be explained by the difference in Moho depth for two dissimilar blocks. The geomagnetic variations (Fig. 4.2 to 4.4) seem to indicate that the discontinuity runs deeper than the Moho. This could mean that two different lithospheric plates are involved.

The modelling of these curves evolved in a sequential manner. First the ocean of 2 km. depth abutting a uniform continent was tried. The transfer functions for this were too high suggesting that a near surface high conductivity layer was needed to dampen the response. Following the results of Caner et al., a high conductivity layer was placed at 15 km. beneath the continent. The seismic profile of Johnson et al., (1972) suggested that this high conductivity layer and the intermediate seismic layer were the same. Accordingly a layer of similar conductivity to the Caner layer was placed beneath the ocean. These two layers were connected by a downwarped zone beneath the Queen Charlotte Islands since the seismic evidence suggested this connection between the two layers. This model still required modifications in surface conductivities to obtain an adequate match with the observed data. To achieve this an integrated conductivity was used in the final model (Fig. 4.5 and 4.6) for the upper 5 km. of both the ocean and Queen Charlotte Islands sections. Thus the uncertainty in the locations of the surface and subsurface boundaries of the sediments and water produced an indeterminancy in the location of the equivalent integrated conductivity

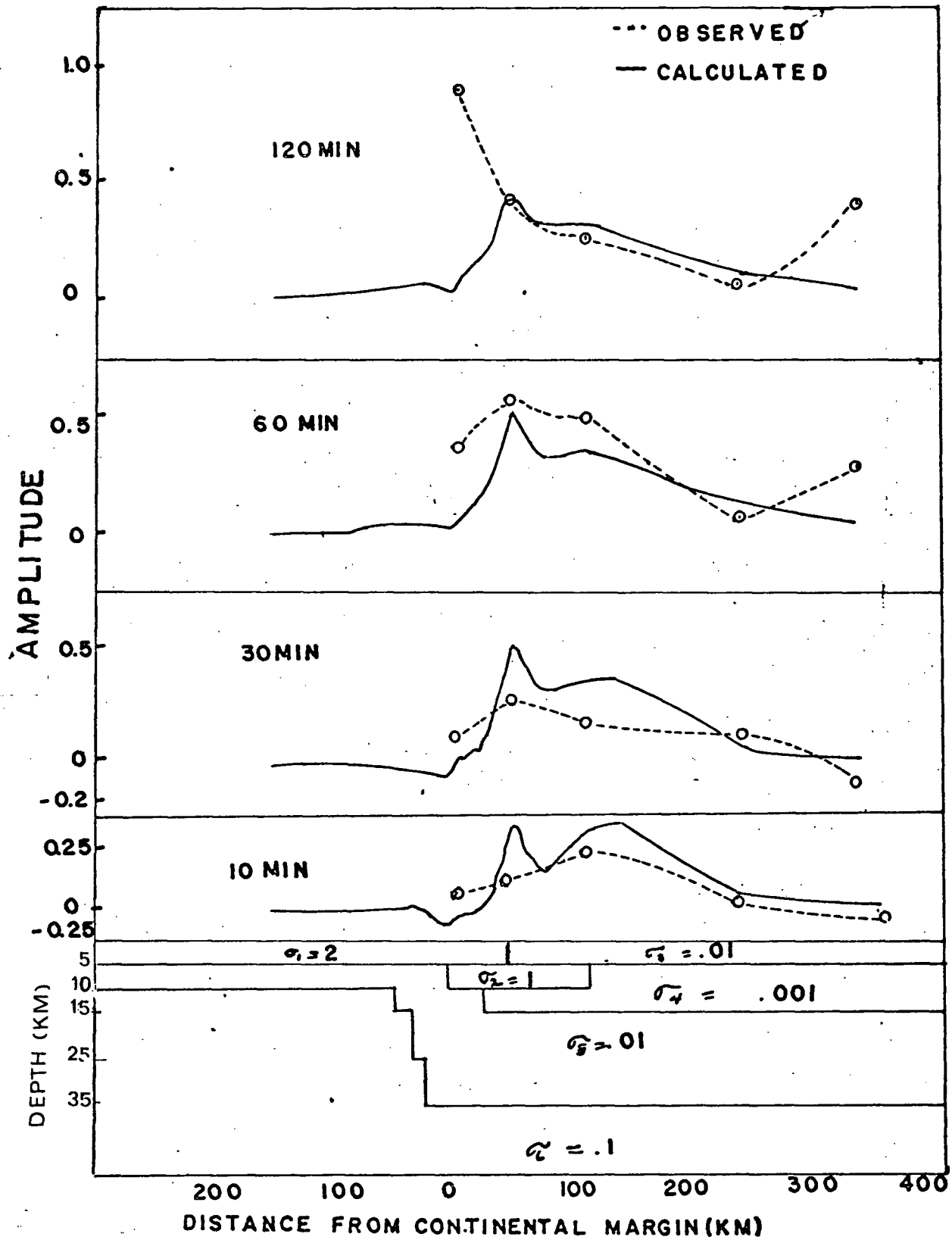

Fig. 4.5 Calculated and observed in phase transfer function magnitude resolved on a line perpendicular to coastline. Final model shown with all conductivities in units of $(\text{ohm m})^{-1}$.

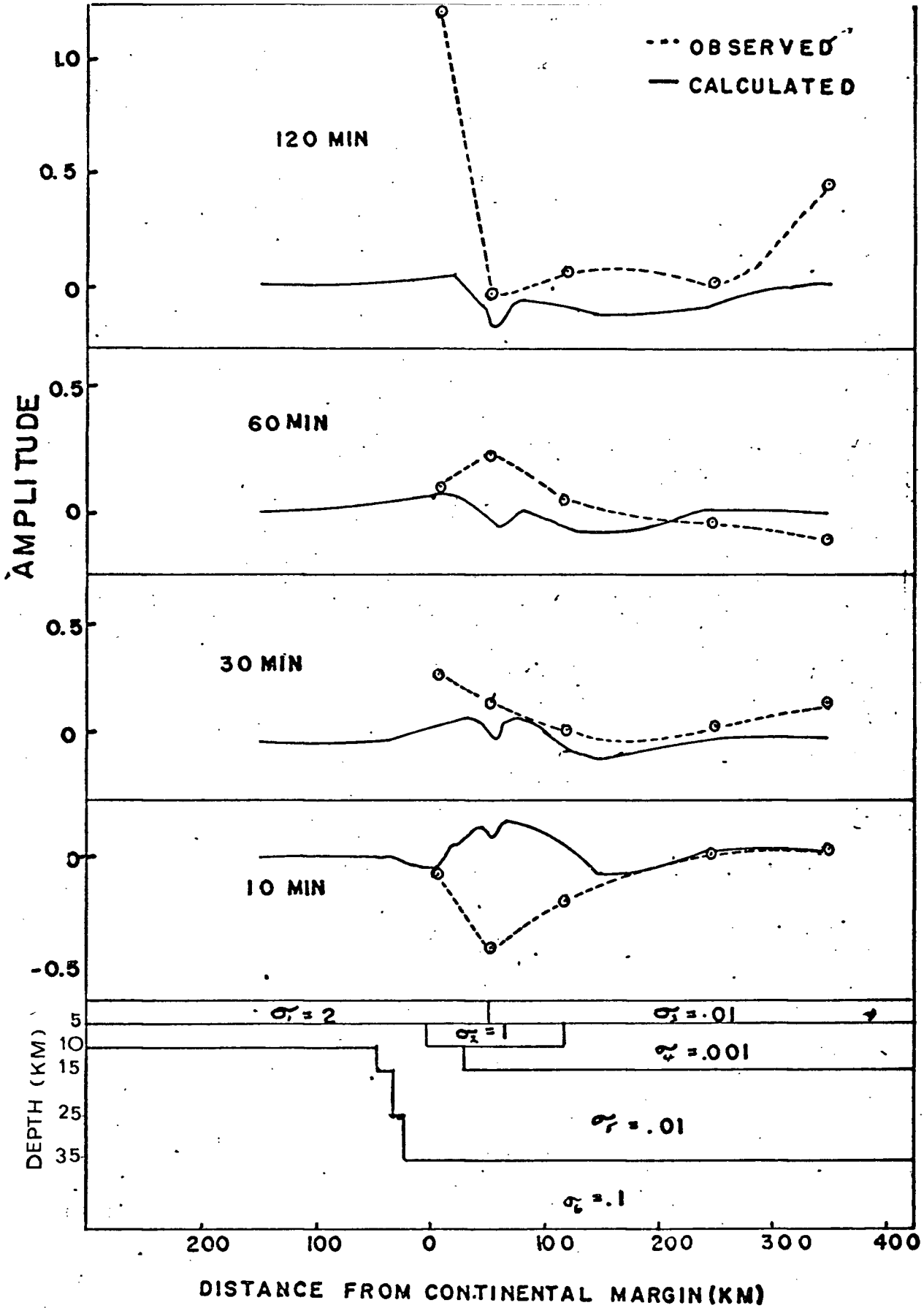

Fig. 4.6 Calculated and observed out of phase transfer functions resolved on a line perpendicular to the coastline. Final model shown with all conductivities in units of $(\text{ohm m})^{-1}$.

boundary. This indeterminancy is responsible for the misfit at short periods particularly for the out-of-phase components.

B) Analog Models

The induction arrows and ellipses derived from the analog models using the techniques of Appendix 6 show considerable variation with source orientation and frequency (Fig. 4.7, 4.8, and 4.9). The strongest response is at 4160 Hz. for the source parallel to the graphite-brine boundary, corresponding to the E polarization case. Here it is to be noted that the magnitude increases as one progresses away from the boundary, then decreases at the two innermost locations. The results for all frequencies show that the largest vector does not necessarily occur at the station nearest the coast. These results also show that considerable rotation of the arrow may occur. For all locations and frequencies the out of phase response is small compared with the in phase part indicating that little mutual inductive coupling is present. This is expected since there is no vertical structure to provide separate induced currents which may couple only by mutual induction.

The induction ellipses show essentially the same results as the induction arrows. The presence of relatively large minor axes at various frequencies supports the idea that the observed ellipticities (Chapter 3) are caused by the presence of two almost perpendicular conductors. The large minor axes at Bella Bella for 695 Hz. and Sandspit for 4160 Hz. and E polarization shows that effects such as those

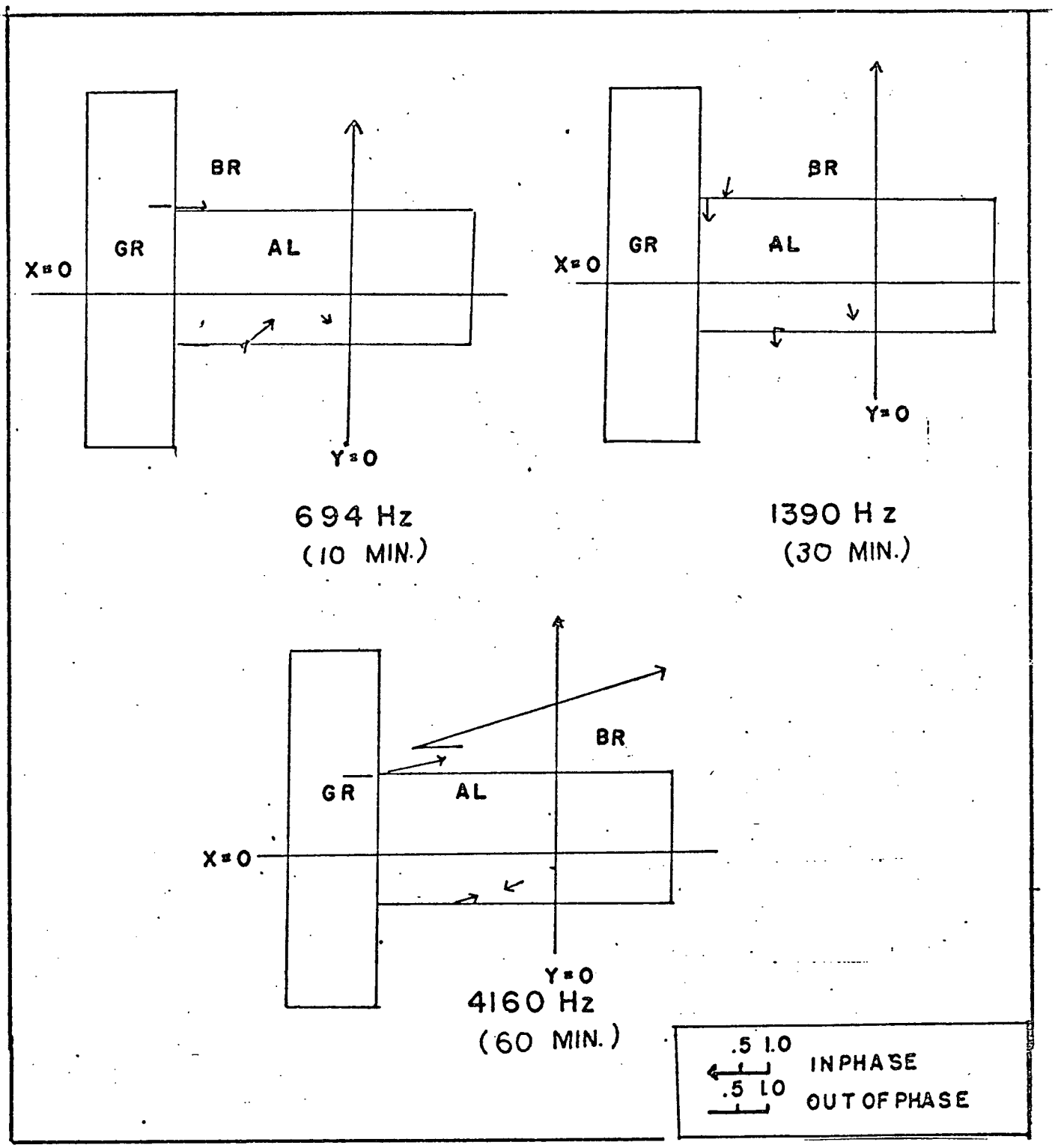

Fig. 4.7a Induction arrows from analog models as a function of frequency and source orientation.

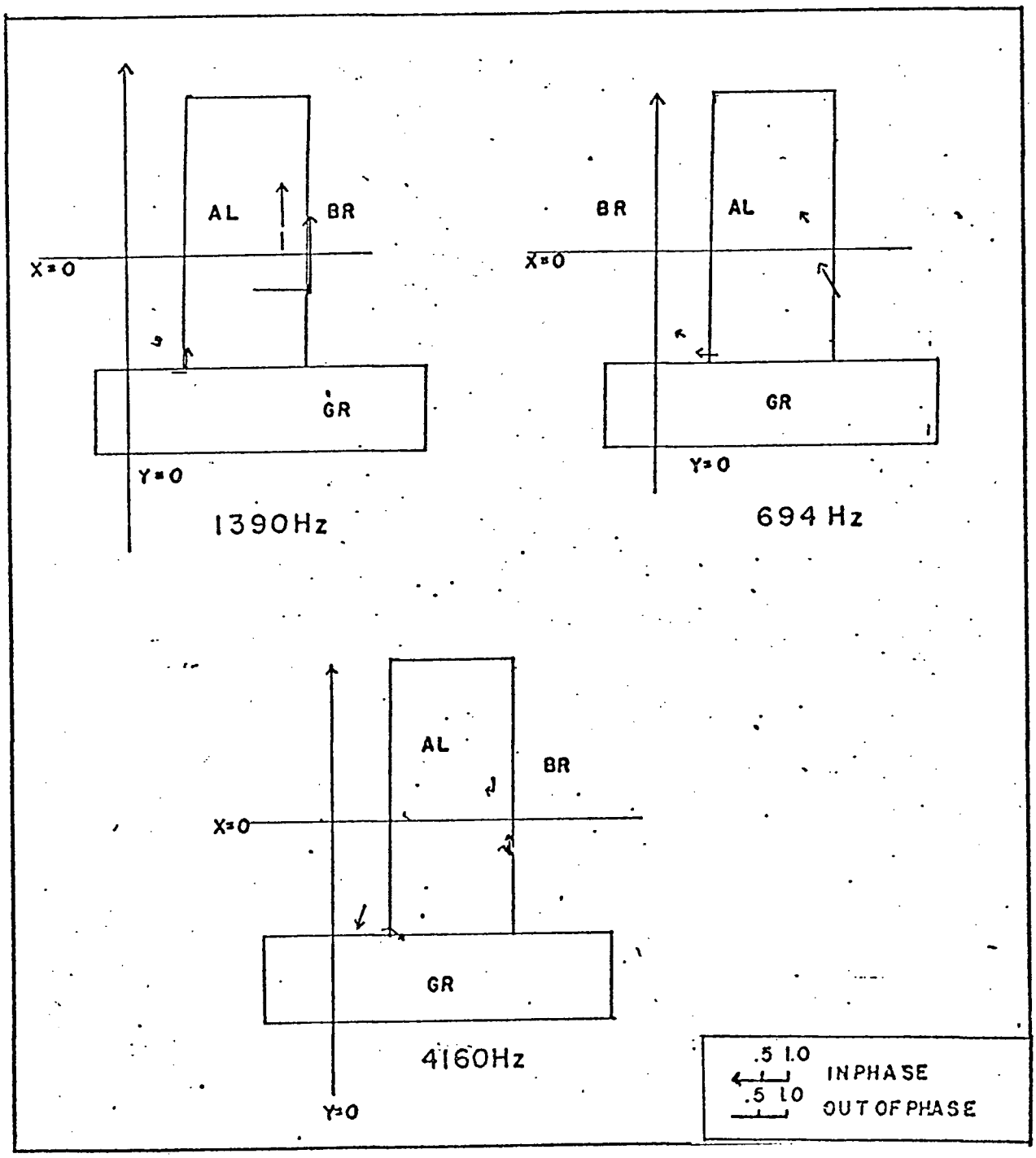

Fig. 4.7b Induction arrows from analog models as a function of frequency and source orientation.

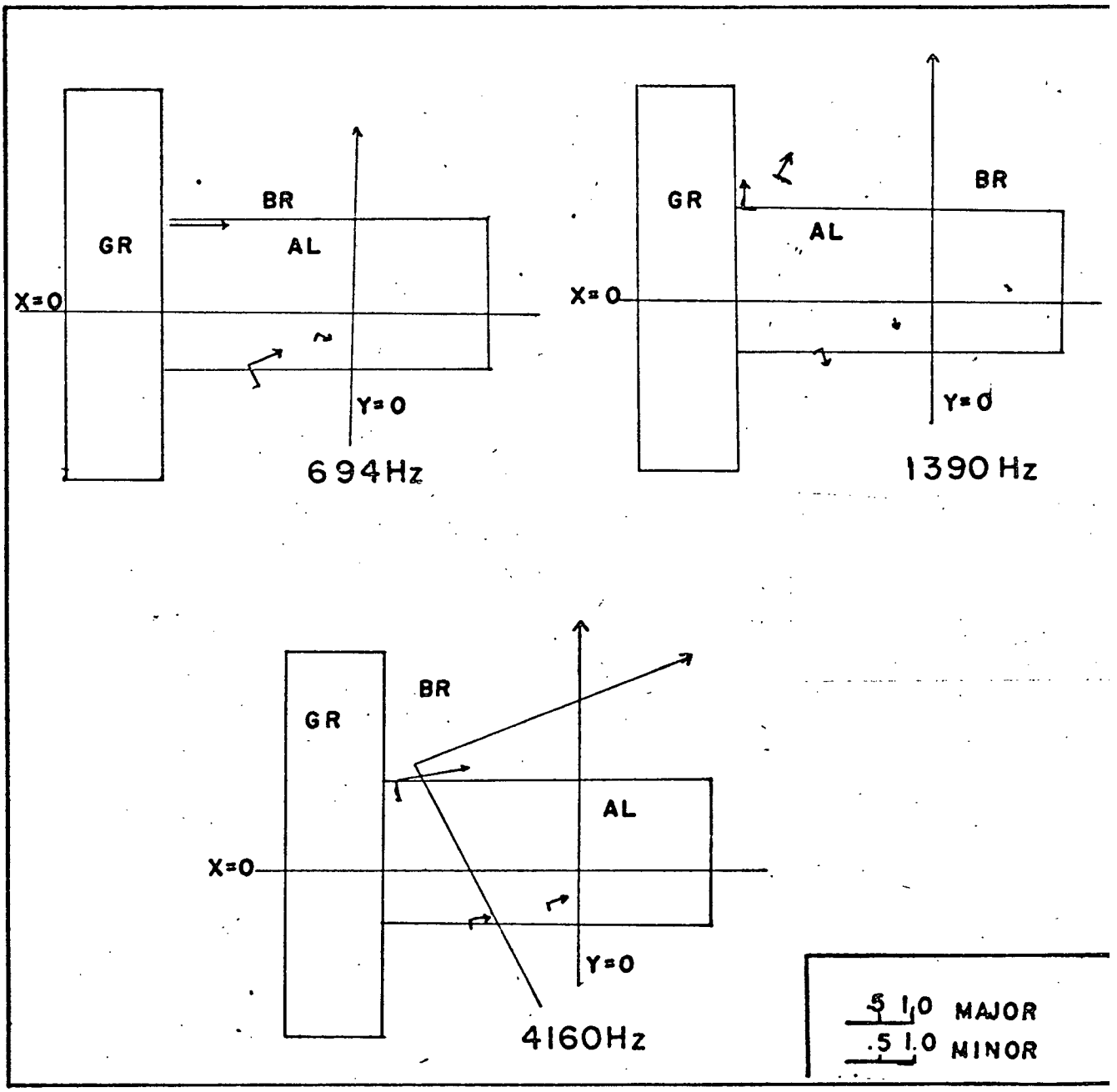

Fig. 4.8a Induction ellipses from analog models as a function of frequency and source orientation.

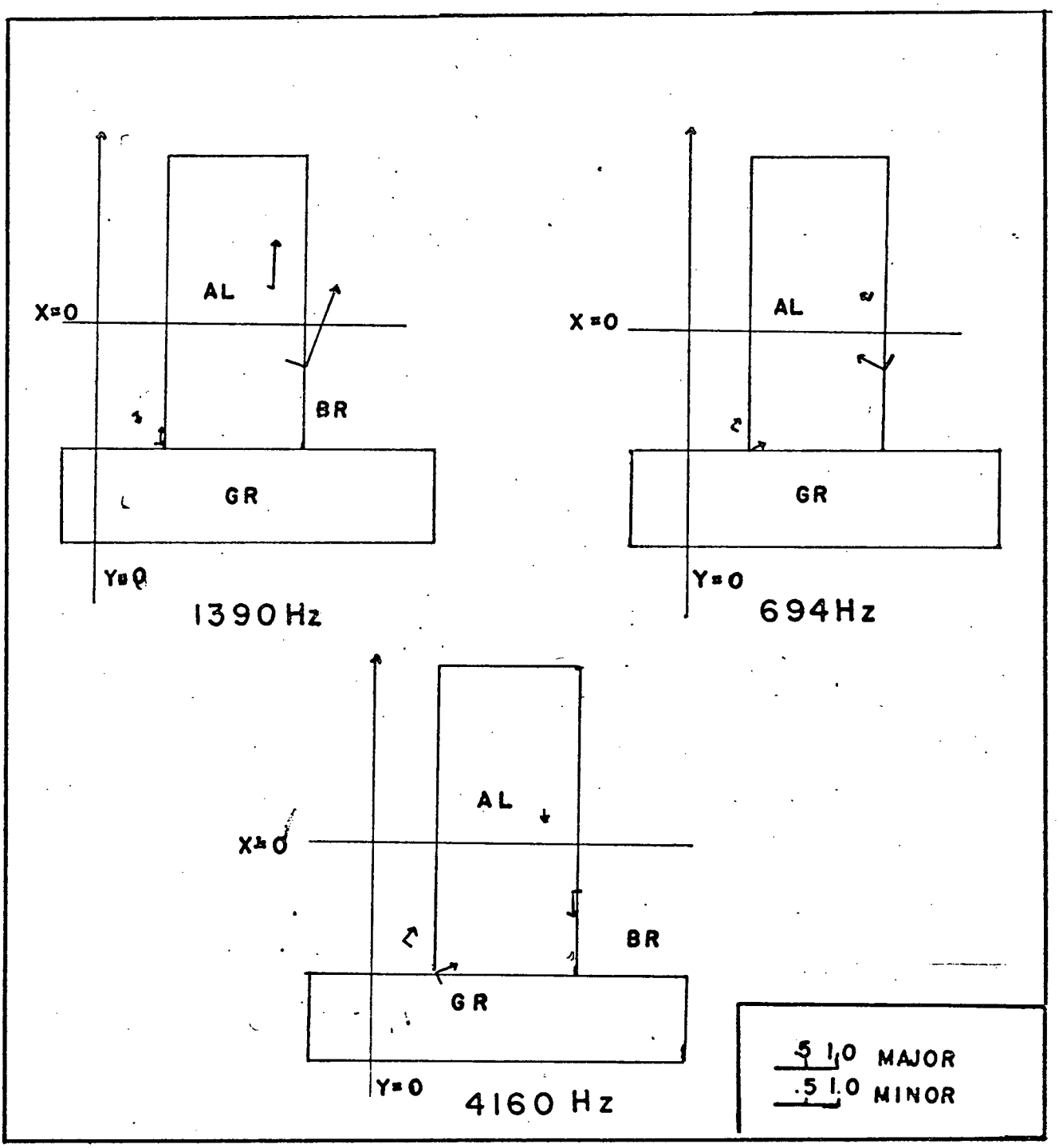

Fig. 4.8b Induction ellipses from analog models as a function of frequency and source orientation.

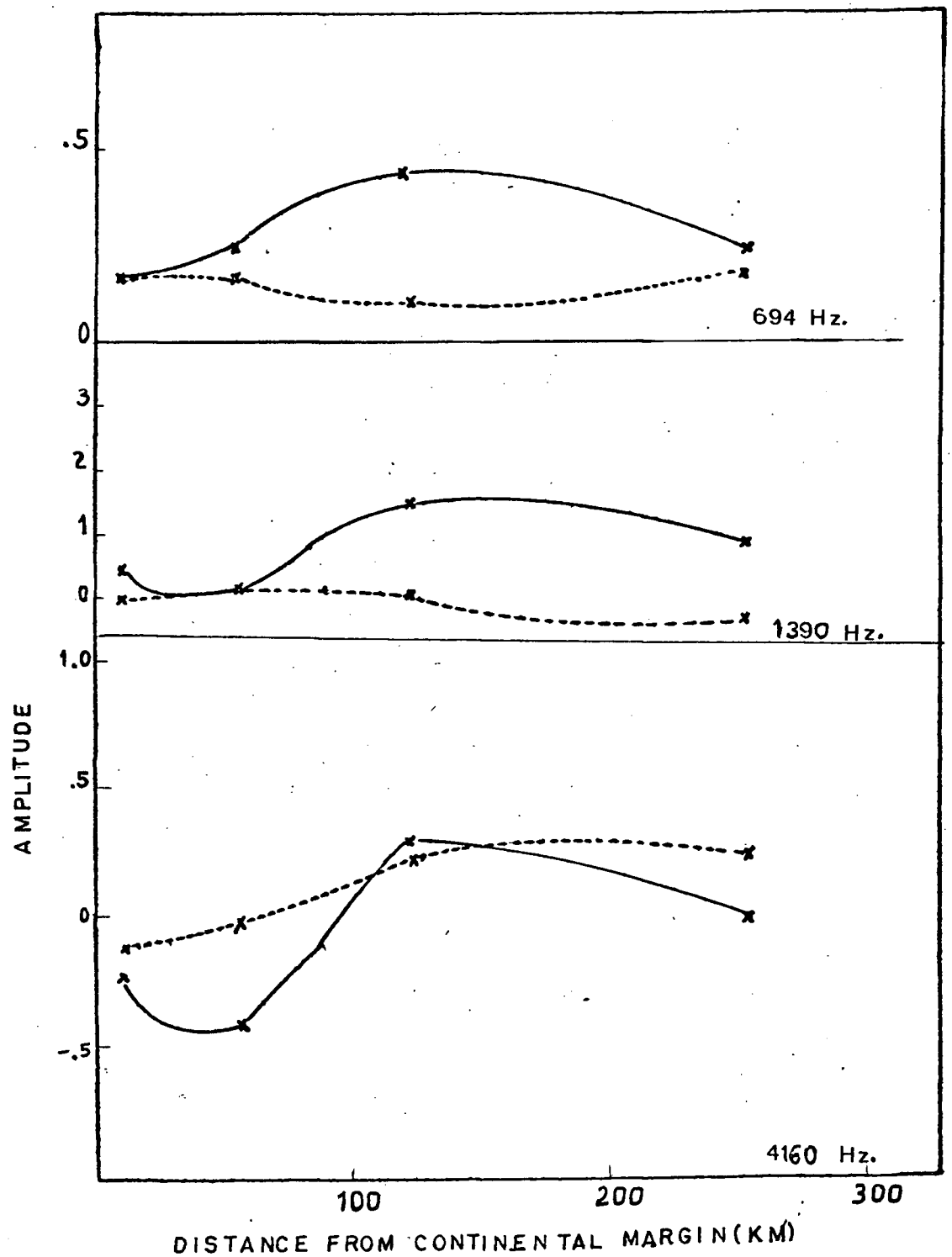

Fig. 4.9b. In phase and out of phase transfer function magnitudes from analog models resolved on a line perpendicular to graphite for E perpendicular to graphite.

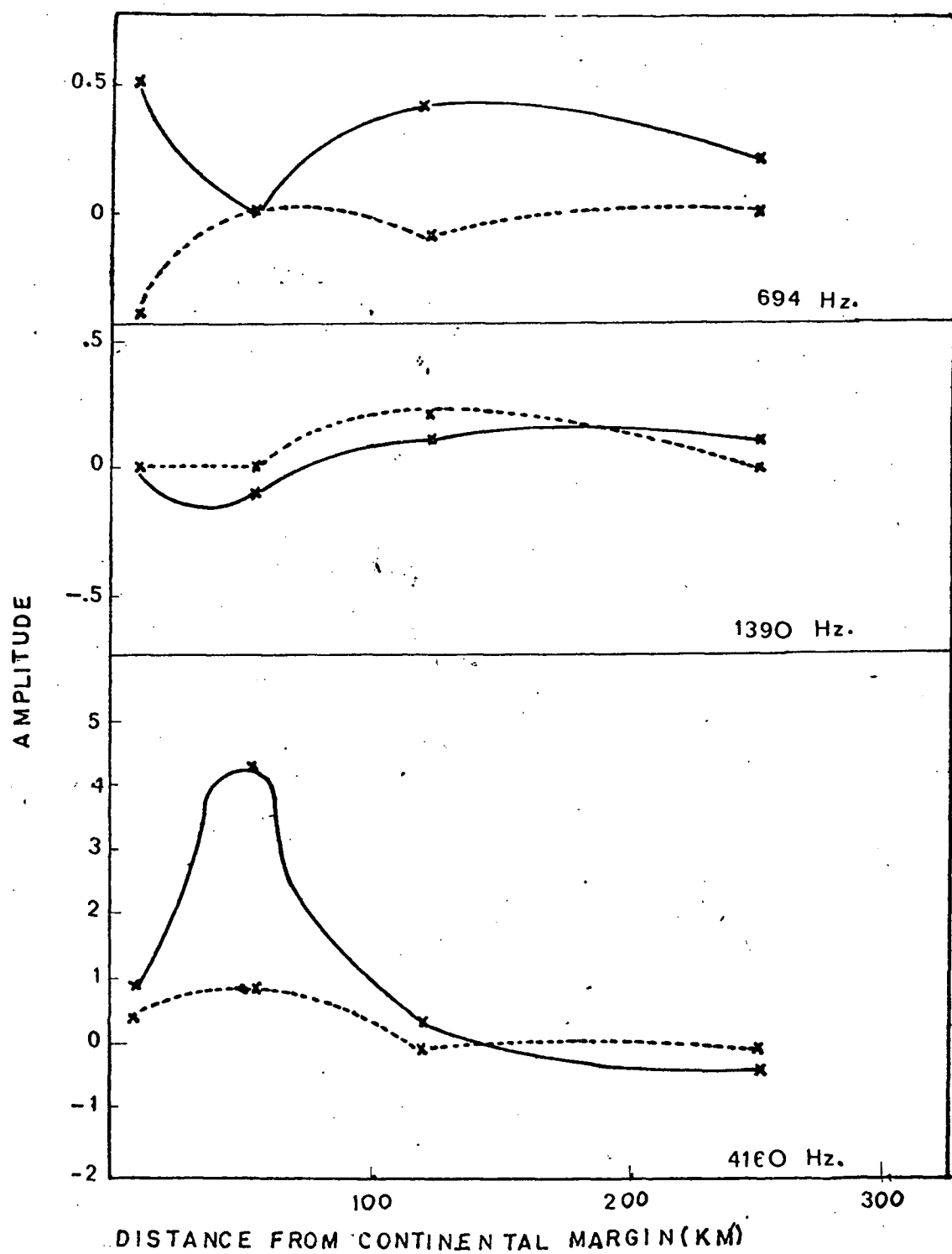

Fig. 4.9a In phase and out of phase transfer function magnitudes from analog models resolved on a line perpendicular to the graphite for E type polarization.

observed at Sandspit and Tasu for 120 minutes (Fig 3.10 to 3.18) and Bella Bella for shorter periods are caused by the presence of a second conductor.

The variation of the transfer function response at the model location equivalent to Tasu and Sandspit shows that considerable variation in the response may occur for different source orientations. This could explain the large error bars at Sandspit and Tasu, since the source fields may be biased towards some direction in one storm and a different one in the next storm, thus inducing a completely different response typified by the transfer functions.

4.5 Tectonic Implications

The model studies have added more evidence to the knowledge of tectonic structure in British Columbia. The numerical models as compared with the primary data suggest major currents induced beneath the Queen Charlotte Islands and at the boundary between the Coast Plutonic belt and the Insular Trough (Fig. 4.5). The resolved transfer functions of Cochrane and Hyndman (1970) (Fig. 4.2 to 4.4) suggest significant structural change at depth beneath the Georgia Strait (120 to 150 km. from the continental margin). This would be consistent with Jacoby's profile of thechanges in depth to Mohorovicic discontinuity below southern British Columbia. The Forsyth (1973) seismic profile in the same region as the Dragert (1973) geomagnetic profile suggests that several deep cutting faults penetrate to the Moho, the structural boundaries in the region also occur near the stations on the Dragert profile showing most appreciable out-of-phase components, and the Jacoby profile for southern British Columbia suggests that the Moho depth

changes beneath the various structural provinces. The numerical model studies show the effect of one such boundary (Bella Bella, 120 km. from the margin), so that the higher magnitude transfer functions observed by Dragert may be explained by induced currents at the base of the crust. The presence of the Souther volcanic zone to the south is not needed to explain the direction of Dragert's long period induction arrows.

The east-west volcanic zone is needed however to explain the azimuthal response of the induction arrows from the present survey. The in-phase and out-of-phase components of the transfer functions on a line perpendicular to the coast line may be explained by induced currents at the continental margin in the ocean and underlying structure which may be an ancient zone of subduction. The persistence of the relatively large amplitude inland may be explained by the presence of induced currents at the boundary between the Interior Trough and the Coast crystalline belt. The small major/minor ellipse axes ratios and the orientations of the induction arrows indicate that the Souther volcanic belt running east-west influences the results. Since the exact location of this belt is poorly defined, and since its presence is indicated at all periods it is assumed this zone has considerable depth. The volcanic material released is also indicative of deep fissures in the crust since its origin is at considerable depth. But there appears to be no other published reports of the existence of such a zone in geological or geophysical literature. Berry et al., (1971) suggest that there is considerable differences in structure in central and southern British Columbia but propose no definite demarcation line. On the basis of the geomagnetic data analysed in this thesis it would appear that the Souther volcanic zone is the demarcation line. The zone may thus be

considered a major structural feature. The northern profile analysed in this thesis (Dragert, 1973) provides evidence of a similar zone to the north of the Prince Rupert to Prince George profile. Thus a crustal block is postulated having boundaries on the north of this northern zone, on the south by the Souther volcanic zone, on the east by the boundary between the Interior Trough and Omineca geanticline, and on the west by the boundary between the coast crystalline belt and the Interior Trough. Berry et al., (1971) also present aeromagnetic evidence for the eastern and western boundaries (Fig. 4.10, Block A). It is to be noted that the existence of this block with these boundaries provides a reasonable explanation for the Dragert (1973) data as well as the data from the present survey. The Cochrane and Hyndman (1970) data are compatible with this interpretation and also provide evidence for a second block bounded by the Strait of Georgia-Coast crystalline belt discontinuity discussed earlier.

The Cache Creek and Hope data are no longer anomalous in light of this discussion above. Cache Creek sees both the eastern and western boundaries of the first block proposed above. In addition it is influenced by the presence of an east-west conductor which runs between it and Hope. No tectonic explanation can be proposed for this conductor unless it is a westward continuation of a deep conductor associated with the Kootenay Arc which Berry et al., (1971) think may mark another boundary of the ancient craton. Lajoie (1970) provides geomagnetic evidence for the existence of the Kootenay Arc conductor in southeastern British Columbia.

The proposed conductors and boundaries enable the geomagnetic variation anomalies to be explained in terms of the known tectonics of the area and in terms of two new zones which have not previously been examined.

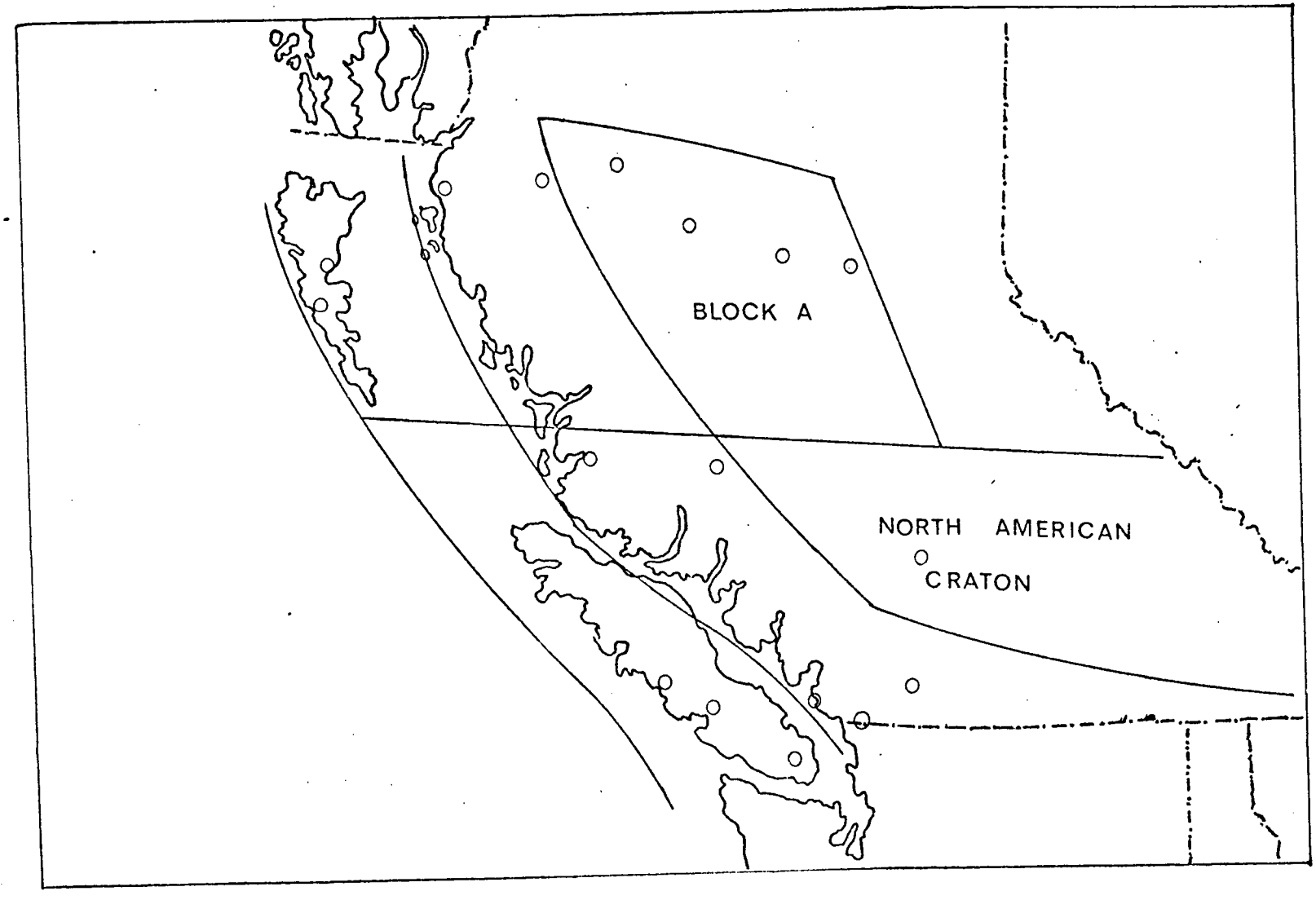

Fig. 4.10 Boundaries indicated by geophysical studies (after Berry et al., 1971) and the present study (cf. Fig. 1.2).

CHAPTER 5

SUMMARY AND CONCLUSIONS

Geomagnetic depth sounding techniques are a recent addition to the geophysicists methods for deducing subsurface structure. Prior to this study several profiles across British Columbia had been analysed in terms of one or more isolated conducting zones. In this study the data from three profiles running from the continental margin to the central interior of the province have been interpreted. The following conclusions may be drawn:

1) The coast effect observed in British Columbia is due to the interaction of the geomagnetic effect of the ocean coupled with the geomagnetic effect of buried conducting structures parallel to the ocean-land boundary. These conductors appear to be associated with a subduction zone beneath the Queen Charlotte Islands in the north and Vancouver Island in the south. It is not possible to delineate by model studies the depth of burial of such a zone, hence no distinction between the northern and southern areas may be made.

2) The persistence in the magnitude of the transfer functions as one proceeds inland on the Prince George - Prince Rupert profile can be explained by induced currents flowing along the boundaries between the structural provinces. The exact location of such currents is not known but the variation in the depth to the Mohorovicic discontinuity beneath these provinces suggests that current concentrations could occur at depths corresponding to the Mohorovicic discontinuity. Such currents explain

the magnitude response of the transfer functions on both the northern and southern profiles. For the southern region a structural discontinuity across the Strait of Georgia is indicated. To the north structural discontinuities are indicated at the Coast Range - Interior Trough and Interior Trough - Omineca Geanticline boundaries.

3) The azimuthal directions of the transfer functions for the central and northern profiles suggests that there is an east-west conductor having considerable depth. The Souther (1970) volcanic zone correlates well with such a conductor. Its presence as a deep conductor is given credence by the analog models.

4) The error bars on the magnitude of the transfer functions may be explained by variations in source orientations and by the interaction of these sources with the complex geology.

5) Two new zones of east-west induced currents are proposed. The first to the north of the Prince Rupert to Prince George profile marks the northern boundary of a crustal block which extends south to the Souther volcanic zone. The eastern and western boundaries are the Omineca geanticline and the coast crystalline belt respectively. The second zone is a possible extension of the Kootenay Arc to the south of Cache Creek. This may represent an extension of the craton further west than previously suspected.

This interpretation represents the first time that the geomagnetic data from a large area of the province has been integrated with

the available geological and geophysical evidence in a total picture. By analysing the data in this way it was possible to postulate the new features and to explain the geomagnetic coast effect in terms of known structure by means of model studies.

The complex structural picture of coastal British Columbia requires considerable further geomagnetic and other geophysical study. It could be rewarding to operate a geomagnetic array on the Queen Charlotte Islands alone. This should be possible using the available logging camps, mines, and towns, in addition to some portable sites using self-contained gasoline or propane generators. By using a floating system as in this thesis, the system can operate on battery power while the generators are being serviced. The operation of such a portable array would permit stations to operate as close as 5 km. from the continental margin. By covering the Queen Charlotte Islands more effectively with recording sites the location of the Souther volcanic zone may be more accurately delimited. Also the operation of an array would enable the internal-external fields to be separated. Thus the anomalous contributions could be determined more precisely and a more detailed analysis produced. If some way of coupling the array with the broad band instruments (Dragert and Caner, 1972) could be achieved it would then be possible to do model studies which could take into detailed account the known geological formations. Such a study should provide much more information about the variations in the coast effect near the margin. A similar array study at any of the other structural boundaries would be extremely instructive.

Other geophysical surveys should be integrated into the study proposed above. The most useful would probably be deep crustal

reflection studies and several refraction profiles parallel to the discontinuity and perpendicular to it. It is realized that such studies in the detail required are extremely expensive, but in light of the present knowledge of the deep structure of British Columbia these studies along with detailed gravity surveys in the north central part of the province are necessary to enhance our understanding of the evolution of the area.

REFERENCES

Atwater, T. Implications of plate tectonics for Cenozoic tectonic evolution of western North America. Bull., Geol. Soc. Amer., 81, 3513-3536, 1970.

Bendat, J. S. and A. G. Pierson. Measurement and analysis of random data. New York, Wiley, 1966.

Berry, M. J., W. R. Jacoby, E. R. Niblett, and R. A. Stacey. A review of the geophysical studies in the Canadian Cordillera. Can. J. Earth Sci., 8, 788-801, 1971.

Cagniard, L. Basic theory of the magnetotelluric method of geophysical prospecting. Geophysics, 18, 605-635, 1953.

Caner, B. Electrical conductivity structure of the lower crust and upper mantle in western Canada. Unpublished Ph. D. thesis, University of British Columbia, Vancouver, 1969.

Caner, B. and D. R. Auld. Magnetotelluric determination of upper mantle conductivity structure at Victoria, British Columbia, Can. J. Earth Sci., 5, 1209-1220, 1968.

Caner, B. and W. H. Cannon. Geomagnetic depth-sounding and correlation with other geophysical data in western North America. Nature, 207, 927-928, 1965.

Caner, B., W. H. Cannon and C. E. Livingstone. Geomagnetic depth-sounding and upper mantle structure in the Cordillera region of western North America. J. Geophys. Res., 72, 6335-6351, 1967.

Caner, B., P. A. Camfield, F. Anderson, and E. R. Niblett. A large scale magnetotelluric survey in western Canada. Can. J. Earth Sci., 6, 1245-1261, 1969.

Caner, B. and H. Dragert. Instrumentation for wide-frequency-band (0.01-100 millihertz) geomagnetic induction work. Zeitschrift fuer Geophysik, 38, 121-132, 1972.

Cannon, W. H. Geomagnetic depth-sounding in southern British Columbia and Alberta. Unpublished M. Sc. thesis, University of British Columbia, Vancouver, 1967.

Chapman, S. and J. Bartels. Geomagnetism. Oxford, Clarendon Press, 1940.

Cochrane, N. A. and R. D. Hyndman. A new analysis of geomagnetic depth-sounding data from western Canada. Can. J. Earth Sci., 7, 1208-1218, 1970.

Culbert, R. R. A study of tectonic processes and certain geochemical abnormalities in the Coast Mountains of British Columbia. Unpublished Ph.D. thesis, University of British Columbia, Vancouver, 1971.

Dickinson, W. R. Plate tectonic models of geosynclines. Earth and Planetary Science Letters, 10, 165-174, 1971.

Dosso, H. W. Analogue model measurements for electromagnetic variations near a coastline. Can. J. Earth Sci., 3, 917-936, 1966.

Dosso, H. W. and J. A. Jacobs. Analogue model measurements of electromagnetic variations in the near field of an oscillating line current. Can. J. Earth Sci., 5, 23-29, 1968.

Dosso, H. W. Induction in laterally non-uniform conductors - Scale model experiments. Invited paper presented at conference on electromagnetic induction held at University of Edinburgh, September, 1972. Reprint of paper for publication in conference volume.

Dragert, H. A geomagnetic depth-sounding profile across central British Columbia. Umpublished M.Sc. thesis, University of British Columbia, Vancouver, 1970.

Dragert, H. A transfer function analysis of a geomagnetic depth-sounding profile across central B.C. Can. J. Earth Sci., 10, 1089-1098, 1973.

Edwards, R. N., L. K. Law, and A. White. Geomagnetic variations in the British Isles and their relation to electrical currents in the ocean and shallow seas. Phil. Trans. Roy. Soc. London, 270, 289-323, 1971.

Everett, J. E. and R. D. Hyndman. Geomagnetic variations and electrical conductivity structure in southwestern Australia. Phys. Earth Planet. Int., 1, 24-34, 1967.

Forsyth, D. A. G. A refraction survey across the Canadian Cordillera. Unpublished M.Sc. thesis, University of British Columbia, Vancouver, 1973.

Haines, G. V., W. Hannaford, and R. P. Riddihough. Magnetic anomalies over British Columbia and adjacent Pacific Ocean. Can. J. Earth Sci., 8, 387-391, 1971.

Hermance, J. F. Model studies of the coast effect on geomagnetic variations. Can. J. Earth Sci., 5, 512-522, 1968.

Hyndman, R. D. and N. A. Cochrane. Electrical conductivity structure by geomagnetic induction at the continental margin of Atlantic Canada. Geophys. J. R. Astr. Soc., 25, 425-446, 1971.

Hyndman, R. D. and D. W. Hyndman. Water saturation and high electrical conductivity in the lower continental crust. Earth and Planet Sci., Lett., 4, 427-432, 1968.

Jacoby, W. R. A refraction profile across the southern Canadian Cordillera (abstract). Trans. Am. Geophys. Un., 51, 356, 1971.

Jenkins, G. M. General considerations in the analysis of spectra. Technometrics, 3, 98-131, 1961.

Johnson, S. H., R. W. Couch, M. Gemperle, and E. R. Banks. Seismic refraction measurements in Southeast Alaska and Western British Columbia. Can. J. Earth Sci., 9, 1756-1765, 1972.

Jones, F. W, and A. T. Price. The perturbation of alternating geomagnetic fields by conductivity anomalies. Geophys. J. R. Astr. Soc., 20, 317-334, 1970.

Keller, G. V. and F. C. Frischknect. Electrical methods in geophysical prospecting. Oxford Pergammen Press, 2nd ed., 566p., 1970.

Lajoie, J. J. The geomagnetic variation anomaly at Kootenay Lake, B.C. Unpublished M.Sc. thesis, University of British Columbia, Vancouver, 1970.

Lambert, A., and B. Caner. Geomagnetic depth-sounding and the coast effect in western Canada. Can. J. Earth Sci., 2, 485-509, 1965.

Lines, L. R. A numerical study of the perturbation of alternating geomagnetic fields near island and coastline structures. Unpublished M.Sc. thesis, University of Alberta, Edmonton, 1972.

Madden, T., and C. M. Swift. Magnetotelluric studies of the crust and upper mantle, in the Earth's crust and upper mantle. Geophys. Monogr. Ser., vol., 13, 469-479, AGU, Washington, D.C., 1969.

Monger, J. W. H. Oceanic crust in the Canadian Cordillera. Publ. Earth Phys. Branch, 42, No.3, 59-64, 1972.

Neiaber, W., D. R. Auld, and H. W. Dosso. Analysis of anisotropic magnetotelluric measurements at Victoria, B.C. Can. J. Earth Sci., 10, 557-570, 1973.

Oxburgh, E. R., and D. L. Turcotte. Thermal structure of island arcs. Geol. Soc. Am. Bull., 81, 1665-1688, 1970.

Parkinson, W. D. Directions of rapid geomagnetic fluctuations. Geophys. J., 2, 1-14, 1959.

Porath, H., D. W. Oldenburg, and D. K. Gough. Separation of magnetic variation fields and conductive structe in western United States. Geophys. J., 19, 237-260, 1970.

Rikitake, T. Electromagnetism and the earth's interior. Elsavier publishing Company, Amsterdam, 1966.

Roddick, J. A., J. O. Wheeler, H. Gabrielse, and J. G. Souther. Age and nature of the Canadian part of the Circum-Pacific orogenic belt. Tectonophysics, 4, 319-337, 1967.

Schmucker, U. Anomalies of geomagnetic variations in the southwestern United States. J. Geomagn. Geoelec., 15, 193-221, 1964.

Schmucker, U. Anomalies of geomagnetic variations in the southwestern Unites States. Bull. Scripps Inst. Oceanog., 13, University of Calfornia, 1970.

Souther, J. G. Volcanism and its relationship to recent crustal movements in the Canadian Cordillers, Can. J. Earth Sci., 7, 553-568, 1970.

Stacey, R. A. Gravity anomalies, crustal structure, and plate tectonics in the Canadian Cordillera. Can. J. Earth Sci., 10, 615-629, 1973.

Swift, C. M. Theoretical magnetotelluric and Turam response from two-dimensional inhomogenities. Geophysics, 36, 38-52, 1971.

Tiffin, D. L., B. E. B. Cameron, and J. W. Murray. Tectonics and depositional history of the continental margin off Vancouver Island, British Columbia. Can. J. Earth Sci., 9, 280-286, 1972.

Topping, J. Errors of observation and their treatment. Chapman and Hall Ltd., London, 1955.

Watanabe, Hiroshi. Measurements of electrical conductivity of basalt at temperatures up to 1500^{0}C. and pressures to about 20 kilobars. Special contribution, Geophysical Institute, Kyoto University, 10, 159-170, 1970.

Weaver, J. T., and D. J. Thompson. A solution of the "coastline effect". Geophys. J. R. Astr. Soc., 28, 163-186, 1972.

Wright, J. A. The magnetotelluric and geomagnetic response of two dimensional structures. Gamma 7, Inst. fuer Geophysik u. Meteorologie, Tech. Univ. Braunschweig, 1969.

APPENDIX 1

DATA PREPARATION

1) SPECTRA

The solution of equations (A1.1), which are equations (2.9), requires the computation of the auto and cross power spectra from the observed time series for the magnetic components.

$$z_D = \frac{S(HH)\,S(ZD) - S(HD)^{*}\,S(ZH)}{S(DD)\,S(HH) - |S(HD)|^2}$$

$$z_H = \frac{S(DD)\,S(ZH) - S(HD)^{*}\,S(ZD)}{S(DD)\,S(HH) - |S(HD)|^2} \qquad \text{(A1.1)}$$

The techniques used to obtain the spectra and the weighting factors for the spectra used in determining the "best" average transfer function are derived and discussed.

a) Digitizing

The time series observed may be considered a number of bandwidth limited records independent of one another. The frequencies present in the observed signal range from dc to the cut-off frequency of the recording system. At the chart advance speed used, the highest frequency which can be detected is about 0.03 sec^{-1} (30 seconds period). The digitizing for the Askania records was undertaken using a grid which had a 2 minute (frequency of 0.833×10^{-3} sec^{-1}) digitizing interval. The lowest frequency which can be expected is dc. Record lengths of 22 hours were digitized and extended by 60 zeros to provide estimates of the daily variation.

b) Harmonic and Trend Removal

Chapman and Bartels (1940) show that the geomagnetic field has strong daily and semidiurnal periodicity. To remove the effect of these, their principal harmonics, and the dc and linear trend components is necessary to avoid contamination of the low frequency part of the spectrum (Bendat and Piersol, 1966). The longest period of interest for analysis is three hours, so harmonics having periods of 24, 12, 8, and 6 hours were removed before the records were spectrally analysed. These harmonics were not used in further analysis as the coast effect in the period range of 10 minutes to 180 minutes was being examined.

The dc, trend, and harmonic components were removed using UBC DPLQF (UBC Computing Centre) to fit the following equation to the data.

$$y(t) = a_0 + a_1 x(t) + \sum_{n=1}^{N} a_{2n} \cos nx(t) + a_{2n+1} \sin nx(t)$$

where N is the number of harmonics of the daily variation component to be removed. Here N = 4.

$$x(t) = \frac{2\pi t}{T}$$

where T is the record length and t is the time from the start of the digitized record.

The data remaining to be analysed now has the form

$$y_1(t) = y_0(t) - y(t) \qquad \text{(A1.2)}$$

where $y_0(t)$ is the original data.

c) Whitening

Spectral analysis of geomagnetic records (Lambert and Caner, 1965) has shown that the spectral energy density tends to decrease with increasing frequency. To obtain uncontaminated estimates of the spectral energy at high frequencies and to minimize spectral leakage it is necessary, therefore, to suppress the low frequency content relative to the higher frequency range before calculating the spectra. For analysis of geomagnetic data the following two point filter has been used to achieve the desired suppression of low frequencies.

$$y_2(t) = y_1(t) - \alpha y_1(t + \tau) \qquad \text{(A1.3)}$$

where $y_2(t)$ is the whitened data

$y_1(t)$ is the data from b) above

α is the whitening factor determined below

τ is the digitizing interval

Traditionally in geomagnetic work a whitening factor of 0.99 has been used. (A1.3) shows that such a whitening factor has the same effect as a 1st derivative filter and enhances the high frequency. Based upon discussions between R. D. Hyndman and the candidate, the decision to use a data adaptive technique to determine α evolved. Following the approach of Maximum Entropy Spectral Analysis, the optimum whitening factor may be calculated to be

$$\alpha = \frac{\sum_{i=0}^{N-1} x(t_i)\, x(t_i + \tau)}{\sum_{i=0}^{N-1} x(t_i)\, x(t_i)} \qquad \text{(A1.4)}$$

Using this approach a separate whitening factor may be computed for each record section.

The time series $y_2(t)$ were then transformed using the Fast Fourier Transform (UBC FOURT, UBC Computing Centre). The transformed data were recoloured and the power spectra were computed at each frequency.

d) Smoothing Spectra

These power estimates are rough estimates which must be smoothed. Smoothing of spectra decreases the variance of the spectral estimates at the expense of frequency resolution. The objective for geomagnetic depth sounding is to obtain these transfer functions at enough points in the frequency domain to enable a smooth response curve to be determined. Thus a statistically stable estimate of the spectra is more important than fine resolution.

Several smoothing windows exist, each having its own characteristic bandwidth, variance, and side lobing properties. The window used is a Parzen window (Jenkins, 1961) of the form

$$\frac{3\pi}{4m^3}\left[\frac{\sin m\omega}{\sin \omega}\right]^4$$

The window was chosen for its rapid attenuation of side lobes.

The window width was varied linearly as a function of frequency with three points being used at a period of 480 minutes and 70 points employed for smoothing at a period of 5 minutes. Smoothed estimates of the spectra for frequencies whose period was a multiple of 5 minutes and 180 minutes. These points were considered sufficient to determine the frequency response of the transfer functions in this study.

2A) TRANSFER FUNCTION COMPUTATIONS

Given the smoothed auto and cross spectra for each component and combination of components calculated for a given record section, the transfer functions at the various frequencies may be calculated for each location using (2.9). The problem now is to calculate the "best" average transfer function for a given location using all storms analysed at that location. By computing an average transfer function using the results of several storms the effect of source effects may be minimized and estimates of the reliability of the best average may be obtained without recourse to the complicated error analysis which would be required from equation (2.9, A1.1). A system of empirical weights to be applied to the spectra calculated above before computing the "best" average transfer function have been devised by Cochrane and Hyndman (1970) and the candidate. These weights are as follows:

i) The Record Length Weight From a consideration of the statistical properties of spectral analysis, it is known that the variance of the smoothed spectral estimate decreases linearly as the record length increases (Bendat and Pierson, 1966). Cochrane and Hyndman (1970) suggest, therefore, that in averaging transfer functions a weight T_i/T_{max} be applied to all spectral values for a given storm, where T_i is the length of the storm and T_{max} is the length of the longest storm analysed.

ii) The Record Energy Weight The computation of the "best" average transfer function requires the total energy from all storms for each spectral frequency component. Use of the spectral energy computed in 1) biases the average value toward the strongest storm i.e. the one having

the most energy. To reduce this bias the spectral components for a given storm are normalized by dividing all spectral estimates for that storm by the total energy in the vertical component for that storm. t Then:

$$\overline{S_i(AB(J))} = \frac{S_i\ (AB(J))}{\sum_{j=1}^{N} S_i\ (ZZ(J))}$$

where $\overline{S_i\ (AB(J))}$ is the normalized spectral energy at frequency J for storm i

$S_i\ (AB(J))$ is the observed spectral energy at frequency J for storm i

$\sum_{j=1}^{N} S_i\ (ZZ(J))$ is the total spectral energy in the vertical component for storm i

iii) The Coherence Weight The two weights above, devised by Cochrane and Hyndman (1970) do not consider the signal to noise ratio at a given frequency for a particular storm. It is conceivable that the spectral energy density for a given frequency may be above the mean noise level for one storm and closer to the noise level in another storm. In such a situation, in the candidate's opinion, it is desirable to weight in favor of the energy density having the higher signal to noise ratio. The quantity which provides a measure of the signal to noise ratio is the spectral coherence. Given the energy spectra for the three components it is possible to compute three coherences, a, b, c, and combine these to give a weight to be applied to the spectral energy at a given frequency for a given storm. The coherences a, b, c, are defined as follows:

$$a = \sqrt{\frac{|\overline{S(HZ(J))}|^2}{S(HH(J))\ S(ZZ(J))}}$$

$$b = \sqrt{\frac{|\overline{S(DZ(J))}|^2}{S(DD(J))\ S(ZZ(J))}}$$

$$c = \sqrt{\frac{|\overline{S(HD(J))}|^2}{S(HH(J))\ S(DD(J))}}$$

Then the weight to be applied to the J^{th} frequency for storm i is $W_i(J) = abc$. The weight is applied to all spectral energies of frequency J for the given storm.

All of these weights may be applied to the smoothed spectra to calculate the total spectral energy at a given frequency as follows:

$$\overline{S(AB(J))} = \sum_{i=1}^{m} \frac{T_i}{T_{max}} \frac{S_i(AB(J))\ W_i(J)}{\sum_{J=1}^{N} S_i(ZZ(J))} \qquad \text{(A1.5)}$$

where m is the number of storms.

2B) TRANSFER FUNCTIONS

Given the weighted total smoothed spectral energy calculated from (A1.5) above, for each of the cross and auto spectra required in (2.9), the equation (2.9) may be solved for z_D and z_H. Individual values of z_D and z_H from each storm for a given frequency may be calculated. By calculating the scatter of these individual values around the "best" average transfer function, the standard error of estimate in z_D and z_H may be calculated using the usual error analysis techniques (Topping, 1955). These "best" average transfer functions may then be used for analysis (Chapter 2 and 3).

APPENDIX 2

INDUCTION ARROWS

The transfer functions z_H and z_D are the ratio of the induced vertical field to the induced horizontal fields in the magnetic northward and eastward directions at a given frequency. Since in general a structure will not be parallel to either of these directions, it is more instructive for interpretation to combine the real parts of these to give the in phase induction arrow and combine the imaginary parts to give the out of phase induction arrow. By analogy with the Parkinson arrow (Chapter 2) the resultant in phase induction arrow will be perpendicular to the strike of the conductor if only a single conductor is involved. In such a case the out of phase part should be zero. If the induction arrows are the resultants of several induction arrows from a multiplicity of conductors each with its own strike, then the in phase arrow will not point to the major conductor nor will the out of phase arrow be zero. Such complex situations may be better interpreted by the induction ellipse discussed in Appendix 3.

The derivation of the in phase and out of phase parts of the induction arrows proceed from z_D and z_H at a given frequency as follows.

Let AINP = the real part at a given frequency of the induction arrow

AZIMR = the azimuthal direction of AINP measured clockwise with respect to magnetic north.

QUAD = the imaginary part at a given frequency of the induction arrow.

AZIMQ = the azimuthal direction of QUAD measured clockwise from magnetic north.

Then at a given frequency

$$\begin{aligned} \text{AINP} &= \{\mathcal{R}(z_H)\}^2 + \{\mathcal{R}(z_D)\}^2 \\ \text{AZIMR} &= \arctan \frac{\mathcal{R}(z_D)}{\mathcal{R}(z_H)} \\ \text{QUAD} &= \{\mathcal{I}(z_H)\}^2 + \{\mathcal{I}(z_D)\}^2 \\ \text{AZIMQ} &= \arctan \frac{\mathcal{I}(z_D)}{\mathcal{I}(z_H)} \end{aligned} \tag{A2.1}$$

In this form the phase angle can be computed by resolving the imaginary part on the real part and taking the ratio of the two.

$$\text{PHASE} = \arctan \frac{(z_D) \quad \cos\ (\text{AZIMR} - \text{AZIMQ})}{(z_D)} \tag{A2.2}$$

These quantities may be used for qualitative analysis of a general induction situation or if the problem is two dimensional the magnitudes may be used for numerical studies. If the in phase component is not perpendicular to the conductors being modelled numerically, it is necessary to reduce the problem to a two dimensional one by resolving the observed AINP andQUAD on to a line perpendicular to the strike of the conductor. This reduces AINP and QUAD to:

$$\begin{aligned} \text{RINP} &= \text{AINP} \quad \cos\ (\text{AZIMR} - \text{COAST}) \\ \text{RQUAD} &= \text{QUAD} \quad \cos\ (\text{AZIMQ} - \text{COAST}) \end{aligned} \tag{A2.3}$$

where RINP is the resolved in phase component

RQUAD is the resolved out of phase component

RQUAD is the resolved out of phase component

COAST is the direction perpendicular to strike

and all other terms are previously defined.

The phase angle for the resolved induction arrows may be computed from:

$$\phi = \arctan \frac{\text{RQUAD}}{\text{RINP}} \qquad \text{(A2.4)}$$

As discussed in Chapter 2 this angle ϕ indicates the degree of coupling between structures. An abrupt change in ϕ from one location to the next indicates a discontinuity in structure.

Using the measures calculated from z_H and z_D in this Appendix a through analysis of a two dimensional problem is possible. Three dimensional problems where one conductor predominates may also be analysed though not with the same thoroughness. The induction ellipse technique (Appendix 3) may be used for a detailed interpretation of such problems. For the general many conductor problem detailed interpretation is not possible using either technique.

APPENDIX 3

INDUCTION ELLIPSES

Schmucker (1964) and Everett and Hyndman (1967) show that an induction ellipse may be derived from the z_D and z_H calculated from (2.9). The general form for this ellipse is

$$R = z_H \cos\theta + z_D \sin\theta \qquad \text{(A3.1)}$$

where θ is the angle between magnetic north and the axis whose magnitude is is R.

Two axes may be calculated by maximizing (A3.1) with respect to θ as follows

$$\text{Let} \qquad z_D = \alpha + i\beta$$
$$z_H = \gamma + i\delta$$

Then it can be readily shown that

$$\tan 2\theta_{max} = \frac{2(\alpha\gamma + \beta\delta)}{\alpha^2 + \beta^2 - \gamma^2 - \delta^2} \qquad \text{(A3.2)}$$

By definition $\theta_{min} = \theta_{max} + 90^0$

Having θ_{max} and θ_{min}, R_{max} and R_{min} can be obtained from (A3.1) and z_H and z_D.

The phase angles can be obtained from

$$\phi_{max} = \arctan \frac{\mathcal{J}(R_{max})}{\mathcal{R}(R_{max})}$$

$$\phi_{min} = \arctan \frac{\mathcal{J}(R_{min})}{\mathcal{R}(R_{min})}$$

The major axis of this ellipse points in the horizontal direction which has maximum coherence with the vertical field. For a single conductor the direction of the major axis is perpendicular to the strike of the conductor, and the magnitude of the minor axis is zero. In this simple situation the induction arrow (Appendix 2) and the induction ellipse are equivalent.

For the case of two conductors perpendicular to one another (Fig. A3.1) the major axis should be perpendicular to the stronger conductor and the minor axis perpendicular to the second conductor. This situation, of course will depend upon the relative strength of the two conductors. If both the responses of the conductors are equal then the major axis will be perpendicular to neither conductor. The minor axis will be the same magnitude as the major indicating two equal conductors. If two intersecting conductors which are not perpendicular to one another are involved, the major axis will be perpendicular to neither one if the two are approximately equal in strength. Obviously if one is much stronger than another the major axis will tend to be perpendicular to it. For more than two conductors the major axis will not necessarily point to either conductor. The magnitude of the minor axis will be an indication that two or more conductors are involved, but no detailed interpretation in terms of the locations of the conductors would be possible.

In summary, the ellipse technique enables the four parameter problem i.e. in-phase and out-of-phase induction magnitudes and directions to be considered in terms of five ellipse parameters: the in-phase and out-of-phase parts of the major and minor axes together with the orientation of the major axis. In the case of two conductors the ellipse technique is superior to the induction arrow technique since it attempts a separation of the contribution from each conductor.

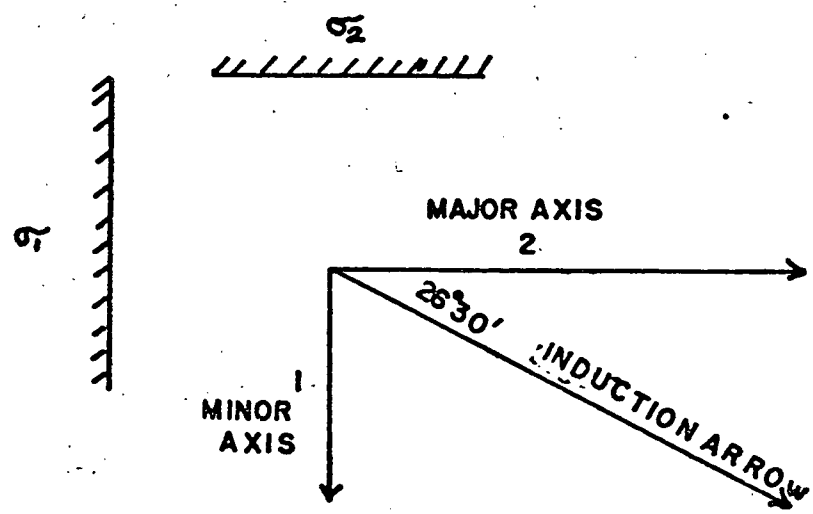

Fig. A3.1 Induction Ellipse and induction arrows for the special case of two perpendicular conductors. The major/minor axis ratio is 2:1.

APPENDIX 4

I RATIOS

Prior to the widespread use of power spectral analysis techniques in geomagnetic analysis pseudo frequency domain techniques such as the I ratio were used (Lambert and Caner, 1965). The I ratio is simply the ratio of the change in the vertical component in a given time interval to the change in the total horizontal component in that same time interval. That is

$$I(\tau) = \frac{\left|Z(t) - Z(t+\tau)\right|}{\sqrt{\{H(t) - H(t+\tau)\}^2 + \{D(t) - D(t+\tau)\}^2}} \qquad \text{(A4.1)}$$

This equation is the same as the Parkinson arrow, the only difference being that Parkinson computed the changes in the components for a specified interval over the whole record length, whereas Caner and his followers only computed I for selected events, which showed bay type disturbances of deviation 2τ, in which they were interested.

Since spectral analysis allows the spectral energy at a particular frequency corresponding to a period τ to be readily determined, the candidate has computed an I ratio at selected periods of 10, 30, 60, and 120 minutes from the spectral energy as follows, where all symbols are as

$$I(J) = \sqrt{\frac{\overline{S(ZZ(J))}}{\overline{S(HH(J))} + \overline{S(DD(J))}}} \qquad \text{(A5.1)}$$

defined in previous Appendix.

This I ratio should be the same as the average I ratio computed

by Caner. Like the I ratio computed in the time domain it does not consider coherence between the various components. In the computation of (A5.1) it is assumed that source effects are small and are removed by the averaging of the spectra discussed in Appendix 1 since the I ratio is computed from the total weighted spectra. These ratios are only used to indicate areas of possible induced current concentration. No numerical analysis is based upon them, therefore estimates of the variability of I(J) were not calculated.

APPENDIX 5

NUMERICAL MODELLING

Transmission Line Analogy

The method used in this thesis is the transmission line analogy as programmed by Hyndman and Cochrane (personal communication). This technique follows Swift (1971) and solves the resultant mesh equations by an over-relaxation procedure. Only the E polarization case will be considered here since it gives a vertical magnetic field and a horizontal field perpendicular to the strike which in the transfer function approach in the direction of maximum coherence between the vertical and horizontal components.

Maxwell's equations as before may be written as

$$\overline{\nabla} \times \overline{E} = -\frac{\partial \overline{B}}{\partial t} = -\mu \frac{\partial \overline{H}}{\partial t}$$

$$\overline{\nabla} \times \overline{H} = \sigma \overline{E} + \frac{\partial \overline{D}}{\partial t} = \sigma \overline{E} + \varepsilon \frac{\partial \overline{E}}{\partial t} \qquad \text{(A5.1)}$$

$$\overline{\nabla} \cdot \overline{B} = 0 \qquad \overline{\nabla} \cdot \overline{D} = 0 \qquad \sigma \overline{E} = \overline{J}$$

Now for a coordinate system such that x is parallel to strike, y perpendicular in horizontal plane to strike, and z positive downward i.e. right hand coordinate system and $\overline{E} = (E,0,0)$ and the time dependence is of the form $e^{i\omega t}$ the above equations become

$$\frac{\partial E_x}{\partial x} = 0 \Longrightarrow H_x = 0$$

$$- i\mu\omega H_y = \frac{\partial E_x}{\partial z}$$

$$i\mu\omega H_z = \frac{\partial E_x}{\partial y}$$

$$\text{and} \quad (\sigma + i\omega\varepsilon)E_x = \frac{\partial H_z}{\partial y} - \frac{\partial H_y}{\partial z}$$

Putting $(\sigma + i\omega\varepsilon) = \sigma'$ yields

$$\sigma' E = \frac{\partial H_z}{\partial y} - \frac{\partial H_y}{\partial z} \tag{A5.2}$$

Now the equations for the propogation of a disturbance along a transmission surface are

$$\nabla V = ZI \quad \text{and} \quad \nabla \cdot I = - YV$$

which reduce to

$$\frac{\partial V}{\partial y} = -ZIy \qquad \frac{\partial V}{\partial z} = -ZIz$$

$$\text{and} \qquad \frac{\partial I_y}{\partial y} + \frac{\partial I_z}{\partial z} = -YV \tag{A5.3}$$

where Z,Y are lumped impedances associated with the grid points. Combining these it is evident that

$$\frac{1}{Z} \nabla^2 V + YV = 0 \tag{A5.4}$$

which is analogous to

$$\nabla^2 E + i\mu\omega\sigma E = 0 \tag{A5.5}$$

where $i\mu\omega\sigma = ZY$

By comparing (A5.2) and (A5.3) the following analogy is made.

E Polarization	Transmission Surface
E_x	V
$-H_z$	I_y
H_y	I_z
Y	σ
Z	$j\mu\omega$

Then the equation

$$\frac{\partial I_y}{\partial y} + \frac{\partial I_z}{\partial z} = -YV$$

may be rewritten in terms of the voltage at a given grid point and an adjacent point as

$$\sum^{A} \frac{V_{neighbouring} - V_{ij}}{Z_{connecting}} + Y_{ij} V_{ij} = 0 \qquad \text{(A5.6)}$$

From the analogy drawn it is seen that the grid points are linked by inductive reactance to one another and be a resistive admittance to ground.

Equation (A5.6) must be solved at each grid point subject to the boundary conditions already mentioned.

It should be noted that the impedances and admittances used in equation (5.6) are the lumped values which incorporate the dimensions of the block for which they are given hence:

$$Z_H(\text{lumped}) = Z\,\Delta y_i/\Delta z_i \qquad \text{where } y_i,\ z_i \text{ are distances between grid points.}$$

$$Z_V(\text{lumped}) = Z\,\Delta z_i/\Delta y_i$$

$$Y_{ij}(\text{lumped}) = Y\,\Delta y_i \Delta z_i$$

If one defines the parameters for the blocks between grid points rather than for the grid points one eliminates the uncertainty about where the ends of the block lie, but it is then necessary to define the lumped impedance as twice the parallel combination of the impedances on either side of the inter-nodal line and to make the nodal admittance one quarter of the sum of the admittance of adjacent blocks.
The boundary conditions then require that one must move above the air-conductor surface to such a height that H_z is zero. This in the transmission analogue implies that $I_y = 0$ which means $Z_y \Longrightarrow \infty$ i.e. infinite wavelength.

At the edges of the grid it is also required that $H_z = 0$ which again implies no horizontal current flow in the transmission line analogy, which means that Z_y again tends to infinity and Z is the characteristic impedance

The major problem once the equations and boundary conditions have been enunciated is in obtaining stable solutions after a significant number of iterations. By using a relaxation parameter of 1.5 it was found that the process rapidly converged even for the most complicated models. Since the impedance parameters are frequency dependent the whole iterative procedure has to be repeated to calculate the response for each frequency for which results are desired.

APPENDIX 6

ANALOG MODEL ANALYSIS

The anomalous magnetic field component and its phase is obtained for each of three orthogonal directions using the data collected from the analog model traverses. This data may be combined to give the in-phase and out-of-phase induction arrows for the model as follows:

$$\Delta Z = \Delta \mathcal{Z} \exp i\Delta\phi_z$$
$$\Delta X = \Delta \mathcal{X} \exp i\Delta\phi_x$$
$$\Delta Y = \Delta \mathcal{Y} \exp i\Delta\phi_y$$

where $\Delta \mathcal{Z}$, $\Delta \mathcal{X}$, $\Delta \mathcal{Y}$, are the magnitudes and $\Delta\phi_z$, $\Delta\phi_x$, $\Delta\phi_y$ are the phases of the three magnetic field components.

Then the total anomalous horizontal field is given by

$$\Delta H = \Delta \mathcal{H} \exp i\phi_H$$

The real part of ΔH is defined by

$$\Delta H_R = \{\mathcal{R}(\Delta X)\}^2 + \{\mathcal{R}(\Delta Y)\}^2$$

and the imaginary part is defined by

$$\Delta H_I = \{\mathcal{I}(\Delta X)\}^2 + \{\mathcal{I}(\Delta Y)\}^2$$

The phase angle of the horizontal field is then

$$\phi_H = \text{arc tan } \frac{\Delta H_I}{\Delta H_R}$$

The azimuthal direction relative to the X axis of the in-phase component of the horizontal field is given by

$$\text{AZIMR} = \text{arc tan } \frac{\mathcal{R}(\Delta Y)}{\mathcal{R}(\Delta X)}$$

Similarly the azimuthal direction of the out-of-phase component of the horizontal field is

$$\text{AZIMQ} = \text{arc tan } \frac{\mathcal{I}(\Delta Y)}{\mathcal{I}(\Delta X)}$$

The single station transfer function i.e. induction arrow is then given by

$$\text{STF} = \frac{\Delta \mathcal{Z}}{\Delta \mathcal{H}} \exp i(\Delta\phi_z - \phi_H)$$

This may be considered as two induction arrows: the in-phase of magnitude $\mathcal{R}$ (STF) and azimuthal direction given by AZIMR and the out-of-phase of magnitude $\mathcal{I}$ (STF) and azimuthal direction AZIMQ. The phase angle of the transfer function is then

$$\delta = \Delta\phi_z - \phi_H$$

The single station transfer function may be analysed by the ellipse

technique discussed in Appendix 3 by resolving the induction arrows in two mutually perpendicular directions as follows

$$z_x = \mathcal{R}\,(\mathrm{STF})\ \cos\ \mathrm{AZIMR} + i\ \mathcal{I}\ (\mathrm{STF})\ \cos\ \mathrm{AZIMQ}$$

$$z_y = \mathcal{R}\,(\mathrm{STF})\ \sin\ \mathrm{AZIMR} + i\ \mathcal{I}\ (\mathrm{STF})\ \sin\ \mathrm{AZIMQ}$$

These may be substituted into the appropriate equations in Appendix 2 to give the major and minor ellipse axes with their orientations.